CANADIAN THESES

THÈSES CANADIENNES

NOTICE

The quality of this microfiche is heavily dependent upon the quality of the original thesis submitted for microfilming. Every effort has been made to ensure the highest quality of reproduction possible.

If pages are missing, contact the university which granted the degree.

Some pages may have indistinct print especially if the original pages were typed with a poor typewriter ribbon or if the university sent us an inferior photocopy.

Previously copyrighted materials (journal articles, published tests, etc.) are not filmed.

Reproduction in full or in part of this film is governed by the Canadian Copyright Act, R.S.C. 1970, c. C-30.

AVIS

La qualité de cette microfiche dépend grandement de la qualité de la thèse soumise au microfilmage. Nous avons tout fait pour assurer une qualité supérieure de reproduction.

S'il manque des pages, veuillez communiquer avec l'université qui a conféré le grade.

La qualité d'impression de certaines pages peut laisser à désirer, surtout si les pages originales ont été dactylographiées à l'aide d'un ruban usé ou si l'université nous a fait parvenir une photocopie de qualité inférieure.

Les documents qui font déjà l'objet d'un droit d'auteur (articles de revue, examens publiés, etc.) ne sont pas microfilmés.

La reproduction, même partielle, de ce microfilm est soumise à la Loi canadienne sur le droit d'auteur, SRC 1970, c. C-30.

THIS DISSERTATION HAS BEEN MICROFILMED EXACTLY AS RECEIVED

LA THÈSE A ÉTÉ MICROFILMÉE TELLE QUE NOUS L'AVONS REÇUE

Synthesis and X-Ray Crystallography of Some Metal Carbonyl Complexes Containing the TRIPOD ligand, $HC(PPh_2)_3$.

Antoni Vincent Peters

A Thesis

in

The Department

of

Chemistry

Presented in Partial Fulfillment of the Requirements
for the Degree of Master of Science at
Concordia University
Montréal, Québec, Canada

September 1985

ISBN 0-315-30605-X

ABSTRACT

Synthesis and X-Ray Crystallography of Some Metal Carbonyl Complexes Containing the Tripod Ligand, $HC(PPh_2)_3$

Antoni Vincent Peters

This thesis reports the syntheses and/or single crystal diffraction studies of some metal carbonyl complexes coordinated by the TRIPOD ligand, $HC(PPh_2)_3$.

The molecule $Mo(CO)_4[HC(PPh_2)_3]$ was prepared and characterized by both ^{31}P NMR and a single crystal X-ray structure determination. The x-ray study revealed the molecule to possess near mirror symmetry with the TRIPOD ligand in a chelate bonding mode. The pseudo-mirror plane bisects the molecule through the Molybdenum atom, the chelate metallocycle and two carbonyl groups. The chelating bite angle was determined to be 67.06° and the distance from Molybdenum to the non-bonded phosphino function was found to be 4.332A.

The molecule $MoCl(CO)_2(\pi\text{-allyl})[HC(PPh_2)_3]$ was prepared by the Osborn group.[1] The crystal structure determination was undertaken to determine structural differences between itself and that of the tetracarbonyl analogue. In this case no pseudo-symmetry was found. The distance between Molybdenum and the non-bonded phosphino function was found to be 5.033A and the

chelate bite angle determined to be 63.90°. The allyl group adopts a cis-configuration with respect to the chloride in a distorted octahedral coordination sphere. The chelating phosphine functions also are cis to the chloride. One of these functions is trans to the allyl ligand while the other is trans to a terminal carbonyl.

The complex formulated as $[RhCl\{HC(PPh_2)_3\}]_2$ was prepared by direct combination of $[RhCl(CO)_2]_2$ with the TRIPOD ligand at room temperature. The product was recovered immediately only when using wet, non-deoxygenated THF assolvent. Difficulties with solubility, spectral characterization and the inability to grow suitable single crystals made the assignment of an unequivocal structure impossible.

This product was reacted with $Co_2(CO)_8$ in a 1:4 molar ratio to yield the complex $RhCo_3(CO)_9[HC(PPh_2)_3]$. A single crystal structure determination revealed the novel crystallographic result that four formula units comprising two asymmetric units were found to pack into a unit cell with space group P1. Included in this result was the two formula units displayed disorder such that the Rhodium atom, which is always one of the three metals coordinated to TRIPOD, could occupy any one of three possible positions.

A final synthesis involved the reaction of the TRIPOD ligand with $Co_2(CO)_8$ in a 1:1 molar ratio at 25°C yielding a product displaying more than two types of

carbonyl groups. The ^{31}P NMR spectrum showed a familiar resonance pattern (doublet:triplet) indicating either a symmetric bridging between both metal centres or an asymmetric bridging with two of the ligand functions coordinated to one Cobalt atom and the third singly coordinated to the second Cobalt. Geometric and intensity data were collected for the x-ray structure but the structure was not solved due to phasing difficulties.

Acknowledgements

I would like to express my appreciation to Dr. P. H. Bird for introducing me to valuable preparative techniques as well as his guidance through the process of several x-ray structure determinations. Also, my thanks to him for tolerating my idiosynerasies.

Secondly, I would like to thank my parents for supporting me through my undergraduate years.

I should also like to extend special mention to Mr. Paul Cahill for his skillful glass-blowing as well as the technical support team of Francesco Nudo and Miriam Posner.

Thank you to Dr. L. D. Colebrook for introducing me to FT-NMR.

To

Marie-Josée

Table of Contents

List of Tables

TABLE 5.4.1. Unit Cell Dimensions With e.s.d.'s for Reaction Product from $Co_2(CO)_8$ and $HC(PPh_2)_3$

List of Figures

1. GENERAL INTRODUCTION [2-9]

1.1 BACKGROUND

Homogeneous catalysts are compounds which function in the same phase as reactants and serve to facilitate or increase the rate of given chemical reactions. The main drawback in the use of these catalysts is the difficulty encountered separating the catalyst from the product(s).

Conversely the attractive features associated with the use of these catalysts are often: a) enhanced stereoselectivity and b) milder reaction conditions under which many homogeneous catalytic conversions occur.

More recently the synthesis of metal carbonyl clusters has given rise to investigation of whether catalysis by metal clusters occurs in a mono or multimetallic fashion. Specifically, if a carbonyl cluster is added to a reaction mixture, is the catalytically active species a mono- or multimetallic composite? Metal carbonyl clusters often fragment at elevated temperatures or in the presence of a coordinating solvent. In order to explore the possibility of multimetallic or cluster catalysis it is desirable to prepare molecules in which the metal skeleton is supported by multidentate ligands. The resulting complexes should display enhanced structural integrity in turn minimizing cluster degradation.

The work undertaken in this study has been primarily an investigation into the possible products formed by

reactions of metal carbonyls and chloro-bridged carbonyls with the ligand tris-1,1,1,-diphenylphosphino methane, $HC[PPh_2]_3$. The ligand is also referred to as TRIPOD. TRIPOD can be prepared as outlined in the paper by Isslieb and Abicht[2] or similarly as reported by Osborn et al[3]. Of course, the ligand need not be limited to phosphines or species with C_{3v} symmetry. Furthermore, interesting combinations containing alkyl pi-bonding derivatives may generate a greater number of possible metal complexes than the aryl precursors in view of their higher expected nucleophilicity (FIG.1).

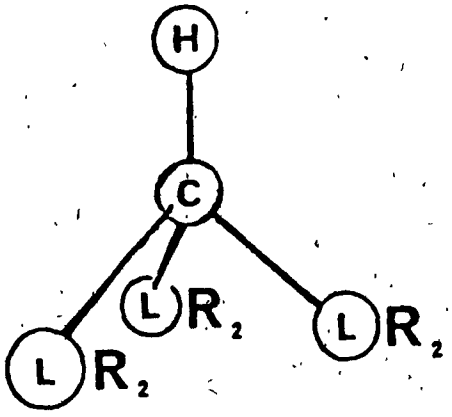

R = Alkyl, Aryl

L = P, As, Sb

(Fig.1)

It is useful to review the possible bonding modes of this ligand to mono and multinuclear metallic systems, which are very diverse.

The monometallic complex may exhibit two bonding modes, the first being a simple displacement of one carbon monoxide molecule by one of the three phosphino functions leaving two phosphino functions dangling. This case is

exemplified by the reaction of $Fe(CO)_5$ and TRIPOD in a 1:1 molar ratio in hydrocarbon solvent. Fig.2 displays the resulting product, $Fe(CO)_4$TRIPOD.

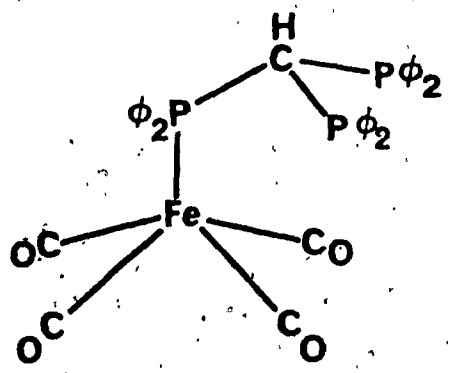

(Fig.2)

The second bonding mode is chelation. Two phosphino functions are coordinated to the metal, the remaining one is dangling. An example of this is $Fe(CO)_3$TRIPOD.[4] (Fig.3.)

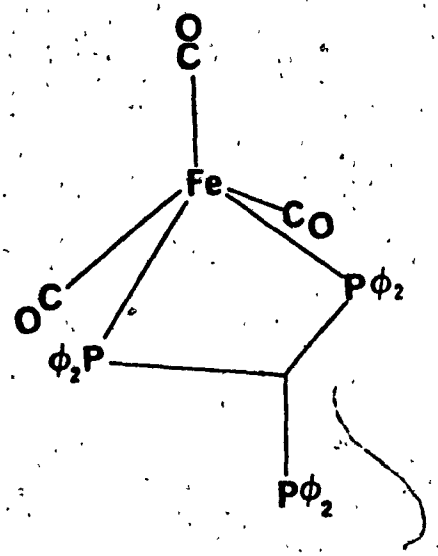

(Fig.3)

It has also been demonstrated that multinuclear

clusters may be synthesized using mononuclear metal complexes, the cluster template being the TRIPOD ligand. The example cited here is the reaction of TRIPOD with excess $Ni(CO)_4$.[6] Initial complex formation gives a chelated nickel dicarbonyl moiety with a dangling phosphino group. The free $-PPh_2$ function may substitute for one CO on a second $Ni(CO)_4$ molecule giving a binuclear species with no observed Ni-Ni bond. Subjecting to vacuum leads to removal of excess $Ni(CO)_4$ and free CO with subsequent condensation to a triangular Nickel array tricapped by TRIPOD. The complex is formulated as $Ni_3(CO)_6$TRIPOD and it is the only example of a Nickel(0) trimer. (Fig. 4.)

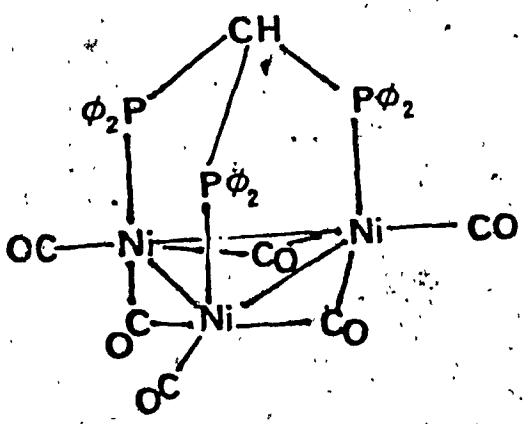

(Fig.4)

Alternatively, a triangular cluster may be capped by TRIPOD forming an analogue to the Nickel example above. The capping process occurs in a symmetrical fashion[7] but difficulties in product formation are encountered if the cluster initially exhibits structurally rigid axial-equatorial carbonyls only. Such cases exist for $Ru_3(CO)_{12}$ and

$Os_3(CO)_{12}$.

This observation has been made in a preliminary communication from Harding, Nicholls and Smith.[8] The product, $Ru_3(CO)_9$TRIPOD is formed by reaction of equimolar quantities of $Ru_3(CO)_{12}$ and TRIPOD. It is believed to have the structure given in Fig. 5.

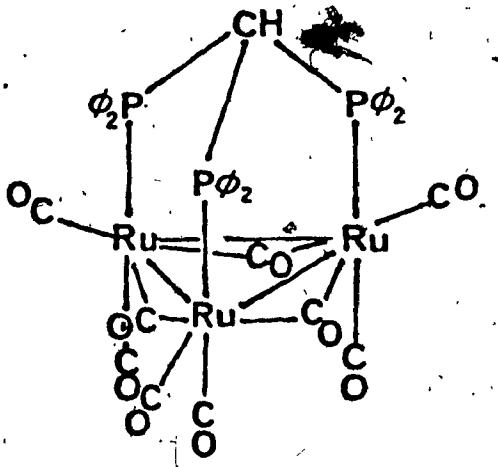

(Fig.5)

Under vigorous conditions, clusters may also be destroyed in the presence of excess ligand forming mononuclear metal complexes with bonding modes previously discussed.

Tetranuclear clusters exhibit promising reactivity to TRIPOD. Capping a triangular face proceeds more smoothly and completely since the carbonyl groups replaced are not so structurally rigid as are those in $Ru_3(CO)_{12}$ (ie:axial or equatorial).[3] The capping occurs preferentially on the triangular face whose edges support bridging carbonyls. Many examples of this type of complex formation have al-

ready been investigated.[3,7] In particular, a capped product, $Co_4(CO)_9$TRIPOD has been prepared by the action of TRIPOD upon $Co_4(CO)_{12}$. Mild reflux in toluene affords almost quantitative conversion to the π-toluene complex.[3] (Fig. 6)

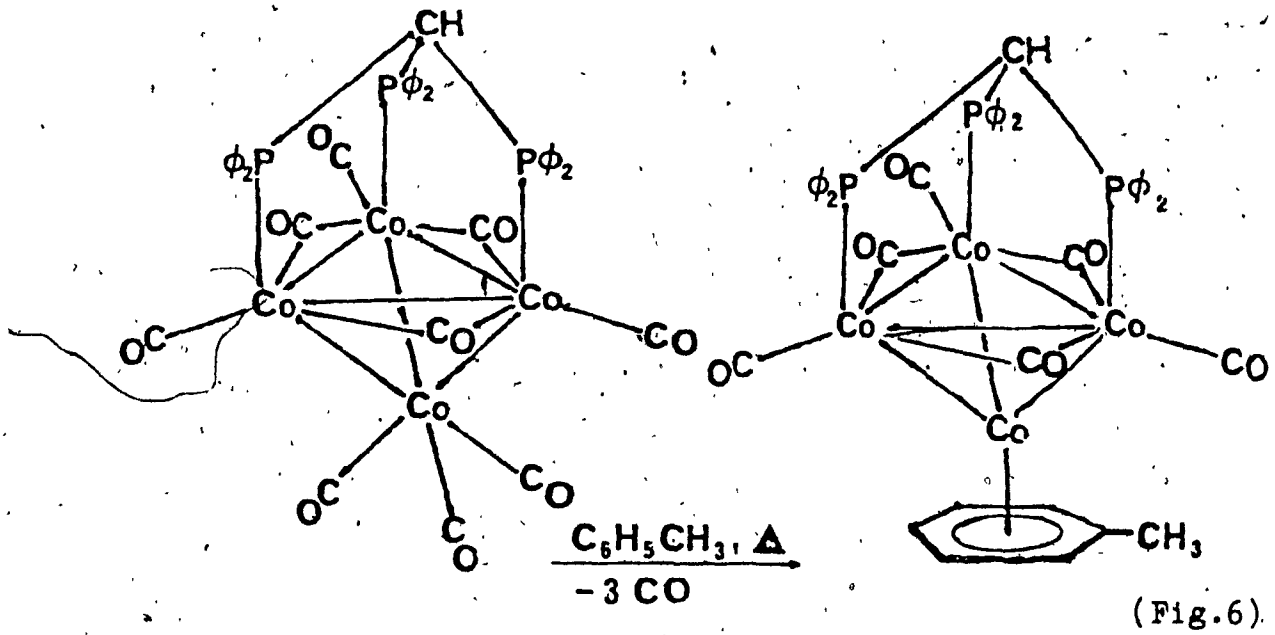

(Fig.6)

The Osborn group[1] has been most active in preparing and characterizing TRIPOD complexes with close collaboration in the structural part of this work byour own group (Bird et al.). A list of tetranuclear species can be found in Table 1. Very lately, the crystal structure of $Ir_4(CO)_9$TRIPOD was reported showing an all-terminal carbonyl framework.[9] This is the only known tetranuclear carbonyl cluster containing phosphine ligands which exhibits the all-terminal carbonyl structure except for the hydride complex $H_4Ru_4(CO)_9[HC(PPh_2)_3]$.[10] All other metal carbonyl clusters posessing the all-terminal carbonyl ar-

rangement form bridging carbonyls upon phosphine substitution.[3,7]

TABLE 1.[3]

Some tetranuclear clusters containing TRIPOD.

METAL CARBONYL	LIGAND	PRODUCT	COLOR
$Co_4(CO)_{12}$	$HC(PPh_2)_3$	$Co_4(CO)_9HC(PPh_2)_3$	green
$Rh_4(CO)_{12}$	"	$Rh_4(CO)_9HC(PPh_2)_3$	purple-red
$Ir_4(CO)_{12}$	"	$Ir_4(CO)_9HC(PPh_2)_3$	yellow
$Co_2Rh_2(CO)_{12}$	"	$Co_2Rh_2(CO)_9$ "	dark-purple
$HFeCo_3(CO)_{12}$	"	$HFeCo_3(CO)_9$ "	dark-violet
$H_4Ru_4(CO)_{12}$	"	$H_4Ru_4(CO)_9$ "	deep red

Interestingly, a third type of bonding mode is possible with binuclear complexes. This mode makes use of the two modes available to monometallic complexes. One metal in the complex is chelated by two phosphino functions while the third phosphino function coordinates to the second metal centre. The first example of this class of complex was prepared by the Osborn group and crystallographically characterized by Bird et al.[4]

This novel complex was formed by reacting equimolar quantities of $Fe(CO)_3$TRIPOD and $[RhCl(CO)_2]_2$ in THF. The product consists of a heterobimetallic cation supported by the TRIPOD ligand in which Fe remains chelated and Rh is coordinated by the dangling phosphino function.

The counteranion is cis-dichlorodicarbonyl Rh(1). Schematic representation of the structure is shown in Fig.7.

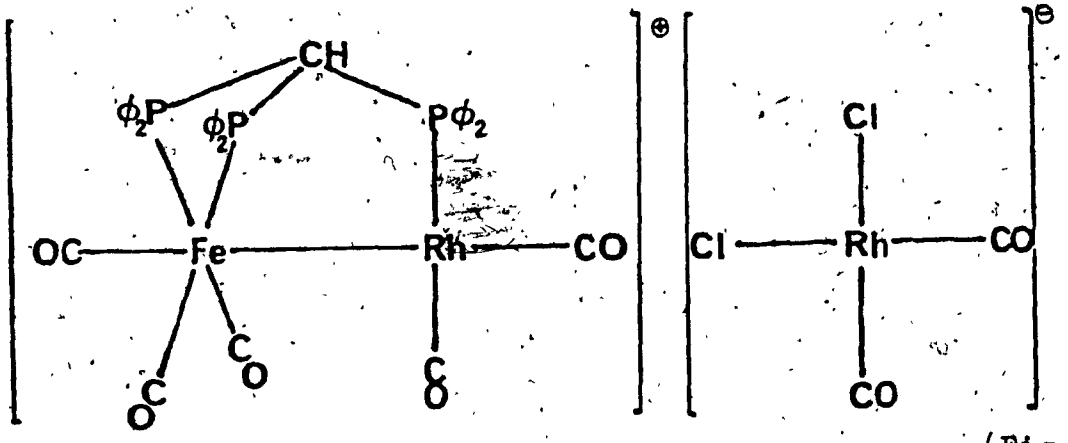

(Fig.7)

1.2. DESCRIPTION OF WORK DONE

The complex $[(CO)_2Rh\{HC(PPh_2)_3\}Fe(CO)_4]^+ [RhCl_2(CO)_2]^-$ (Fig.7)[4] was inspirational for the first part of this investigation. The preparation of this complex was performed to supply the starting material for conversion of the complex to one with a non-catalytically active anion. The anion $[cis\text{-}RhCl_2(CO)_2]^-$ is well known in homogeneous catalysis as a hydroformylation catalyst. Hence, any investigation of the cation in terms of catalytic activity would necessitate the replacement of the anion for one which is inert.

Repeated attempts to replace the Rhodium anion by large, inert anions such as BF_4^-, PF_6^- and triflate were unsuccessful. It has since been revealed in a personal

communication from the Osborn group that the carbonyl dimer should first be converted to a salt using AgX in which X includes the anions used above.

At this point it was decided that preparation of other complexes of the same general type could shed more light upon the synthetic limitations the formation of polymetallics supported by TRIPOD. Some monometallic complexes were prepared and reacted with Chlorodicarbonyl Rhodium (1) dimer, however, the chemistry was generally not clean, giving rise to either a large number of products or decomposition of the starting materials. The complex, $[HC(PPh_2)_3]Mo(CO)_4$ was prepared and characterized by ^{31}P NMR and X-ray crystallography (vide-infra). The Tungsten analogue was prepared in such low yield, probably owing to the thermodynamic stability of $W(CO)_6$, that further investigation of this complex was not undertaken. A crystal structure of $MoCl(\pi\text{-allyl})(CO)_2[HC(PPh_2)_3]$ was also undertaken so as to complement the structure of the tetracarbonyl analogue.

A second part of this investigation was to attempt to cap two triangular faces of a tetrahedral metal carbonyl cluster with TRIPOD. Insight into the syntheses of the aforementioned target molecule was obtained from a review by Chini and Heaton in "Topics in Current Chemistry"[11] wherein the reactions in equations (1) and (2) were given.[12,13]

$$2[RhCl(CO)_2]_2 + 3Co_2(CO)_8 \rightarrow 2Rh_2Co_2(CO)_{12} + 2CoCl_2 + 8CO \quad (1)$$

$$2[RhCl(PF_3)_2]_2 + 3Co_2(CO)_8 \rightarrow 2Rh_2Co_2(CO)_8(PF_3)_4 + 2CoCl_2 + 8CO \quad (2)$$

If reaction (2) was possible, then perhaps the following reaction is feasible:

$$2[RhCl\{HC(PPh_2)_3\}]_2 + 3Co_2(CO)_8 \rightarrow 2Rh_2Co_2(CO)_6[HC(PPh_2)_3]_2 \quad (3)$$

It was reasoned that to prepare a tetranuclear cluster supported by two TRIPOD ligands the Rhodium dimer in equation (3) must be prepared by reaction (4). Subsequent reaction of this product with $Co_2(CO)_8$ as given by reaction (3) ought to lead to a duly TRIPOD-capped product (assuming the reaction proceeded along the same line as reaction (2).

$$[RhCl(CO)_2]_2 + 2HC(PPh_2)_3 \rightarrow [RhCl\{HC(PPh_2)_3\}]_2 + 4CO \quad (4)$$

In fact, reaction (4) leads to a complex which was not completely characterized. Details of the preparation and attempts to spectroscopically analyze the product are given in Section 3.2.3. Reaction of this compound with $Co_2(CO)_8$ yields a singly-capped $RhCo_3$ tetrahedral nonacarbonyl derivative in which preparative and spectral details are given in Section 3.2.4. An x-ray crystal structure analysis of the unexpected product is given

in Section 5.3.1.

The final type of reaction to be attempted was to bridge a preformed binuclear complex with TRIPOD. Although much time was lost attempting to bridge the heterobinuclear complex $Cp(CO)Fe(\mu\text{-}CO)_2Co(CO)_3$, [14, 15] it was decided that the complex $Co_2(CO)_8$ would be a good candidate since the electron count for the anticipated product (Fig. 8) was favorable with regard to the eighteen-electron configuration. Crystallographic details pertaining to the attempted structure solution are given in Chapter 5.

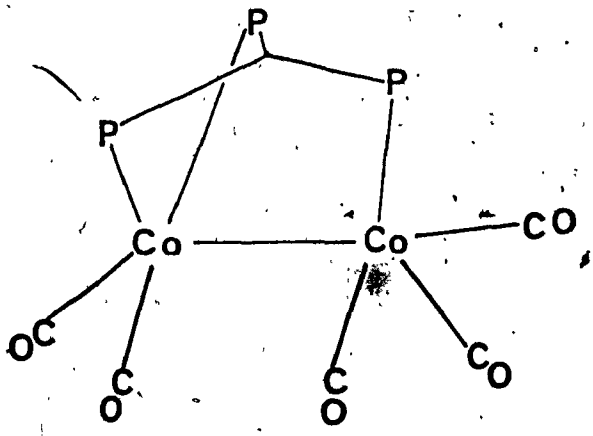

(Fig.9)

While no catalytic testing of the products synthesized in the course of this work has been done, the products may serve either to inspire further preparative work in this area and/or to provide the catalytic chemist with some new complexes to evaluate.

2. INTRODUCTION TO PREPARATIVE TECHNIQUES

Work with metal carbonyls, phosphine ligands and organometallics in general requires reaction conditions which are essentially oxygen-free. The methods utilized to keep reactions oxygen-free in the course of the following experiments will be briefly explained.

There are many ways in which anaerobic conditions may be obtained.[16] Some less-effective methods are encountered in undergraduate transition-element chemistry courses.[17]

In most cases, these methods provide adequate conditions for experiments which have been tried and tested on numerous occasions. However, in dealing with previously untried reactions, to ensure maximum product formation and minimum side-reactions, more rigorous precautions should be employed. For reasons of versatility and convenience the Schlenk technique is the obvious choice of most preparative organometallic chemists. The technique makes use of a double-manifold vacuum/nitrogen line (Fig. 2.1a) with which a vessel referred to as a Schlenk-tube (Fig. 2.1b) is employed. This vessel is used for reactions and solution transferral. Transferral and/or filtration may be accomplished oxygen-free by use of rubber septa and double-tipped flexi-needles (Fig. 2.1c). Reactions may be carried out under atmospheric pressure by connecting the reaction flask to a Mercury bubbler or under approximately 7 p.s.i. of N_2 (Fig.2.1d). Solvents may be rigorously deoxygenated by exposure to alternate cycles of vacuum/dinitrogen

(Fig. 2.1e). More complete degassification of solvents is achieved by simultaneous ultrasonication and evacuation. Filtration of solvents through highly activated silica gel may serve to remove traces of moisture and in the same fashion solutions may be filtered through Celite filter-aid (Fig. 2.1f).

This technique affords the preparative chemist the convenience of working in the open with the benefit that no compound or solution need be exposed to the external atmosphere. The possibility of poisoning through skin con-

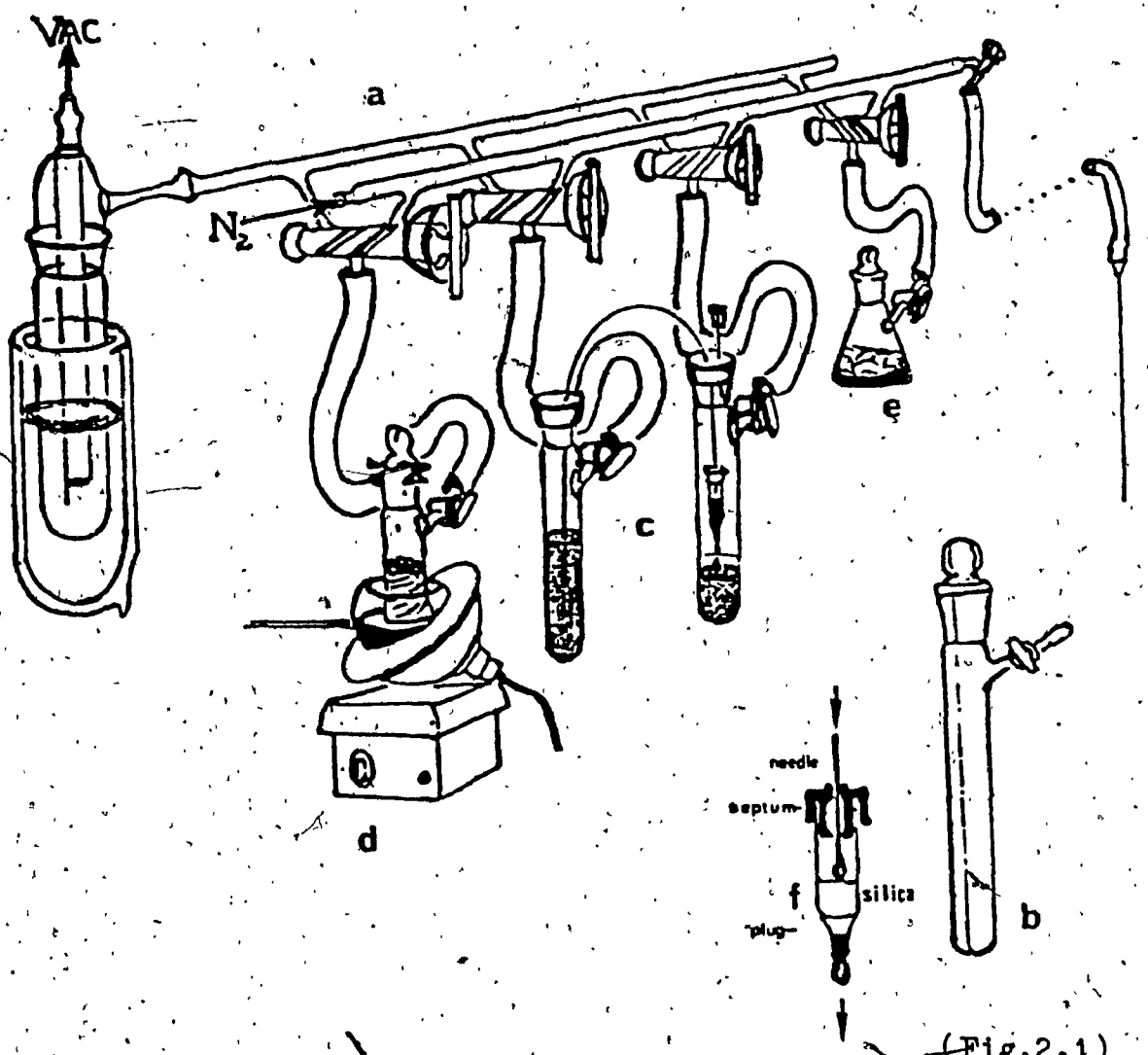

(Fig.2.1)

3. PREPARATIVE

3.1. GENERAL

All reactions were carried out using standard Schlenk techniques. All materials and solvents were reagentgrade. Solvents were rigorously deoxygenated by multiple alternate exposure to vacuum/dinitrogen unless otherwise specified. All ^{31}P NMR spectra were recorded on a Bruker WP-80 FT-NMR spectrometer at 30°C. Samples were dissolved in CD_2Cl_2 (MSD Isotopes) for deuterium lock. 10 mm. Wilmad NMR sample tubes were employed. All sample manipulations were performed using an adapted Schlenk technique under an atmosphere of dinitrogen. Samples were filtered through Celite filter-aid directly into dinitrogen-purged sample tubes and sealed. Infrared spectra of the carbonyl region were obtained on a Perkin-Elmer 599B grating infrared spectrophotometer using solution-injectable infrared cells with NaCl windows and dichloromethane as solvent.

3.2. EXPERIMENTAL

3.2.1. PREPARATION OF $HC(PPh_2)_3Mo(CO)_4$

$Mo(CO)_6$ (.465 g.- 1.76 mmol.) and 1.0 g (1.76 mmol.) $HC(PPh_2)_3$ were dissolved in 20 ml. 1,2-dimethoxyethane and refluxed 24 hrs. under N_2 while being magnetically stirred. The solution turned pale yellow within the first hour of

reflux. (Refer to Fig. 2.1d of Chapter 2 for preparative setup). The solvent was removed from the resulting solution in-vacuo and redissolved in a minimum of dichloromethane. Cyclohexane was added until turbid and the mixture was refrigerated overnight. A white solid composed of unreacted starting material crystallized out and the yellow product solution was filtered from the solid and hexanes were added to further precipitate out any unreacted starting reagents. The solvent was stripped from the remaining solution yielding 0.85 g. $HC(PPh_2)_3Mo(CO)_4$ (1.09 mmol). (62% based on Mo.)

Crystallographically suitable crystals were grown from a saturated acetone solution of the product by evaporation.

The $^{31}P\{^1H\}$ NMR spectrum of the product revealed a doublet centred at 130.1 ppm and a triplet centred at 85.1 ppm relative to trimethylphosphite (J_{P-P} = 23.222 Hz.) with relative intensities being 2:1, respectively. Comparison of the spectrum with those of $HC(PPh_2)_3Fe(CO)_3$ and $HC(PPh_2)_3Fe(CO)_4$ indicated the product to be chelated by two of the three phosphino functions of TRIPOD. (Fig. 3.2.1.1. -next page). Elemental analyses yielded the following results:

Calculated; C(63.32%), H(3.99%), P(11.97%), Mo(12.36%).

Analyzed; C(60.24%), H(3.96%), P(11.06%), Mo(13.88%).

Fig. 3.2.1.1. Comparison of ^{31}P NMR spectra of product with Iron analogues. Scales are in ppm relative to TMP.

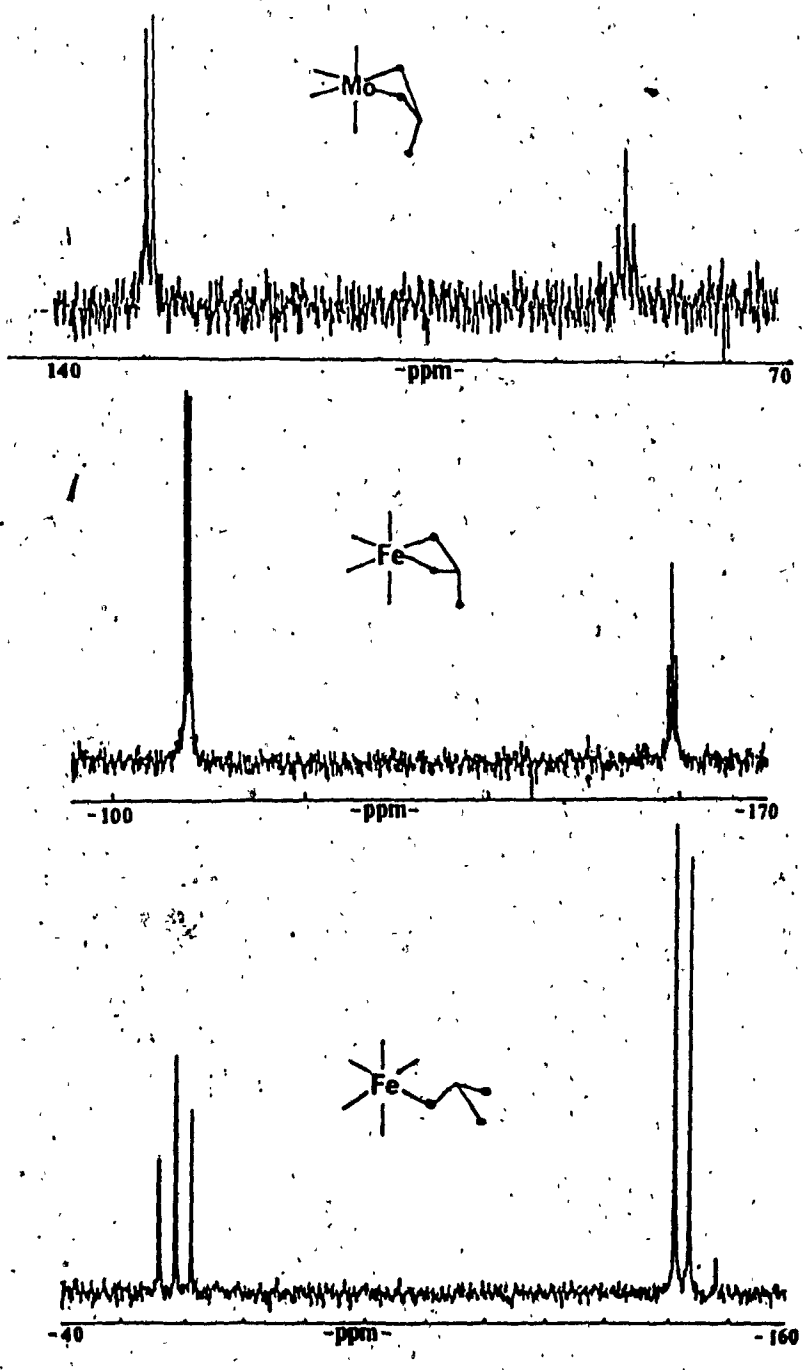

3.2.2. PREPARATION OF $[RhCl\{HC(PPh_2)_3\}]_2$

$[RhCl(CO)_2]_2$ 0.35 g.(.088mmol.) and 1.00g. (1.76 mmol.) $HC(PPh_2)_3$ were deposited as solids into a clean Schlenk vessel. Twenty ml. of wet, non-degassed reagent grade THF was quickly added to the solid mixture with magnetic stirring. The vessel was quickly stoppered and a vigorous evolution of gas ensued-presumably CO, and hence to drive the reaction, the vessel was evacuated. A hot air gun was used to warm the reaction mixture and the vessel was intermittently evacuated to remove any more evolved gases. The process was stopped when the solution no longer evolved gas bubbles. A solid product began to precipitate out of solution almost immediately after the addition of the THF.

The product is poorly soluble in THF, methanol, and dichloromethane but somewhat more soluble in chloroform. This was convenient for the washing step since the starting materials are very soluble in THF and dichloromethane. Yield is 88% (1.61 mmol.) tentatively based on the assumed formulation. Elemental analysis yielded the results:

Calculated; C(62.84%), H(4.39%), P(12.58%), Cl(5.10%), Rh(14.58%)

Analyzed; C(61.58%), H(4.65%), P(12.58%), Cl(4.67%), Rh(13.70%)

The infrared spectrum showed no carbonyl bands in the region from 2500 to 1500 cm.-1. $^{31}P\{^1H\}$ NMR spectra were very difficult to interpret on an 80 MHz spectrometer.

What was interpretable was a quartet centred at 146.3 ppm relative to trimethyl phosphite, (J_{P-P} = 452 Hz.; J_{Rh-P} = 129 Hz.) and what seemed to be a very scrambled triplet in which the centre was not accurately defined. The quarted:triplet intensity was approximately 2:1. The spectrum is shown in Fig. 3.2.2.1.

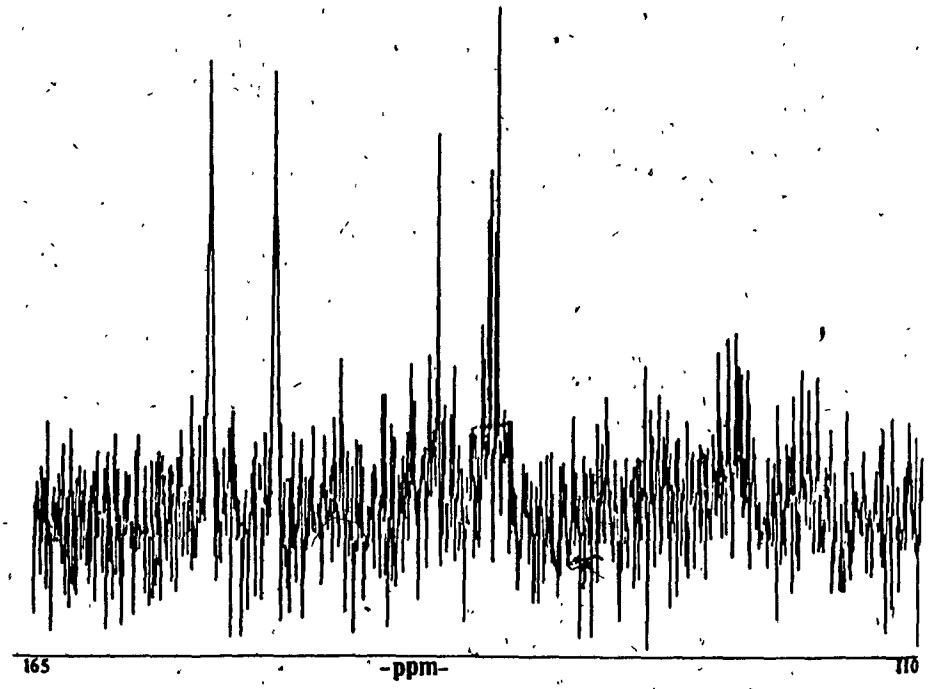

Fig. 3.2.2.1. ^{31}P NMR spectrum of Rhodium-TRIPOD complex.

This evidence would support the basic structural deduction (Fig. 3.2.2.2.) that each Rhodium is chelated by two phosphino groups with the third phophino group uncoordinated.

The possibility exists that the product is polymeric in nature. This point is discussed in Chapter 6.

Suitable crystals for single-crystal x-ray structure analysis were not successfully grown. Techniques to induce crystallization included 1) refrigeration from a cold,

saturated solution; 2) elevated temperature growth in an evacuated, sealed vessel; 3) vapor diffusion in chloroform/heptane.

The third method yielded large blocks which lost solvent upon drying and formed rosettes (multiply-twinned aggregates).

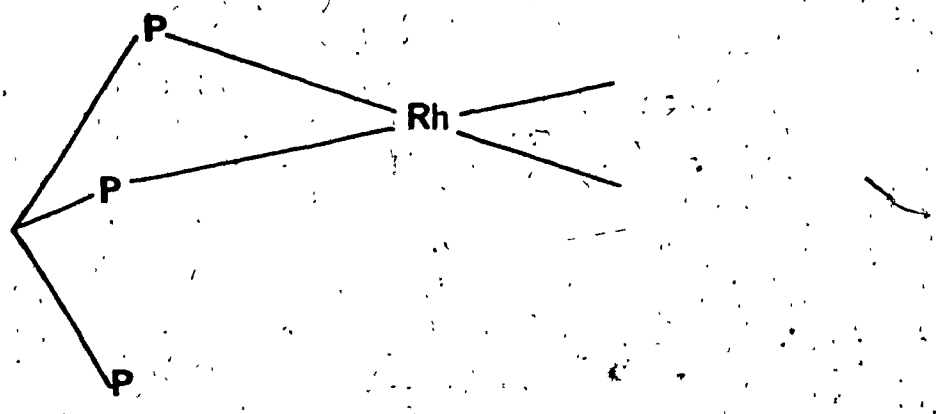

Fig. 3.2.2.2. Proposed coordination sphere for Rhodium.

3.2.3. PREPARATION OF $RhCo_3(CO)_9HC(PPh_2)_3$

$[RhCl\{HC(PPh_2)_3\}]_2$ (0.5 g. ; 0.035 mmol.) and 0.5 g. (0.146 mmol.) $Co_2(CO)_8$ were each dissolved in $CHCl_3$ while being magnetically stirred. A $Co_2(CO)_8$ solution was added to the $[RhCl\{HC(PPh_2)_3\}]_2$ solution rapidly through a double ended syringe needle under 7 p.s.i. dinitrogen at 25°C. Gentle gas evolution was observed for about a half hour. The temperature was raised to 60°C and the solution was

stirred for approximately 2 hours at which point the deep brown color of the $Co_2(CO)_8$, upon careful inspection, exhibited a purple tinge. Heating was stopped. The brown mother liquor was filtered off leaving a very dark purple microcrystalline solid which had caused the filter to clog.

This substance was found to be poorly soluble in chlorocarbon solvents and very poorly soluble in aromatics. The compound was completely insoluble in aliphatic hydrocarbons. It was, however, appreciably soluble in THF in which it was dissolved and filtered. The THF was stripped in-vacuo to dryness since it seemed to be causing decomposition: a green color was observed in solution towards the end of the filtration step. Yield 0.54g.; 70% based on Rh. Elemental analyses yielded the following results:

Calculated; C(50.18%), H(2.82%), P(8.45%), Co(16.10%), Rh(9.36%)

Analyzed; C(42.92%), H(3.03%), P(7.44%), Co(15.03%), Rh(8.76%)

The infrared spectrum of the carbonyl region showed terminal and bridging carbonyls. (Fig. 3.2.3.1.)

$^{31}P\{^1H\}$ NMR spectra were poor due to poor solubility and possible paramagnetic contamination. This was concluded from the extremely broad signal obtained in the NMR experiment.

The complex was dissolved in 1,2-dichloroethane and the solvent was removed until fine solid particles ap-

peared. Refrigeration afforded very fine multiply-twinned block-like crystals. These being too small for single crystal studies were redissolved in the same solvent and sealed under vacuum in a glass tube. The solution was held at 70°C. for several days yielding a crop of larger crystals which were, however, still twinned but not so severely. These crystals were large enough to observe the twin plane. The crystals cleaved easily along this line to yield samples suitable for single crystal analysis which was performed to overcome difficulties encountered in spectral characterization. (Ch. 5).

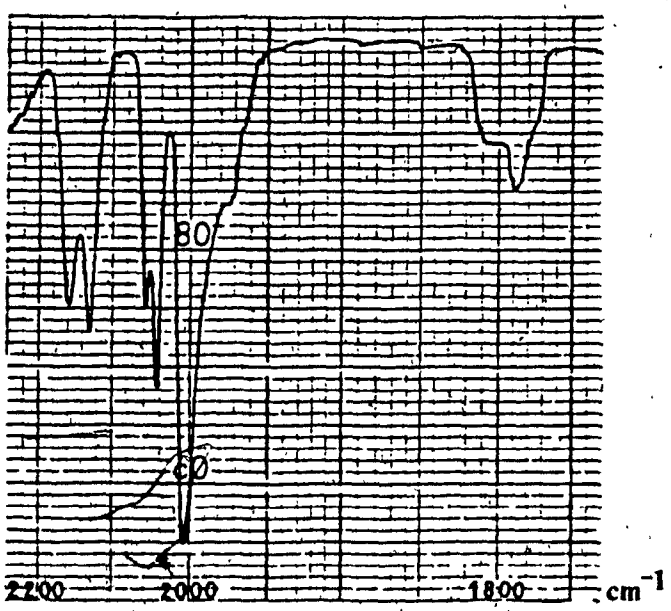

Fig. 3.2.3.1. Infrared spectrum of the carbonyl region.

3.2.4. REACTION OF $Co_2(CO)_8$ and $HC(PPh_2)_3$

$Co_2(CO)_8$ (0.5 g. - 1.46 mmol.) in 10 ml. CH_2Cl_2 was filtered through celite filter-aid directly into a vigor-

ously stirred solution of $HC(PPh_2)_3$ (0.9 g. - 1.58 mmol.) in 10 ml. CH_2Cl_2 at 20°C. under 2 p.s.i. of dinitrogen. Gentle evolution of CO was observed for approximately one hour. During this time the deep-brown colored solution underwent a color change to deep cherry red. This solution exhibited an opacity within thirty minutes. Stirring was continued for fifteen hours (overnight) afterwhich stirring was discontinued allowing the product, a dark, red-orange, microcrystalline solid to settle. The mother liquor was decanted and the solid was washed with a 25 ml. aliquot of CH_2Cl_2 followed by two 25 ml. aliquots of pentane. Yield was 1.08 g.(1.32 mmol.); 90% based on Co assuming the product formulation $Co_2(CO)_5[HC(PPh_2)_3]$.

Elemental analysis yielded the following results:

Calculated; C(60.94%), H(3.75%), P(11.24%), Co(14.27%)

Analyzed; C(58.58%), H(3.63%), P(10.76%), Co(12.96%)

The infrared spectrum showed several types of carbonyl absorption. (Fig. 3.2.4.1.)

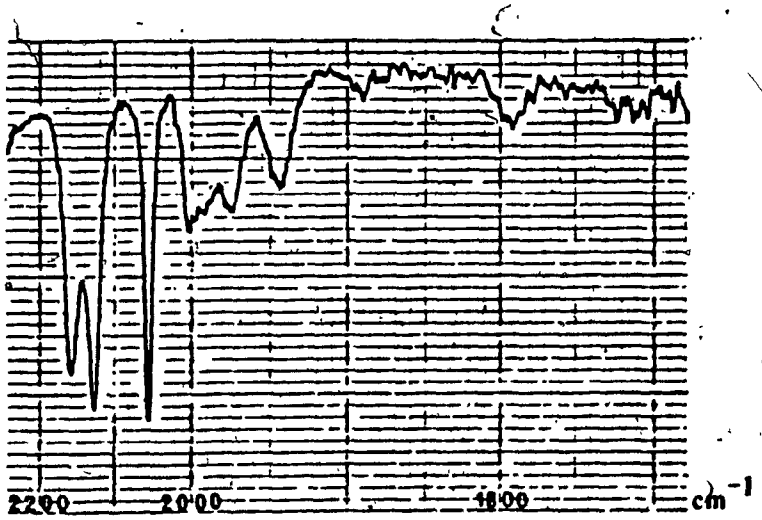

Fig. 3.2.4.1. Infrared spectrum of the carbonyl region.

The low resolution ^{31}P NMR spectrum exhibits what appears to be a triplet:doublet pattern in which J_{P_P} is not well resolved but has been estimated to be 6.19 Hz. The triplet is centred at -80.12 ppm and the doublet is centred at -153.88ppm relative to trimethyl phosphite.

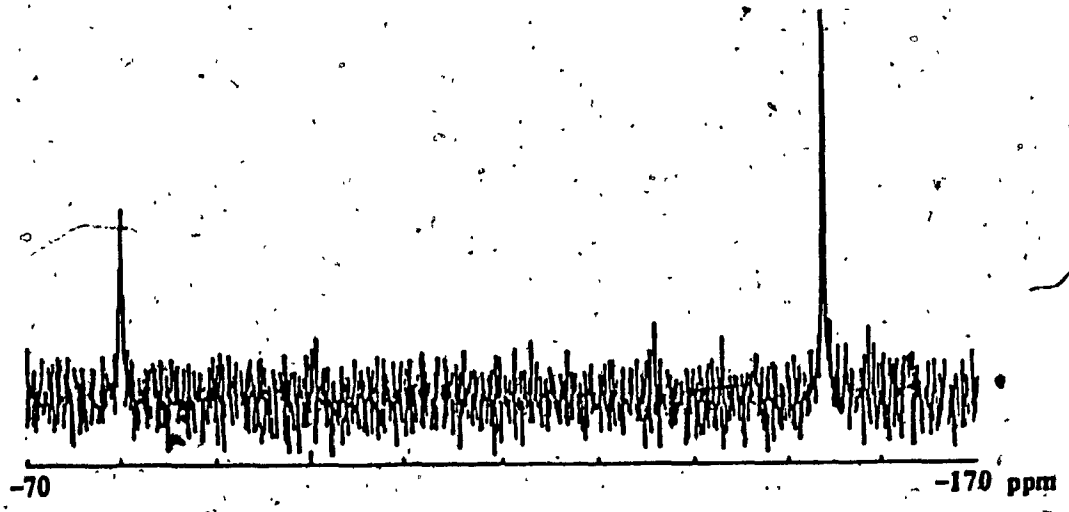

Fig. 3.2.4.2. ^{31}P NMR spectrum of the product from reaction between $Co_2(CO)_8$ and $HC(PPh_2)_3$.

Comparison of this spectrum with those on page 16 would indicate the ligand to be singly-coordinated to the Cobalt, however, this is unlikely due to the apparent non-existence of bridging carbonyls in the infrared spectrum.

Crystallographically suitable crystals were grown from a saturated chloroform solution under N_2 at 25° C.

4.CRYSTALLOGRAPHIC

4.1.INTRODUCTION

The process of crystal structure determination is one which relates the diffracted intensities from scattering centres inside the crystal to the spatial electron density of the basic three-dimensional repeat unit of the crystal, the unit cell. The method incorporates x-rays as a source for the diffracted radiation while the crystal acts as a three-dimensional diffraction grating. The diffraction pattern obtained contains all the information necessary to characterize the spatial geometric arrangement of the atoms or molecules contained in the crystal. This phenomenon occurs since the wavelength of x-radiation is of the order of interatomic distances. The radiation interacts with electrons surrounding the nuclei. The net effect is that diffraction of x-rays by a three-dimensional crystal lattice gives rise to constructive and destructive interference so as to produce a three-dimensional periodic interferogram more commonly referred to as the reciprocal lattice.

The intensities of the diffracted rays may be recorded in a spatial reference corresponding to the indices of the reciprocal lattice (h,k,l). The significance of these indices will be elaborated on in the appropriate section of the text. The information obtained by the collection of these intensities is the observed structure factor for the

unit cell. These intensities, summed over all reciprocal space, hkl, are represented by a Fourier series. The Fourier transform of the series is the electron density of the basic three dimensional repeat unit - again the unit cell. This represents a gross over-simplification of the central problem in crystallography. For the sake of development, however, the problem will be deferred to the appropriate section of the text. (4.2.4.).

Refinement of the experimentally obtained electron density by a combination of least squares and Fourier methods causes the construction to converge quite accurately to the interatomic distances and angles between bonded and non-bonded atoms Hence the molecular geometry may be very precisely determined. The degree of accuracy depends upon how closely an observed structure matches that of a theoretically calculated model.

The next two sections will deal with the main theoretical aspects of single-crystal x-ray analysis. The following one will deal with the practical aspects of collecting geometric and intensity data and the subsequent processing of the information to determine crystal structures.

4.2.THEORETICAL

4.2.1.THE RECIPROCAL LATTICE [18-26]

The concept of the reciprocal lattice is one which is of primary importance in the understanding of the collection of x-ray diffraction data.

From a one-dimensional periodic array of scattering centres the phenomenon of x-ray diffraction can be developed. Suppose the array is a row of equispaced atoms with interatomic spacing a and that an x-ray wavefront defined by AC impinges upon the row at some angle ψ_0. This is demonstrated in Fig. 4.2.1.1.

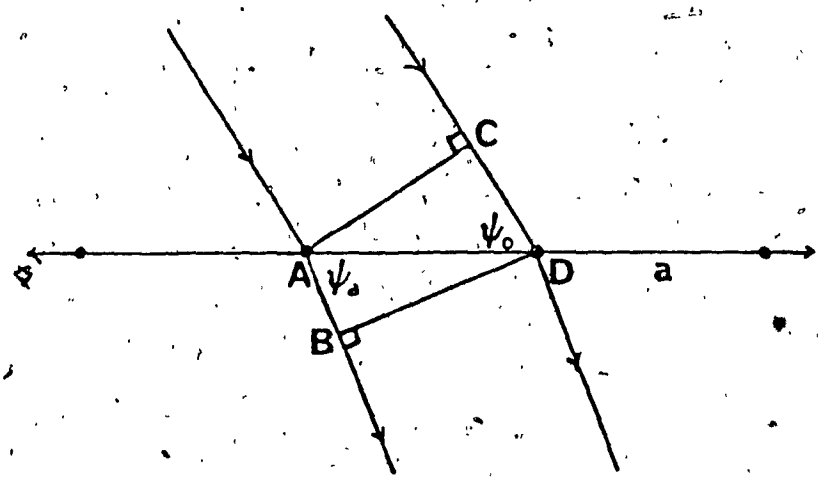

Fig.4.2.1.1.

The resultant wavefront DB leaves the row at some angle ψ_a. Then line segment CD is defined in physical terms as $a\cos\psi_0$, and line segment AB is defined by term $a\cos\psi_a$. The difference in length of the two line segments is an integral number of wavelengths $n\lambda$. The analytical

expression being

$$a\,(\cos\psi_0 - \cos\psi_a) = h\lambda \qquad (4.2.1.1.)$$

Actually, this represents the generating surface of a diffracted cone coaxial with the array. Generally there exists a family of cones for which h takes on values of 0,1,2,...,n. The value of h is referred to the order of the diffracted cone.

Progression to the two-dimensional array yields two conditions. That of equation 4.2.1.1. and the following.

$$b\,(\cos\psi_0 - \cos\psi_b) = k\lambda \qquad (4.2.1.2.)$$

in which the array with interatomic spacing b also generates a family of cones in which equation 4.2.1.2. represents the conical surfaces. The intersection of cones coaxial to the a and b arrays are depicted in Fig. 4.2.1.2.

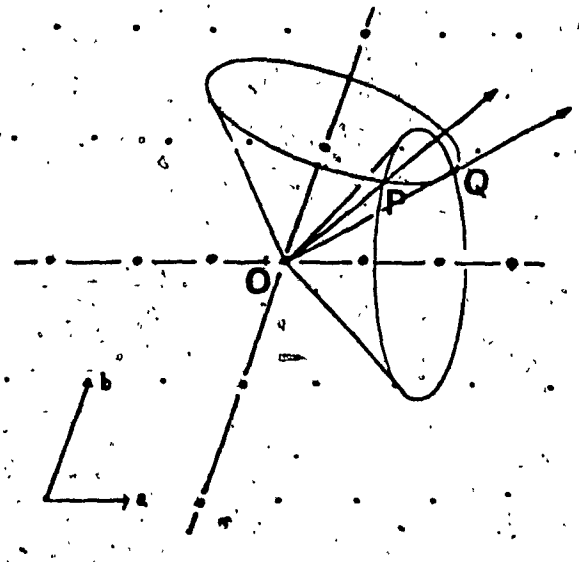

Fig.4.2.1.2.

These intersections are possible directions of a diffracted beam. Therefore, regarding a particular direction of the incident beam, diffracted rays are discretely produced depending on the angle the incident beam makes with the two-dimensional array.

Hence, in the two-dimensional case, only when both equations, 4.2.1.1. and 4.2.1.2. are satisfied is the diffraction phenomenon observed since all other points in space correspond to regions in which destructive interference occurs. The significant point is that the scattering in directions OP and OQ are in-phase.

In the three-dimensional case, three non-coplanar arrays h,k and l of atoms with interatomic spacings a,b and c, respectively, intersect. The c-array gives rise to a third condition

$$c\,(\cos\psi_0 - \cos\psi_c) = l\lambda \qquad (4.2.1.3.)$$

which defines the generating surfaces of a third family of cones coaxial with the c-direction. Here, the three cones may simultaneously intersect only in one line and hence this point satisfies the condition that all three equations are satisfied or are scattering in-phase. The situation is shown in Fig. 4.2.1.3.

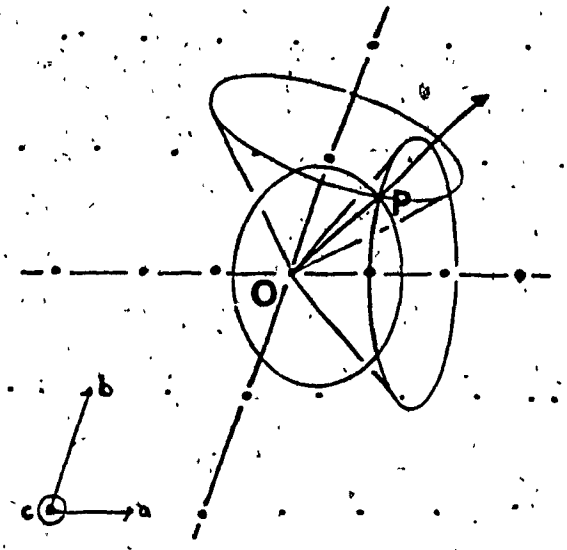

Fig.4.2.1.3.

Equations 4.2.1.1., 4.2.1.2. and 4.2.1.3. are referred to as the Laue conditions[24] from which the reciprocal lattice concept is evolved.

W.L.Bragg[25] published an account in which diffraction of x-rays by crystals could be treated by analogy with reflections by planes running through the lattice. The planes are defined by their indices, hkl. (Fig. 4.2.1.4.)

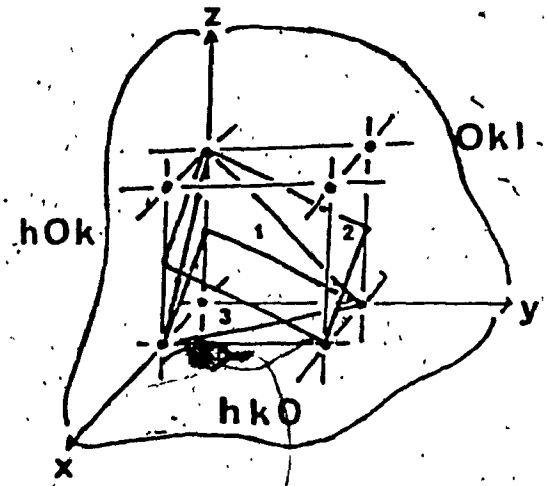

primitive cubic lattice

Fig.4.2.1.4.

In a three-dimensionally periodic repeating structure, many planes are found at varying angles and directions with respect to the coordinate system. In the figure above, the three axial planes defining the unit cell are: the hkO or xy-plane, the hOl or xz-plane and the Okl or yz-plane.

Plane 1 in the diagram corresponds to indices hkl equal to 111. Plane 2 is defined by indices 221 and plane 3 by indices 112. Therefore by inspection the indices hkl represent the intercepts expressed in fractional coordinates on axes a, b and c, respectively. Multiples of the above indices are actually members of a stack of planes running parallel to the general plane hkl.

X-rays "reflected" from such stacks of planes are considered in diagram 4.2.1.5.

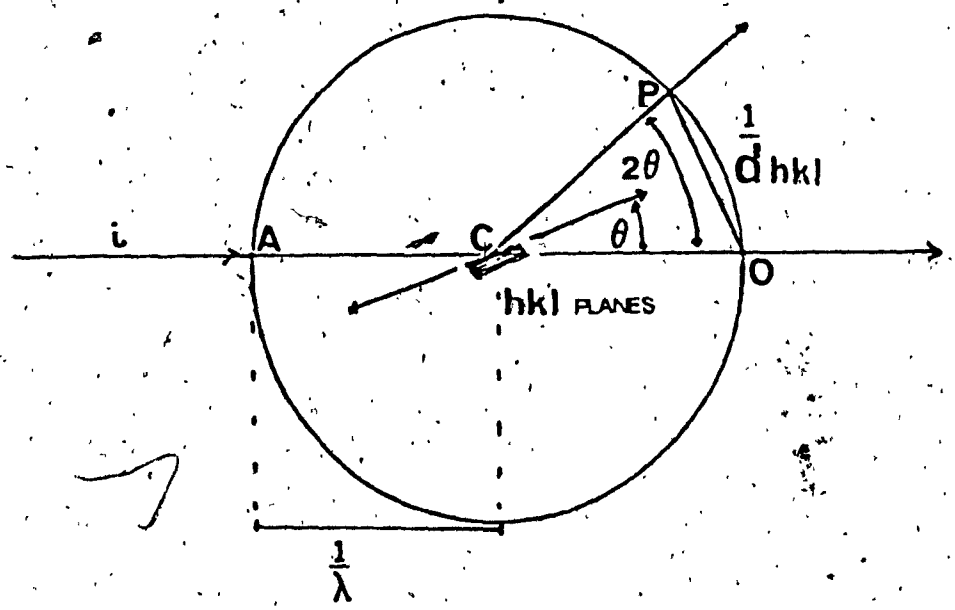

Fig.4.2.1.5.

Incident ray AC impinges on planes hkl at angle θ. Diffracted ray CP makes angle 2θ with the incident ray. If the interplanar spacing normal to the planes in the figure are equal to dhkl then diffracted ray CP defines the reciprocal lattice spacing $1/d_{hkl}$. This condition relates the wavelength λ, the diffraction angle θ and the interplanar spacing in what is known as Bragg's Law.

$$2/\lambda \sin\theta = n/d_{hkl} \quad \text{or} \quad n\lambda = 2d_{hkl} \sin\theta \qquad (4.2.1.4.)$$

Diffraction is observed when a reciprocal lattice point is brought into coincidence with the sphere surrounding the construction by varying the angle θ. This corresponds to an integral number of wavelengths in travelling path ACP. The sphere of radius $1/\lambda$ is referred to as the sphere of reflection or Ewald sphere.[27]

The reciprocal lattice is the three-dimensional construction of the reciprocal of the real or direct cell in which direct unit cell dimensions a, b and c correspond to reciprocal cell dimensions 1/a, 1/b and 1/c or a*, b* and c*, respectively. The reciprocal lattice, the extension of the reciprocal cell, moves in unison with the real cell and therefore any reflection may be observed once the orientation of the crystal is known. The information obtained by measuring the intensity I_{hkl} of the diffracted ray is related to the observed structure amplitude $|F_{hkl}|$.

The volume of the reciprocal unit cell for the most general case is given by

$$V^* = 1/V = a^*b^*c^*[\ 1 - \cos^2\alpha^* - \cos^2\beta^* - \cos^2\gamma^* + 2\cos\alpha^*\cos\beta^*\cos\gamma^*\ ]^{1/2} \quad (4.2.1.5.)$$

in which a*, b* and c* are reciprocal cell dimensions and α^*, β^* and γ^* are reciprocal cell interaxial angles. α^* is defined by the angle made by the intersection of reciprocal axes b* and c*. The two remaining angles are defined in the same manner.

4.2.2. THE STRUCTURE FACTOR [19,21,23,28]

As was mentioned earlier, the crystal acts as a three-dimensional grating transforming the actual crystal electron density in direct space into an interferogram in reciprocal space. This construction can be recorded as will be seen in the following section. Each point (h,k,l) in reciprocal space corresponds to the diffraction from a set of planes defined by the indices, n(h,k,l); n=1,2,3.. . By performing the inverse Fourier transform of the summation of (theoretically) all points it is possible to obtain the electron density distribution of the unit cell. To aid in the explanation of the structure factor it is desirable to consider the scattering due to a point atom. For a point atom, the scattering factor is defined as the quantity, f_{point}. The scattering factor of a real atom is a function

of the number of electrons Z, the angle the diffracted ray makes with the plane (h,k,l), the irradiating wavelength λ, and the thermal parameter B.[27,29]

The isotropic thermal parameter is given by

$$B = 8\pi^2 \overline{u^2} \qquad (4.2.2.1.)$$

where $\overline{u^2}$ is the mean squared amplitude of vibration. In view of equations 4.2.1.4. and 4.2.1.5. the isotropic thermal parameter is expressed in the experimental form as

$$\exp\left[-B/4\{(2\sin\theta_{hkl}/\lambda)^2\}\right] = \exp\left[-B/4\,(1/d_{hkl})^2\right] \qquad (4.2.2.2.)$$

in which

$$1/d_{hkl} = [\, h^2a^{*2} + k^2b^{*2} + l^2c^{*2} + 2hka^*b^*\cos\gamma^* + 2hla^*c^*\cos\beta^* + 2klb^*c^*\cos\alpha^* \,]^{1/2} \qquad (4.2.2.3.)$$

the scattering factor for a real atom in terms of a point atom can be expressed as follows, assuming Z equals 1.

$$f_{real} = f_{point}\exp[-B(\sin^2\theta)/\lambda^2] \qquad (4.2.2.4.)$$

On an absolute scale the average intensities may be expressed in terms of atomic scattering factors by the expression

$$\overline{I_{abs}} = f^2_{point} \exp[-2B(\sin^2\theta)/\lambda^2] = |F_{abs}|^2 \qquad (4.2.2.5.)$$

However, in terms of the indices (h,k,l), the right-hand side of equation 4.2.2.3. gives little practical information relating to the planes from which the diffracted rays originate. The general exponential form may be utilized to show the structure factor F_{abs} is related to the recoprocal lattice indices.

$$|F| = f_j \exp[i\delta_j] \qquad (4.2.2.6.)$$

and

$$|F_{hkl}| = f_j \exp[2\pi i(hx_j + ky_j + lz_j)] \qquad (4.2.2.7.)$$

where f_j is the scattering factor of the j^{th} atom and the total phase difference between the origin and a point defined by the reciprocal lattice point is $2\pi i(hx_j + ky_j + lz_j)$. Hence, from the Eulerian relationship, equation 4.2.2.5 can be expressed as a Fourier sine and cosine series.

$$|F_{hkl}| = \{[\, f_j \cos 2\pi(hx_j + ky_j + lz_j)]^2 + [\, f_j \sin 2\pi(hx_j + ky_j + lz_j)]^2\}^{1/2} \qquad (4.2.2.8.)$$

The equation 4.2.2.8. represents the magnitude of the structure factor. If the cosine and sine terms in the

square brackets are abbreviated by A_{hkl} and B_{hkl}, respectively, equation 4.2.2.9. results.

$$|F_{hkl}| = (A_{hkl}^2 + B_{hkl}^2)^{1/2} \; ; \; F_{hkl} = A_{hkl} + iB_{hkl} \qquad (4.2.2.9.)$$

and the phase angle ϕ_{hkl} is given by

$$\phi_{hkl} = \tan^{-1} (B_{hkl}/A_{hkl}) \qquad (4.2.2.10.)$$

4.2.3. THE ELECTRON DENSITY EQUATION [19,21,23,28]

The expression for the electron density in terms of the scattering amplitudes can be written in the vector form

$$\rho(r) = \int_v F(s) \exp[-2\pi i \, s \cdot r] \, dv \qquad (4.2.3.1.)$$

Considering that the function F(s) is discontinuous and is defined only at reciprocal lattice points, the discrete form of equation 4.2.3.1. is

$$\rho(r) = 1/V_c \sum_h \sum_k \sum_l |F_{hkl}| \exp[2\pi i \, s \cdot r] \qquad (4.2.3.2.)$$

where V_c is the unit cell volume and **r** and **s** are dimensional units in direct and reciprocal space, respectively. ie:

$$\mathbf{r} = \mathbf{xa} + \mathbf{yb} + \mathbf{zc} \qquad (4.2.3.3.)$$

and

$$\mathbf{s} = \mathbf{ha^*} + \mathbf{kb^*} + \mathbf{lc^*} \qquad (4.2.3.4.)$$

Coefficients x,y and z are fractional coordinates of the direct cell dimensions and h,k and l are reciprocal lattice indices. Hence, the last two equations can be implemented in a form of the electron density equation which relates the direct and reciprocal lattices by the discrete Fourier transformation.

$$\rho(xyz) = 1/V_c \sum \sum \sum |F_{hkl}| \exp[-2\pi i(hx + ky + lz)] \qquad (4.2.3.5.)$$

Consideration of section 4.2.2., specifically equations 4.2.2.6. and 4.2.2.7. allows us to write

$$A_{hkl} = |F_{hkl}| \cos \phi_{hkl} \qquad (4.2.3.6.)$$

and

$$B_{hkl} = |F_{hkl}| \sin \phi_{hkl} \qquad (4.2.3.7.)$$

therefore

$$F_{hkl} = |F_{hkl}| \exp(i \phi_{hkl}) \qquad (4.2.3.8.)$$

Expanding equation 4.2.3.5. results in the equation [28]

$$\rho(xyz) = 1/V_c \sum \sum \sum |F_{hkl}| \cos [2\pi(hx + ky + lz) - \phi_{hkl}] \qquad (4.2.3.9.)$$

where ϕ_{hkl} is the phase angle $|F_{hkl}|$ makes with the origin.

$|F_{hkl}|$ may be measured for any value (h,k,l), however, phase determination may not be accomplished directly from

experiment. Hence, the "phase problem" as it is referred to in the literature (ie: the problem determining the phases of the |F|'s) is the main difficulty associated with solving crystal structures.

4.2.4. STRUCTURE SOLUTION

Although many techniques are available to the crystallographer for solving the phase problem depending upon the type of structure under investigation, two techniques definitely predominate in the structural solution of molecular crystals. These are: 1) the Patterson synthesis and 2) statistical phasing.

4.2.5. PATTERSON SYNTHESIS

In section 4.2.3. the general form of the electron density equation was given as the inverse Fourier transform of the structure factor expression. However, in 1935, Patterson[29] published a paper in which was pointed out that instead of using the measured structure factor magnitudes as input to the electron density equation a quantity $|F_{hkl}|^2$ could be subject to the transformation giving rise to what is now referred to as the Patterson function. Just as a three-dimensional electron density map can be constructed by transforming the structure factor expression, a three-dimensional Patterson function can be obtained by transforming the square of the structure factor expression.

$$P(xyz) = 1/V_c \sum\sum\sum |F_{hkl}|^2 \exp[\ -2\pi i\ h\cdot r\ ] \qquad (4.2.5.1.)$$

From equations 4.2.3.6. and 4.2.3.7. it is apparent that the coefficients $|F_{hkl}|^2$ are real and phaseless quantities. The Patterson is thus expressed as a cosine series.

$$P(xyz) = 1/V_c \sum\sum\sum |F_{hkl}|^2 \cos 2\pi[\ hx + ky + lz\ ] \qquad (4.2.5.2.)$$

Regions of large P(xyz) calculated from such an expression are referred to as Patterson peaks and represent the interatomic vectors between all atoms or regions of electron density in the cell. In a cell containing N atoms there exists N^2 vectors in the Patterson cell. N vectors out of the N^2 will be of zero length and correspond to intraatomic vectors (ie:those from each atom N_i unto itself). These N vectors are concentrated at the origin of the Patterson cell and define the magnitude of the origin. The remaining N^2-N vectors will be distributed throughout the rest of the cell. The net result is that Patterson peaks are severely crowded into the cell volume. They are also broader than the electron density peaks. This is due to the diffuse nature of the $|F|^2$ coefficient and the continuous nature of the electron density in real space which follows from the fact that real atoms are not point scatterers. The relatively featureless Patterson cell, the product of

overlapping peaks, may be modified, however, by a two-step process called origin removal and sharpening. While treatments for these processes will not be described in this summary a good explanation can be found in the literature.[21,30]

The Patterson synthesis is in fact the vector space equivalent of the electron density in which the origin of the Patterson map translates as the origin of vector space for the corresponding electron density.[30]

Some properties of the Patterson function are:

1) All Patterson functions are centrosymmetric.

2) Their lattice-type is the same as that of the original space group (ie:P,C,F,I)

3) Their space group is determined by replacing all translational symmetry elements (screw axes and glide planes) by their non-translational equivalents (rotation axes and mirror planes) respectively,[20] and by adding an inversion centre if one is not already present.

Now that the Patterson function has been summarized its utility as a means for determining the phases for a structure is stated.

Providing a molecule contains a heavy atom the Patterson synthesis will yield a peak considerably greater in magnitude for the $|F_{heavy}|^2$ than peaks resulting from $|F_{heavy}||F_{light}|$ or $|F_{light}|^2$. Thus location of the heavy atom is determined by considering the differences between the equivalent positions[31] defining the space group. These

differences may be solved for x, y and z by comparison with the Patterson peak coordinates and verified by comparison with other Patterson vectors. This procedure will be detailed in the section on practical aspects of crystallography (4.3). Once the heavy atom is placed in position (x_o,y_o,z_o) in the unit cell, a structure factor calculation is performed with the heavy atom defined by type and number thus contained in the cell. Since the phases of the lighter atoms are essentially dominated by that of the heavy atom, the phases of a large number of F_{hkl}'s become fixed. Subsequently, the Fourier map may be calculated possibly revealing the positions of the lighter atoms relative to the heavy atom. By a combination of difference Fourier syntheses and least-squares refinements, the complete structure may be determined (vide-infra).

4.2.6. STATISTICAL PHASING [33,34]

This method of structure solution, falling under the more general heading of "direct methods", is used to determine the phases of a set of data strictly by mathematical methods.

To develope the topic, if we assume arbitrary ϕ_{hkl}'s for a real set of $|F_{hkl}|$ data and generate $\rho(xyz)$ from the electron density equation (4.2.3.9.), the resulting synthesis would probably yield a three-dimensional distribution of random density. This distribution may also contain re-

gions of negative density, a condition defying expectation for a real structure. Hence, a suitable criterion for increasing the probability of obtaining the correct set of phases for the $|F_{hkl}|$ data is to constrain the ϕ_{hkl}'s such that the computed $\rho(xyz) \geq 0$. This requirement is met by the Karle-Hauptman determinants.[35]

For direct method calculations it has been found useful to redefine the $|F_{hkl}|$'s in terms of normalized structure factors $|E_{hkl}|$. The normalized structure factor expression is related to $|F_{hkl}|$ by the expression

$$|E_{hkl}|^2 = \frac{K^2 |F_{ohkl}|^2}{\epsilon g_j^2} \qquad (4.2.6.1.)$$

K represents a scaling factor obtained by subjecting the $|F_{hkl}|$ data to Wilson statistics.[36] $|Fo_{hkl}|$ represents the experimentally determined structure factors and g_j is the thermally attenuated scattering factor. The ϵ term is an integer which accounts for special sets of reflections depending upon the space group symmetry.[37]

The reason for using E_{hkl}'s as opposed to other structure factor expressions is to allow normalization of all classes of reflections to a common basis which in turn simplifies probability calculations. Expression 4.2.6.1. also causes the diffraction data to more closely resemble that of a point-atom structure and therefore are less sensitive

to the fall-off of scattering power associated with wide-angle scattering.[33] This results in increased resolving power over conventional $|F_{hkl}|$ data. As the name implies, the normalized structure factor posesses the property that

$$\langle |E_{hkl}|^2 \rangle = 1 \qquad (4.2.6.2.)$$

High-power direct methods of structure solution rely heavily upon probabilistic techniques for the centrosymmetric case. Sayre[38] showed that under certain constraints, any F_{hkl} could be determined by the products of all structure factors whose indices add to give hkl. That is

$$F_{hkl} = C \sum\sum F_{h'k'l'} \cdot F_{h-h',k-k',l-l'} \qquad (4.2.6.3.)$$

or in abbreviated form

$$F(h) = C \sum\sum F(h') \cdot F(k) \qquad (4.2.6.4.)$$

Since the $|E_{hkl}|$'s are formulated from the $|Fo_{hkl}|$'s, the same may be said about the $|E|$'s.

One constraint increasing the probability that equation 4.2.6.4. be useful is that F(h) be large. When F(h) is large, the signs of the series of pairs of F(h') and F(k) tend to be strongly positive or negative.[37] When all three terms are very large the previous equation may be written as

$$S\ F(h) \cong S\ F(h') \cdot S\ F(k) \qquad (4.2.6.5.)$$

where S reads "the sign of" and $\cong$ reads "is probably equal to." The terminology S(h) can replace S F(h) and hence equation 4.2.6.5. can be written

$$S(h) \sim S(h') \cdot S(k) \qquad (4.2.6.6.)$$

or for a number of strong relationships

$$S(hkl) \cong S(h'k'l') \cdot S(h-h'k-k'l-l') \qquad (4.2.6.7.)$$

These expressions are referred to as triple-phase relations and belong to the more general set of expressions known as $\sum_2$-relationships.

In practice one tries to find as many triple-phase relations as possible. The development will be restricted to the primitive centrosymmetric space group for simplicity. For more difficult cases (ie., non-primitive, acentric, etc,) see references 33,34.

The first step is to determine the origin. In centrosymmetric space groups the origin must coincide with a centre of inversion. There are eight distinct inversion centres in a primitive, centric unit cell. These are defined by the positions: (0 0 0), (1/2 0 0), (0 1/2 0), 0 0 1/2), (1/2 1/2 0), (1/2 0 1/2), (0 1/2 1/2), and (1/2 1/2 1/2). In addition each reflection falls into one

of eight parity groups (eee, oee, eoe, eeo, ooe, oeo, eoo, and ooo). The way a reflections' phase changes with origin shifts is summarized in Table 4.2.6.1. By assigning phases arbitrarily to certain reflections the origin may be defined. For example, by choosing a phase for the 542 reflection (oee), the origin is defined as being either one of 1,3,4,7 or 2,5,6,8 and the phases of all other "oee" reflections become fixed relative to reflection 542. Fixing a phase for the 218 reflection (eoe) reduces the choice to one of origins 1,4 or 3,7 or 2,6 or 5,8. Now the relative phases of oee, eoe and ooe reflections are fixed. The third must be selected from one of the remaining groups (eeo, oeo, eoo and ooo, but not eee) to finally fix the position of the origin.

Table 4.2.6.1. Origin - Parity Group Relationships [21]

Origin	Shift	Reflection Parity							
		eee	oee	eoe	eeo	ooe	oeo	eoo	ooo
1 (0 0 0)	0	+	+	+	+	+	+	+	+
2 (1/2 0 0)	a/2	+	−	+	+	−	−	+	−
3 (0 1/2 0)	b/2	+	+	−	+	−	+	−	−
4 (0 0 1/2)	c/2	+	+	+	−	+	−	−	−
5 (1/2 1/2 0)	(a+b)/2	+	−	−	+	+	−	−	+
6 (1/2 0 1/2)	(a+c)/2	+	−	+	−	−	+	−	+
7 (0 1/2 1/2)	(b+c)/2	+	+	−	−	−	−	+	+
8 (1/2 1/2 1/2)	(a+b+c)/2	+	−	−	−	+	+	+	−

Once the initial origin-defining set is fixed it is necessary to generate phases of the remaining reflections by the triple-phase relations.

The following consideration applies to the general case and is not restricted to the primitive centric space groups. It is merely a short developement of the tangent formula.

For a limited vector summation involving r|E| values, equations 4.2.6.5. to 4.2.6.7. may be written in the "ϕ"-symbolism ie:

$$\phi_h \cong \langle \phi_k + \phi_{h-k} \rangle_r \qquad (4.2.6.8.)$$

This can be illustrated using an Argand diagram (Fig.4.2.6.1.) for values of κ .33

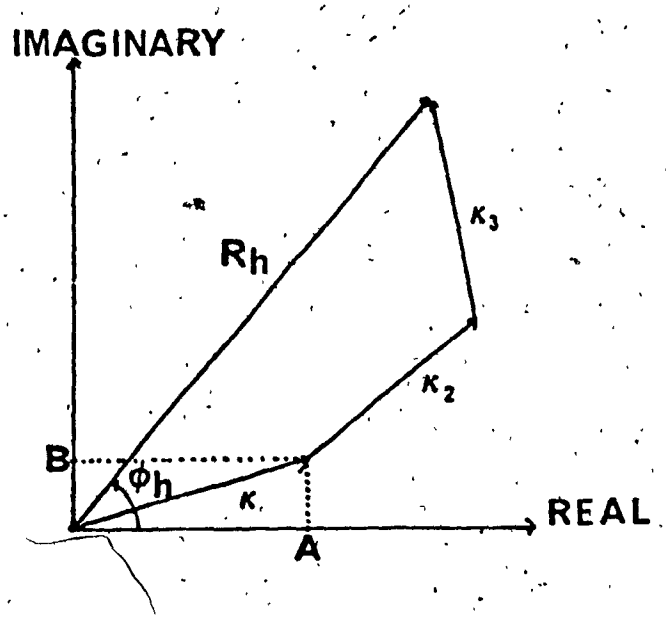

Fig.4.2.6.1.

ϕ_h is the estimated phase angle associated with vector R_h and each vector κ_r depends on the product $|E_k||E_{h-k}|$ which may be resolved into real and imaginary components A and B.

$$A_h = |E_k||E_{h-k}| \cos (\phi_k + \phi_{h-k}) \qquad (4.2.6.9.)$$

$$B_h = |E_k||E_{h-k}| \sin (\phi_k + \phi_{h-k}) \qquad (4.2.6.10.)$$

and

$$\tan \phi_h = \sum W_h B_h / \sum W_h A_h \qquad (4.2.6.11.)$$

This is the weighted tangent formula where W_h is a weighting factor equal to unity or other values which will be elaborated further on. Statistical phasing relies heavily upon equation 4.2.6.11. and the reliability of ϕ_h determined this way may be assessed according to a parameter α_h.

$$\alpha_h^2 = [K_{hk} \cos (\phi_k + \phi_{h-k})]^2 + [K_{hk} \sin (\phi_k + \phi_{h-k})]^2 \qquad (4.2.6.12.)$$

in which

$$K_{hk} = 2 \sigma_3 \sigma_2^{-3/2} |E_h||E_k||E_{h-k}| \qquad (4.2.6.13.)$$

and

$$\sigma_n = \sum Z_j^n \quad ; \quad Z_j = f_j / \sum_{j=1}^{N} f_j \qquad (4.2.6.14.)$$

Z_j is the atomic number of the j^{th} atom in a unit cell containing N atoms.

Relating back to the centrosymmetric case, the probability associated with the triple-phase relations based on large |E|'s is given by

$$P_+(h) = 1/2 \{ 1 + \tanh [\sigma_3 \cdot \sigma_2^{-3/2} |E_h||E_k||E_{h-k}|] \} \quad (4.2.6.15.) \quad 38$$

MULTAN[40]

The MULTAN program for phase determination is a multi solution method which statistically phases experimental intensity data according the following outline:

1) Normalized structure factors are selected from the E_{hkl} data which exhibit intensities greater than some minimum pre-defined intensity, E_{min}. The program then finds all triple-phase relationships with strong reflections such that E_{1s} E_{2s} E_{3s} are greater than a chosen value. Next, it finds some very weak reflections and the associated triples E_w E_{s1} E_{s2} for use in calculating one of the three reliability indices. (PSI-ZERO test - vide infra). It then finds triple-phase relationships among the stronger reflections for immediate phasing (ie: if k = h-k then phase h is positive-according to Sayre's equation).

2) Origin and enantiomorph definition and starting set choice. The starting set choice is obtained through convergence mapping in which a subroutine called CONVERGE is used to form an ordered list of the reflections from the first step. The phase of any reflection in the list can be

obtained from the phases of the reflections preceeding it. The strongest reflections from CONVERGE are used in the phase determination and only those phases for which $_h$ is greater than 5 are considered (eq.4.2.6.12.). The reflection with the poorest phase relation is eliminated with all associated triple phase relationships and a new value is calculated for α_h. This process is repeated and every cycle increases the value of α_h. The process is continued until the calculated value of α_h changes by no more than 2% or the origin can no longer be defined. If the latter is the case, then the last reflection is reinserted into the list and becomes one of the origin-defining reflections. Reflections whose phases cannot be defined by the previous reflections may be selected for the starting set.

The starting set includes:

a) M origin-fixing reflections assigned arbitrary phases on the basis of Table 4.2.6.1. ($m < 3$).

b) One enantiomorph-fixing reflection (if non-centrosymmetric) in which the phase is limited to the range from 0 to 180°.

c) If the structure is centrosymmetric, phases will be restricted to 0 or 180°.

d) N other reflections which cannot be phased by the other reflections from CONVERGE. If the structure is centrosymmetric the starting phases will be assigned all negative or positive combinations. If non-centrosymmetric, they are

assigned all combinations of 45°, 135°, 225°, and 315°. The choice of N is made either automatically or at the discretion of the investigator (usually < 4 for centrosymmetric and < 2 if non-centrosymmetric).

Phase reliability is assessed by eq. 4.2.6.15. for the centrosymmetric case whereas for the non-centrosymmetric case, eq. 4.2.6.12. is used.

At the start of the phase determination α_h cannot be calculated due to the unavailability of phase information. Hence an expectation value of α_h^2, α_e^2 is calculated with values of $_{hk}$:

$$\alpha_e^2 = \sum K_{hk}^2 + \sum \sum K_{hk} K_{hk'} \frac{I_1(K_{hk})\ I_1(K'_{hk})}{I_0(K_{hk})\ I_0(K'_{hk})} \qquad (4.2.6.16.)$$

where I_0 and I_1 are modified Bessel functions of order zero and one, respectively. These functions approximate the behavior of equation eq. 4.2.6.12. in eq. 4.2.6.16.

MULTAN utilizes a modified tangent formula to generate and refine the phases.

$$\tan \phi_h = \frac{Q_{hk} \sin(\phi_h + \phi_{h-k})}{Q_{hk} \cos(\phi_h + \phi_{h-k})} = \frac{B_h}{A_h} \qquad (4.2.6.17.)$$

where

$$Q_h = W_k\ W_{h-k}\ |E_k|\,|E_{h-k}|\,/(1 - |U_h|^2) \qquad (4.2.6.18.)$$

in which

$$W_h = W_k \, W_{h-k} = \tan \left[\sigma_3 \, \sigma_2^{3/2} \, |E_h| \, (A_h^2 + B_h^2)^{1/2} \right] \qquad (4.2.6.19.)$$

and U_h is the unitary structure factor[18,19] defined as

$$|U_{hkl}| = \frac{|F_{ohkl}|}{\exp[+B(\sin^2 \theta / \lambda^2] \sum_j F_{i(point)}} \qquad (4.2.6.20.)$$

In the centrosymmetric case, for N starting sets, 2^N solutions are generated.

The criteria for accepting a particular solution are:

1) The absolute figure of merit, ABS FOM,
2) PSI-ZERO,
3) RESID, and
4) the combined figure of merit, COMBINED FOM.

ABS FOM (Z) is a measure of the internal consistency among the triple-phase relations found in the E_{hkl} data. It is given by the equation

$$Z = \sum (\alpha_h - \alpha R_h) / \sum (\alpha_e - \alpha R_h) \qquad (4.2.6.20.)$$

where αR_h is the α-value expected from a random phase set and is defined by

$$R_h = (\sum \kappa_r)^{1/2} \qquad (4.2.6.21.)$$

α_e comes from equation 4.2.6.16. The larger the value of ABS FOM the greater the reliability that the solution is correct.

The PSI-ZERO (ψ_o) criterion is defined by the expression

$$\psi_o = \sum_h \sum_k |E_k| |E_{h-k}| \quad (51) \qquad (4.2.6.22.)$$

in which the E 's are very close to zero or are zero. The correct solution should have a correspondingly small value of ψ_o. This criterion can help in choosing a solution set when ABS FOM from several solutions exhibit similar values.

RESID (R_k) is calculated from the formula

$$R_k = \sum |E_{oh}| - [\, K\langle |E_k| - |E_{h-k}| \rangle \,] / \sum |E_h| \qquad (4.2.6.23.)$$

in which K is a scale factor. The lowest R_k should correspond to the correct phase set.

Usually the correct phase set can be discerned on the basis of Z and R_k. However, when the choice is still difficult, the COMBINED FOM (C) can be useful. It is given by the expression

$$C = \frac{W_1 (Z - Z_{min})}{(Z_{max} - Z_{min})} + \frac{W_2 (\psi_{omax} - \psi_o)}{(\psi_{omax} - \psi_{omin})} + \frac{W_3 (R_{kmax} - R_k)}{(R_{kmax} - R_{kmin})} \qquad (4.2.6.24.)$$

in which W_1, W_2 and W_3 are weights often equal to unity.

MULTAN will record the solution sets as a Fourier peak file in which the coefficients are the E_{hkl}'s. This file is then used as input to the Fourier program to calculate E-maps. The correctly phased solution is used to generate a map from which a list of peaks in descending order of magnitude is produced. From the map it should be possible to locate and identify the most prominent atoms of the structure. The remainder of the structure can then obtained by performing a combination of least-squares refinements and difference-Fourier syntheses. These are now described.

4.2.7. THE DIFFERENCE FOURIER SYNTHESIS [21,32,41,42]

Often with structures containing heavy atoms location of the lighter atoms of the structure from an F_o-map is not possible. The electron density of the heavy atom tends to swamp the electron density of the rest of the structure. A particularly useful tool in locating light atoms is the difference Fourier synthesis. Once the heavy atom of the structure is located and placed in the cell position, a structure factor calculation is performed and the result of this calculation, F_c may be subtracted from the observed structure factor, F_o giving rise to a quantity, ΔF.

In the centrosymmetric case ΔF is defined by the expression

$$\Delta F = |F_o| - |F_c| \qquad (4.2.7.1.)$$

whereas in the noncentrosymmetric case it is defined as

$$|\Delta F| \exp(i\alpha\Delta) = |F_o| \exp(i\alpha_o) - |F_c| \exp(i\alpha_c) \qquad (4.2.7.2.)$$

in which α_o and α_c are the observed and estimated phases, respectively.

Assuming the phasing of $|F_o|$ data is correct at least for the heavy atom, the electron density difference corresponding to $|\Delta F|$ is

$$\Delta\rho(xyz) = 1/V_c \sum\sum\sum (|F_o| - |F_c|) \exp[i\alpha_c] \exp[2\pi i(hx + ky + lz)] \qquad (4.2.7.3.)$$

since the calculated phase α_c approximately equals the observed phase α_o. The contribution to $|F_o|$ of the heavy atom is subtracted essentially improving the resolution of the light atoms. In addition, since

$$\rho(xyz) = 1/V_c \sum\sum\sum |F_{ohkl}| \exp[-2\pi i(hx + ky + lz)] + R \qquad (4.2.7.4.)$$

and

$$\rho(xyz) = 1/V_c \sum\sum\sum |F_{chkl}| \exp[-2\pi i(hx + ky + lz)] + R' \qquad (4.2.7.5.)$$

then

$$\Delta\rho(xyz) = \rho(xyz) - \rho(xyz)$$
$$= 1/V_c \sum\sum\sum (|F_{ohkl}| - |F_{chkl}|) \exp[-2\pi i(hx + ky + lz)] \quad (4.2.7.6.)$$

The R and R' in the two previous equations are remainders representing the omitted information from finitely limiting the data collection. This is referred to as series termination error.[19] Assuming the magnitudes of R and R' to be nearly equal, the difference, R-R' is nearly zero. Hence the difference synthesis is essentially free of series termination error and the R-terms are not included in equation 4.2.7.6. Difference Fourier syntheses may be used to refine the structure as well, however, the technique of least-squares refinement has predominated in modern crystallographic computing.

4.2.8. LEAST-SQUARES REFINEMENT [21]

The method of least-squares is one in which variables x_i with corresponding coefficients p_i define the function

$$f = \sum_1 p_i x_i \quad (4.2.8.1.)$$

The coefficients are varied so as to minimize the sums of the squares of the differences between the observed and the calculated values of the function for all observations m.

The quantity to be minimized in crystallographic re-

finement is the difference between the observed and calculated structure factors. In the isotropic case the variables whose coefficients are refined are positional (x, y and z) and thermal (B) for every $|F_{hkl}|$.

$$D_{hkl} = \sum W_{hkl} (|F_{ohkl}| - |F_{chkl}|)^2 \qquad (4.2.8.2.)$$

Differentiation of equation 4.2.8.2. followed by setting the derivative equal to zero for every observed reflection gives rise to m normal equations for n unknowns. This results in a series of equations represented by

$$W_{hkl}[(|F_o| - |kF_c(p_1,p_2,\ldots,p_n)|] \frac{\partial}{\partial p_j} kF_c(p_1,p_2,\ldots,p_n) = 0$$
$$; j = 1,2,\ldots,n; \qquad (4.2.8.2.)$$

The function $|F_c|$ can be expressed as a Taylor series and truncated to neglect non-linear terms wherein

$$|kF_c(p_1,p_2,\ldots,p_n)| = |kF_c(a_1,a_2,\ldots,a_n)| + \frac{\partial}{\partial p_1}|kF_c| p_1 + \ldots$$
$$\ldots + \frac{\partial}{\partial p_n}|kF_c| p_n \qquad (4.2.8.4.)$$

in which the p_j's are positional and thermal parameters for variables x, y, z and B and the a_j's are approximate values of p_j. The $p_j = p_j - a_j$ in the Taylor series approximation. Hence, substitution of 4.2.8.4. into 4.2.8.3. results in

$$W_{hkl}\left[\Delta F - \frac{\partial |kF_c|}{\partial P_1} p_1 - \ldots - \frac{\partial |kF_c|}{\partial P_n} \Delta p_n\right] \frac{\partial |kF_c|}{\partial p_j} = 0 \qquad (4.2.8.5.)$$

giving rise to a series of normal equations linear in the p_j's for which they may be solved.

The residual difference between the calculated and observed structure factors, is measured by the residual index R defined as

$$R = \sum(|F_o| - |F_c|)/\sum|F_o| = \sum|\Delta F| / \sum|F_o| \qquad (4.2.8.6.)$$

The smaller the R-value the better the agreement between $|F_o|$ and $|F_c|$ and although R is not a perfect guide as to how correct a structure is, it is a useful criterion to monitor during the process of completion and refinement of the structure.

The isotropic thermal parameter B is usually allowed to vary anisotropically once R attains a valueless than 0.20. From equations 4.2.2.2. and 4.2.2.3. the anisotropic temperature factor is formulated as

$$\exp[-1/4(B_{11}h^2a^{*2} + B_{22}k^2b^{*2} + B_{33}l^2c^{*2} + 2B_{12}hka^*b^*\cos\gamma^* + 2B_{13}hla^*c^*\cos\beta^* + 2B_{23}klb^*c^*\cos\alpha^*)] \qquad (4.2.8.7.)$$

where the B_{ii} are the diagonal coefficients and the B_{ij} are the cross or off-diagonal coefficients. In order to solve m equations in n unknowns, matrix methods have been devised to simplify computations. The method of least squares is

especially suited for matrix manipulation. For the following n normal equations

$$\begin{aligned} a_{11}x_1 + a_{12}x_2 + \ldots\ldots\ldots + a_{1n}x_n &= v_1 \\ a_{21}x_1 + a_{22}x_2 + \ldots\ldots\ldots + a_{2n}x_n &= v_2 \\ \vdots \qquad\qquad & \\ a_{n1}x_1 + a_{n2}x_2 + \ldots\ldots\ldots + a_{nn}x_n &= v_n \end{aligned} \qquad (4.2.8.8.)$$

where

$$a_{ij} = \sum_r W_r \frac{\partial F_{cr}}{\partial P_i} \frac{\partial F_{cr}}{\partial P_j} \quad ; \quad x_j = \Delta p_j \qquad (4.2.8.9.)$$

and

$$v_i = \sum_r W_r(\Delta F_r) \frac{\partial F_{cr}}{\partial P_i} \qquad (4.2.8.10.)$$

then in matrix notation, equation 4.2.8.8. takes the form

$$\begin{bmatrix} a_{11} & a_{12} & \ldots\ldots\ldots & a_{1n} \\ a_{12} & a_{22} & \ldots\ldots\ldots & a_{2n} \\ \vdots & \vdots & & \vdots \\ a_{1n} & a_{2n} & \ldots\ldots\ldots & a_{nn} \end{bmatrix} \begin{bmatrix} x_1 \\ x_2 \\ \vdots \\ x_n \end{bmatrix} = \begin{bmatrix} v_1 \\ v_2 \\ \vdots \\ v_n \end{bmatrix} \qquad (4.2.8.11.)$$

and in matrix shorthand

$$\mathbf{Ax} = \mathbf{v} \qquad (4.2.8.12.)$$

If a solution exists for 4.2.8.8., a matrix A^{-1} exists such that

$$\mathbf{A}\mathbf{A}^{-1} = \mathbf{I} \qquad (4.2.8.13.)$$

where I is the identity matrix. The matrix $\mathbf{A}^{-1}$ or inverse of A can be used to solve for $\mathbf{x}$ in the following way. From equation 4.2.8.13.,

$$\mathbf{A}^{-1}\mathbf{A}\,\mathbf{x} = \mathbf{A}^{-1}\mathbf{v} \qquad (4.2.8.14.)$$

$$\mathbf{x} = \mathbf{A}^{-1}\mathbf{v} \qquad (4.2.8.15.)$$

Full matrix anisotropic least squares include at least eleven parameters to be refined. These are one scale and one overall thermal parameter, and three positional and six thermal parameters per atom. This means that for a 50 atom structure 452 parameters are refined for each cycle of refinement.

The A-matrix will be composed of: one 2x2 block corresponding to the first two parameters, one 3x3 block and one 6x6 block corresponding to three positional and six thermal parameters, respectively, per atom. These are seen to lie symmetrically along the main diagonal of the matrix and hence the modification is termed the "block-diagonal least-squares" approximation. This method seriously decreases the demands of memory space and computation time. The block diagonalized A-matrix can be pictorially represented as in Fig.4.2.8.1.

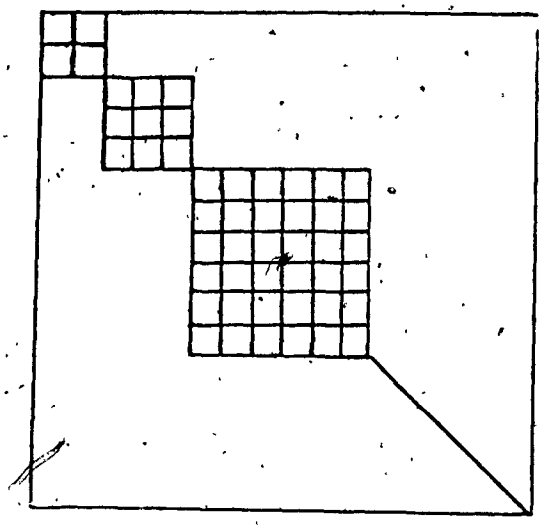

Fig.4.2.8.1.

4.2.9.RETROSPECTUS

From the last two sections it was shown that once the phase problem has been overcome by either method described, a combination of difference-Fourier and least-squares techniques can be used to refine the structure down to respectable limits of confidence. Aside from the residual index R, a weighted residual index R_w is often calculated based upon the weighting of F.

$$R_w = [\{ \quad W_i(F_{oi} - F_{ci})^2 / \quad W_i F_{oi}^{\,2} \}]^{1/2} \quad (4.2.9.1.)$$

Iterative refinement cycles are terminated once the variation on R and R_w is insignificant when compared to the standard deviations computed from successive least squares refinements. A reasonably good structure will be characterized by $R \sim R_w < 0.05$ although under optimum conditions of data collection it may be as low as 0.01 or less.[43]

4.3.CRYSTALLOGRAPHIC TECHNIQUE

This chapter deals with the procedures used in this investigation to collect geometric and intensity data and it may be used as an outline for the data collection of single crystals. Although more modern techniques are available in which almost all preliminary photography is eliminated from the procedure necessary to collect geometric and symmetry information, the following outline is by far the more instructive one. As a teaching exercise it is superior in that the concepts of the reciprocal lattice and space group determination must necessarily be familiar to the student before progression to the intensity data collection and subsequent completion of a given structure.

4.3.1.GEOMETRIC DATA COLLECTION

Geometric data collection includes determination of the unit cell dimensions as well as the space group. The steps used to carry out these determinations will now be described.

Choosing a Crystal.

Using a low power stereo microscope, several crystals are initially selected from a sample with the criteria that they be: 1) Observable to the naked eye but small enough that their shape be relatively undiscernible. 2) Well formed and transparent under low magnification and 3) Homogeneous with respect to transmission and or absorption of

visible light. If not the crystal may be twinned, a condition wherein the apparent single crystal is actually an aggregate of two or more single crystals in which the order of molecular packing is not homogeneous throughout the sample.

If these criteria are met, the best choice is made at the discretion of the investigator and thus the crystal is mounted on a fine lithium borate glass capillary with "5-minute epoxy." The orientation of the crystal is not crucial, however, the alignment routine may be facilitated by choosing at least one crystal edge to be more or less parallel or perpendicular to the axis of the capillary. The more axes visually aligned orthogonal to the rotation axis of the goniometer head the greater the ease in which the crystal may be aligned.

Alignment

The glass capillary supporting the crystal is mounted on the goniometer head using 5-minute epoxy. (Fig 4.3.1.1.) The goniometer head is attached to a Weissenberg camera.[44] (Fig. 4.3.1.2.)

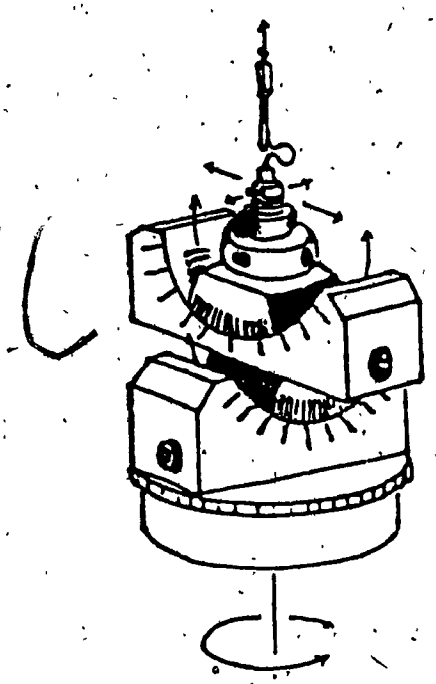

Fig. 4.3.1.1. Eucentric goniometer head with crystal.

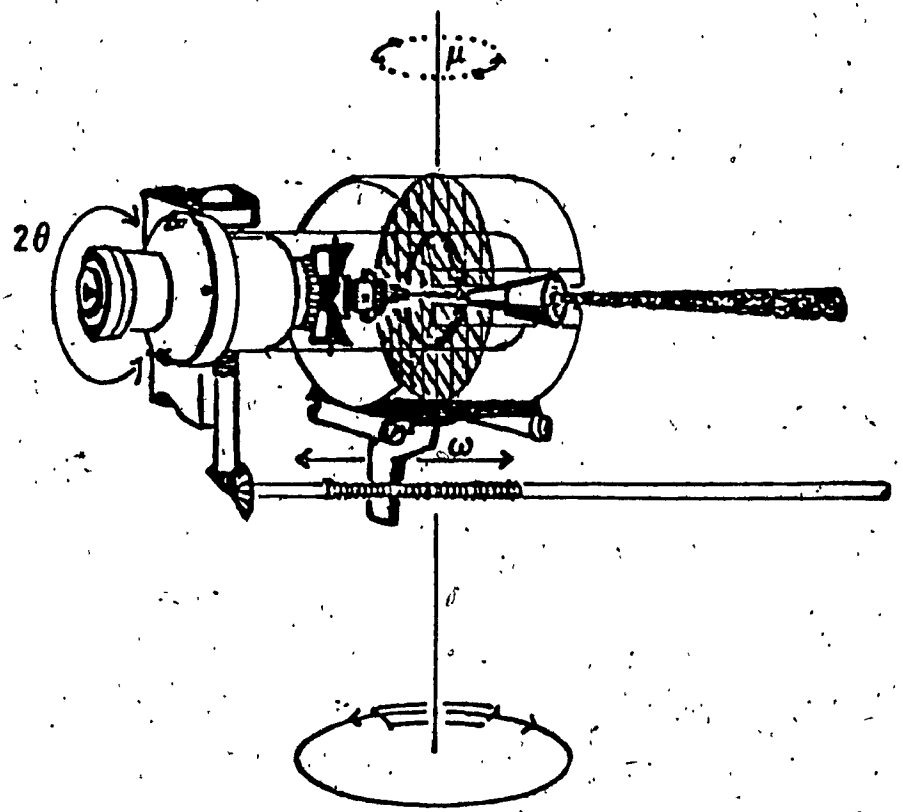

Fig. 4.3.1.2. Essential Weissenberg camera geometry depicting zero-level zone being photographed.

The camera permits the goniometer to be rotated through the 2θ -azimuth. Initially two oscillation photographs are taken. These photographs provide the investigator with the orientation of the reciprocal lattice relative to the camera geometry. Each exposure is made for a fifteen minute interval in which time the crystal is made to oscillate $\pm 5^{\circ}$ through 2θ . One exposure is centred about $2\theta = 180^{\circ}$ and the other at $2\theta = 270^{\circ}$. The developed exposures (Fig. 4.3.1.3.) are used to determine the angular correction to the goniometer arcs in order to orient a reciprocal lattice plane normal to the direction of oscillation.

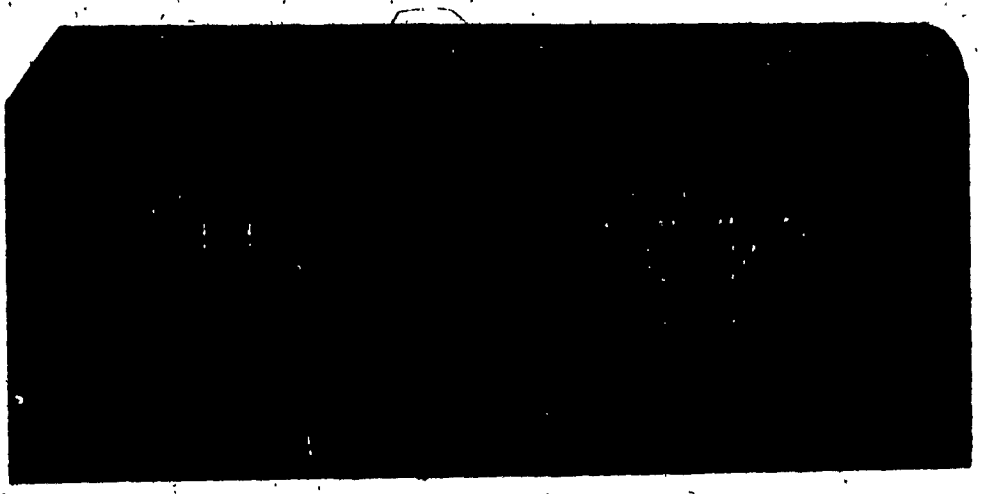

Fig.4.3.1.3. Oscillation photograph at 180° and 270°.

Once this is accomplished, the goniometer arc settings are recorded. A layer-line screen, a tube concentric with the rotation axis of the camera into which a vertical slit is cut, is set in place around the crystal allowing only one reciprocal lattice zone to be photographed for a given exposure.

Weissenberg Photography

The film carriage of the Weissenberg camera (see Fig. 4.3.1.2.) is also concentric with the rotation axis of the camera and fits over the layer-line screen. The film carriage can translate in the direction ω . It is static for oscillation photography where it is manually set into the desired position. For Weissenberg photography, a moving-crystal moving-film method, the film carriage is engaged to translate simultaneously with the rotation of the crystal through a right-hand drive. The camera is designed so that a 2° rotation in the 2θ -azimuth corresponds to a 1-mm. translation in ω . In this fashion, the two-dimensional reciprocal lattice zone can be mapped onto a flat film surface which is loaded into the cylindrical film carriage prior to making the exposure. While the recorded image of the reciprocal lattice zone is a distorted map, it still supplies one with dimensional and symmetry information. (See Fig. 4.3.1.4.)

Fig. 4.3.1.4. Zero-level Weissenberg exposure of b*c* zone.

The zero-order photograph is shown being recorded in Fig. 4.3.1.2.

Rotation of the camera housing through μ allows the upper level to be photographed. The equi-inclination angle can be determined by measuring the horizontal spacing on the oscillation photograph between reciprocal lattice zones perpendicular to the rotation axis. The upper level is exposed in the same way as the zero level and both exposures are compared to reveal any breakdown in symmetry or systematic absences. See Fig. 4.3.1.5. for upper level.

Fig. 4.3.1.5. Upper-level Weissenberg exposure (b*c* zone).

Comparison of the last two figures suggests systematic absences on 0kl for reflections in the b*-direction. Mirror symmetry is preserved.

Precession Photography [22,45]

The precession method is also a moving-crystal moving-film technique. The same type of symmetry and dimensional information can be obtained by this method as with the lat-

ter. The advantage of this method is that the record of the reciprocal lattice zone is undistorted. The basic machinery and essential geometry of the precession camera are depicted in Figs.4.3.1.6. and 4.3.1.7., respectively.

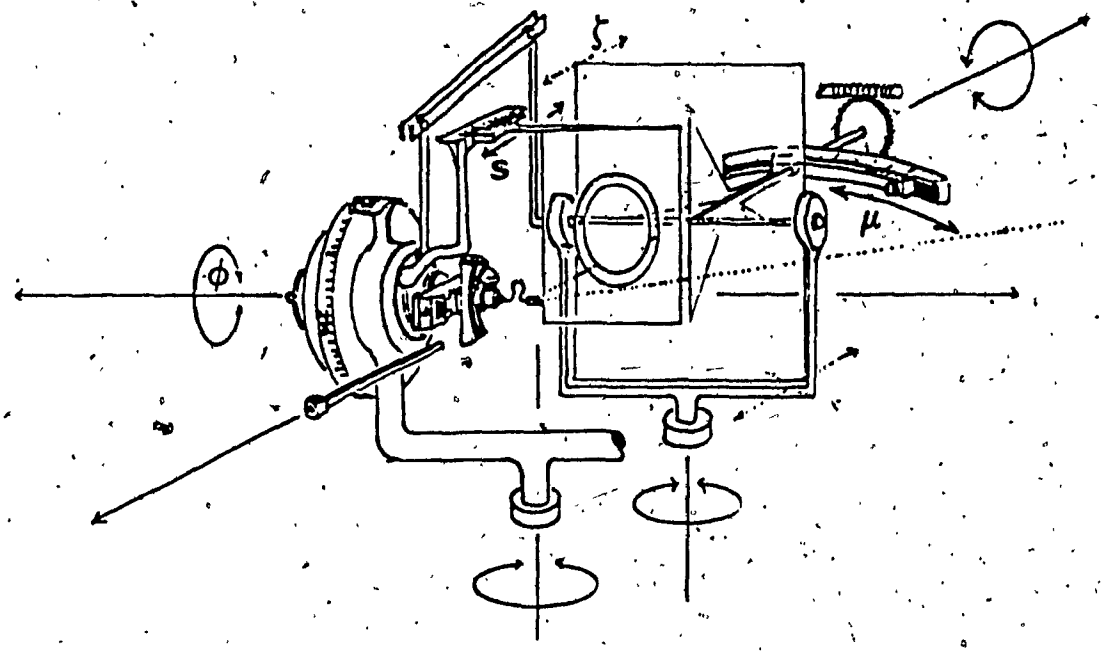

Fig. 4.3.1.6. Precession Camera.

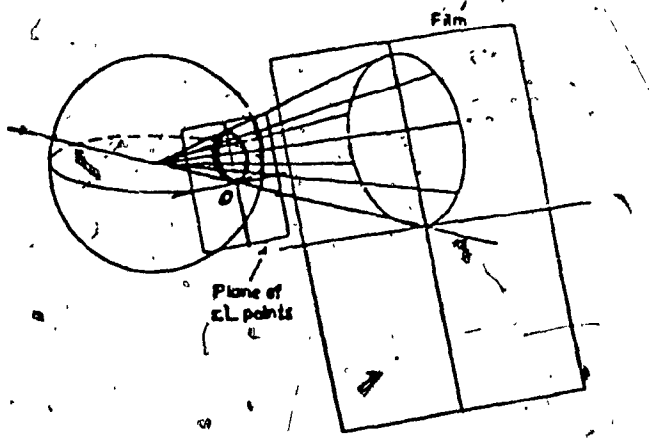

Fig. 4.3.1.7. Essential precession geometry.

As the name suggests, both the crystal and film precess relative to the incident beam in order to bring the reciprocal lattice points into position to satisfy Bragg's law.

In practice one normally proceeds from the Weissenberg step to the precession step. From the zero-level Weissenberg photograph, an axial line is selected and the angular value of 2θ corresponding to the line is used to position the ϕ -azimuth on the precession camera. With the goniometer supporting the same crystal mounted on the precession camera, a fifteen minute alignment photograph is taken. The alignment photograph requires a 10^{o} precession angle and a layer level screen to be placed between the crystal and the film. The screen radius for alignment is 10 mm. The crystal-to-film distance is 60 mm. and the crystal-to-screen distance is 32 mm. The photograph is used to centre the reciprocal lattice zone on the film. Vertical

corrections are performed by adjusting ϕ either up or down and horizontal corrections are effected by appropriately adjusting the goniometer arcs. The procedure is repeated until the alignment satisfactorily centres the zone. The zero level is then photographed using a precession angle of 25°, a layer level screen radius of 15 mm., and a crystal-to-screen distance of 32 mm. A 24-hour exposure of the zone is made revealing the result shown in Fig. 4.3.1.8.

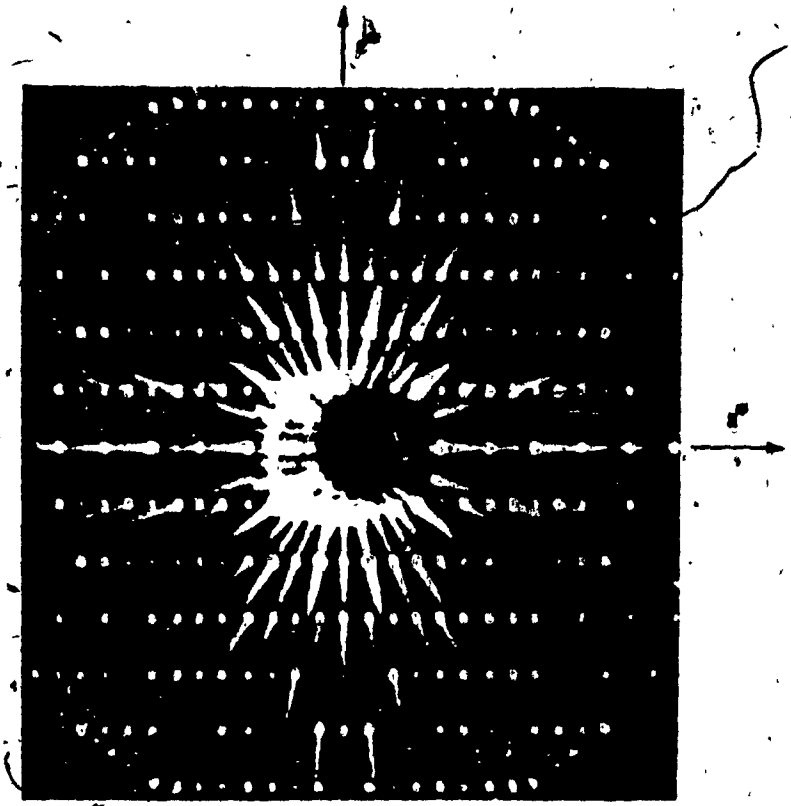

Fig.4.3.1.8. Zero-level Precession photograph of a*c* zone.

Weissenberg photographs illustrated the b*c* zones or the 0kl and 1kl zones. The precession photograph (Fig.4.3.1.8.) reveals the a*c* zone h0l. The upper level precession photograph is made on the basis of the distance between zones normal to the film plane. The spacing is determined by

taking what is referred to as a cone-axis photograph. This photograph is taken on the precession camera by mounting a flat film cassette on the layer-level screen support and setting the precession angle and crystal-to-film distance to 10° and 32 mm., respectively. The exposure time is approximately two hours. The photograph is shown in Fig. 4.3.1.9. and the rings evident in the photograph pertain to the cones of diffraction in the direction normal to the film plane. Measurement of the radius of the second concentric ring (corresponding to the first upper level cone), once scaled for the camera geometry, is used to set the change in the crystal-to-film distance necessary for upper level precession photography.

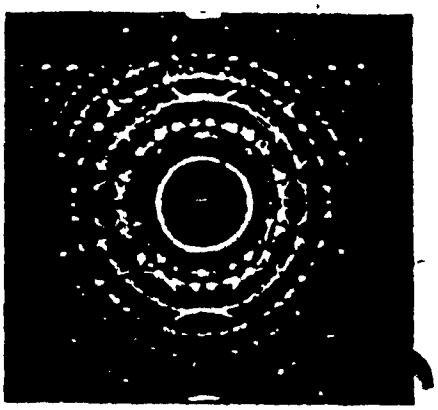

Fig. 4.3.1.9. Cone-axis photograph of a*c* zone.

The upper level photograph is exposed in the same manner as the zero level. The result, Fig. 4.3.1.10., is displayed below. It is observed that every second reflection in the c*-direction in Fig. 4.3.1.8. is systematically absent when compared to Fig.4.3.1.10. Mirror symmetry, however, is preserved about both axes.

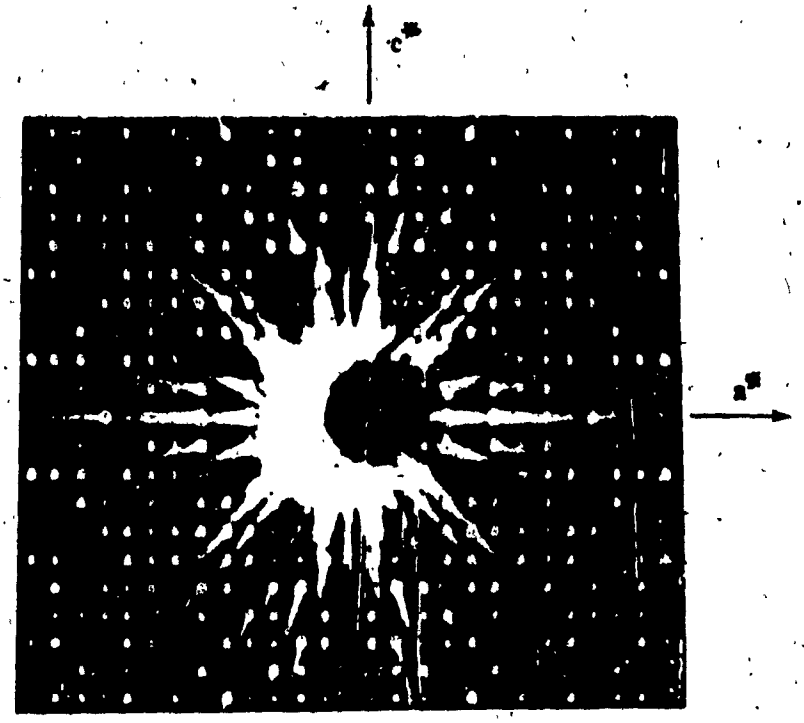

Fig. 4.3.1.10. Upper-level Precession photograph of a*c*.

In order to photograph the a*b* zones, the crystal is rotated through by the appropriate angle determined from the Weissenberg photographs. In this case (orthorhombic) angle = 90°. The hk0 and hk1 zones are then photographed using the same procedure used for the two previous ones. The results are similar to those of the h0l and h1l zones except the absence conditions are in the a*-direction as can be observed from Figs. 4.3.1.11. and 4.3.1.12.

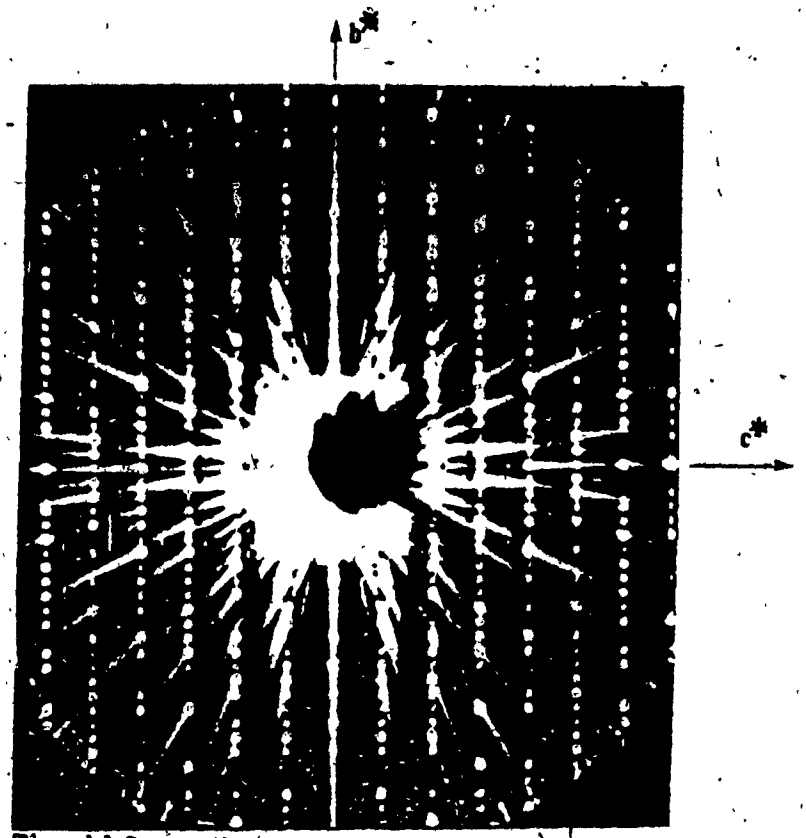

Fig. 4.3.1.11. The hk0 reciprocal lattice net.

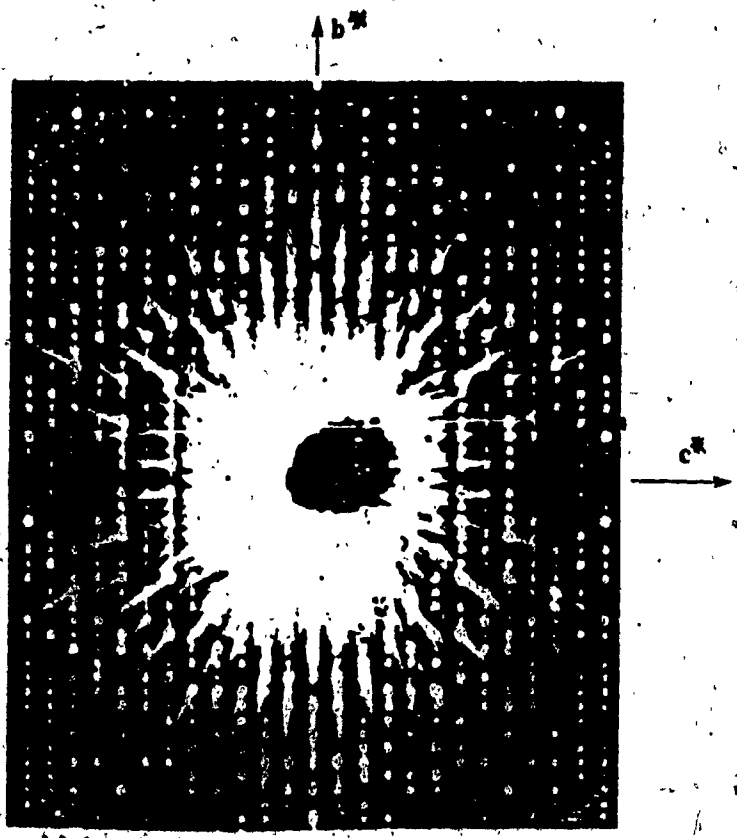

Fig. 4.3.1.12. The hk1 reciprocal lattice net.

Unit cell dimensions and space group determination can now be accomplished by measuring reciprocal lattice interplanar spacings and inspecting the photographs for conditions limiting possible reflections,[30] respectively. The space group is determined unambiguously in this case as Pbca and the unit cell dimensions are: a = 13.41A, b = 23.19A, c= 11.41A; $\alpha = \beta = \gamma = 90^{o}$, V = 3549.67$A^3$..

The camera adjustments are made according to the geometry of the camera and scales relating camera settings to reciprocal lattice constants are supplied by the camera manufacturer.[46]

Once the unit cell parmeters and space group are determined, the density measured by floatation in aqueous ZnI_2 can be used to determine the number of formula units in the unit cell providing a reasonable estimate of the molecular weight is known. At this point, one is prepared to begin intensity data collection.

4.3.2. INTENSITY DATA COLLECTION

Apparatus

The apparatus used to collect intensity data is a diffractometer. An automated, single-crystal, four-circle diffractometer consists of four rotating circles to orient the crystal into any position so that any reflection (F_{hkl}) can be brought into the diffracting condition. In this way the diffracted intensities may be measured. The basic components of the device are displayed in Fig. 4.3.2.1.

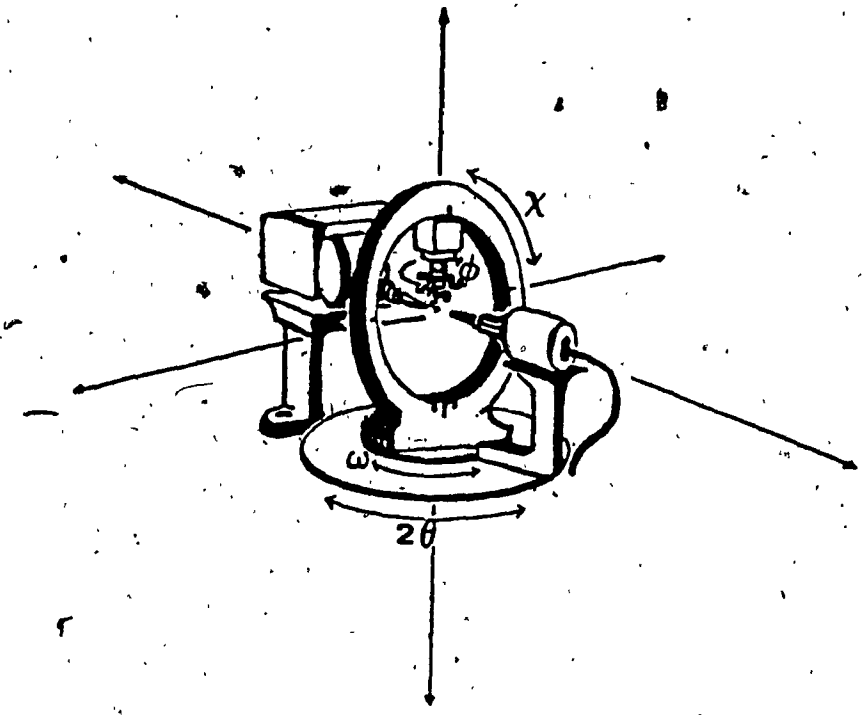

Fig. 4.3.2.1. Four-circle diffractometer (basic geometry).

X-rays are generated and then monochromated using a "crystal" of highly oriented graphite in order to obtain as monochromatic an incident beam as possible. The incident beam bathes the sample crystal which is supported so its orientation is coaxial to the ϕ-circle (with which the goniometer rotation axis is coincident.) Diffracted beams ($|F_{hkl}|$) are detected by a scintillation counter whichis mounted on the 2 -circle.

The ϕ -circle is mounted on the χ-circle and the χ-circle can be rotated through ω. The ϕ and χ -circles thus have unrestricted motion in two independent directions while ω and 2 θ (essentially equi-directional) are limited depending upon the instrumental geometry. The usual high-limit for 2θ is $\pm$ 45° from the incident beam

when employing Mo K radiation.

Hence from the diagram it may be visualized that any reflection ($|F_{hkl}|$) may be caused to diffract once the crystal orientation has been determined by reciprocal lattice photography. Before the detected reciprocal lattice point is recorded it is passed through a pulse-height analyzer and then subject to profile analysis (vide-infra).

Practical

The goniometer is removed from the precession camera and the arcs readjusted to the Weissenberg settings. It is then mounted on the diffractometer with all circles in the zero position. The crystal is then manually centred such that it remains in the incident beam at any orientation. Now the crystal is oriented in such a way that the two axes in the zone photographed by the Weissenberg method lie in the plane circumscribed by the 2θ -circle (upon which the detector is mounted.) The 2θ -circle is set to intercept one of the reflections on either axis defining the zone hOl and a ϕ -scan is performed with the detector slits open wide until the desired reflection is found. Once found, all circles are manually adjusted to maximize the intensity of the detected signal with the slits leading to the detector narrowly open. A 2θ -scan is then performed in order to check the axis by comparing a strip chart recording of the scan with the zero order precession photographs. When the axis is identified, the same procedure is used to locate the second axis in the plane. The third axis is

found by rotating the χ -circle through the appropriate angle and repeating the procedure outlined above. After all axes are identified, three non-colinear reflections are chosen and automatically centred. The indices and angular orientations of the three reflections are used to calculate an initial orientation matrix and the unit cell parameters. Next, about fifteen well-spaced reflections throughout reciprocal space are selected and automatically aligned. The indices and diffractometer angles are used as input to a least-squares refinement of the orientation matrix which provides a more reproducible set of lattice constants with corresponding estimated standard deviations. Line profiles are then measured on some strong reflections to select three reference reflections which are to be monitored at a frequency of once every fifty reflections to ensure instrumental and crystal stability during the data collection. Once all data collection parameters are decided, the space group is entered into the data collection program and data collection may commence. The length of the data collection depends upon the symmetry of the crystal. For an inorganic molecular crystal with monoclinic symmetry approximately 5000 reflections are collected over a period of four to five days

4.3.3. DATA REDUCTION

Data reduction is the process whereby all $|F_{hkl}|$ data are analyzed and brought to a common basis. The data are scaled based upon the variation of the three reference re-

flections from which a scale correction is calculated. The scale correction is applied to attempt to linearize the variation in the $|F_{hkl}|$ data.

During data collection the data are subject to profile analysis.[48] This method of measuring intensity data differs from the conventional method in that, rather than directly measuring the background contribution to the intensity, the background is estimated from the shape of the peak profile. This method is advantageous in its ability to reduce the time necessary to record intensity information by a factor of up to 60%. The collected intensities were processed according to equation 4.3.3.1.

$$I = N - [\ B_1 + [redacted]\ t_s/2t_b\ ] \qquad (4.3.3.1.)$$

where N is the peak count for the scan time t_s. B_1 and B_2 are the background counts on either side of the peak each of which are measured for time t_b. I-values of magnitude less than 3 σ (I) are considered unobserved. σ (I) is calculated using equation 4.3.3.2.

$$\sigma(I) = [\ N + \{(B_1 + B_2)/2\}\ (t_s/t_b)^2 + (DN^2)\ ]^{1/2} \qquad (4.3.3.2.)$$

in which the D in the equation is referred to as the "ignorance factor."

Lorentz and polarization corrections are then applied.

In order to compensate for the diffraction-angle-velocity of reciprocal lattice points as they pass through the sphere of reflection during observation and the polarization of the incident and diffracted beams by both monochromator and sample crystals, the combined expression correcting for the two effects, which is specific to the diffractometer design, is given by equation 4.3.3.3.

$$Lp = (\cos^2 2\theta_m + \cos^2 2\theta_s)/[\sin 2\theta_s(\cos^2 2\theta_m + 1)] \qquad (4.3.3.3.)$$

where θ_m and θ_s are the diffraction angles at the monochromator and sample crystals respectively. The magnitude of the relative structure factor $|F_{rhkl}|$ is then calculated from equation 4.3.3.4.

$$|F_{rhkl}| = [\ \overline{I_{hkl}}/Lp\ ]^{1/2} \qquad (4.3.3.4.)$$

The diffractometer data is then subject to a statistical analysis whereby an approximate overall thermal parameter and an absolute scale factor are calculated. These relate the relative structure factors $|F_{rhkl}|$ to the absolute structure factors $|F_{ahkl}|$. The procedure is to perform a Wilson plot.[36] From equation 4.2.2.3., an expression relating the absolute intensity to the mean atomic scattering factor of a point atom, it can be inferred that

$$\overline{I_{abs}} = f_{oj}^2 \exp[-2B(\sin^2\theta / \lambda^2)] \qquad (4.3.3.5.)$$

in which f_{oj} is the mean atomic scattering factor of the j^{th} atom. Plotting $\ln [\sum f_{oj}^2/I_{rel}]$ vs $\sin^2\theta / \lambda^2$ gives the linear equation 4.3.3.6.

$$\ln [\sum f_{oj}^2/Irel.] = 2B\sin^2\theta / \lambda^2 + \ln C \qquad (4.3.3.6.)$$

where B is obtained from the slope of the line and C, the scale factor is applied to bring the $|F_{rhkl}|$ to an absolute scale wherein

$$|F_{ahkl}| = |F_{rhkl}|/C^{1/2} \qquad (4.3.3.6.)$$

At this point the phase problem is ready to be tackled.

4.3.4. PATTERSON SOLUTION

The remaining procedure to be outlined for structure solution is solving the Patterson for the heavy atom.

Consider a Patterson map calculated from $|F_{hkl}|^2$ for all data $|F_{hkl}|$. Generally, a peak listing in order of decreasing P(xyz) is produced as output from the program calculating the Patterson map. Table 4.3.4.1. gives a partial peak listing for a crystal of space group P $2_1/c$.

Table 4.3.4.1. Partial Patterson Peak Listing

PEAK	REL.HEIGHT	X	Y	Z
1	9169.92	0.0000	0.0000	0.0000
2	2829.85	0.4604	0.5000	0.0363
3	2718.85	0.0000	0.0248	0.5000
4	1240.44	0.5369	0.4769	0.4644

By preparing a table of the equivalent positions for this space group from the International Tables for X-Ray Crystallography[31] one can calculate the interatomic vectors between equivalent positions. (Table 4.3.4.2.)

Table 4.3.4.2.Interatomic Vectors From Equivalent Positions

VECTOR	COMPONENTS	MULTIPLICITY
1	0,0,0,	4
2	+2x, 1/2, 1/2 + 2z	2
3	0, 1/2 + 2y, 1/2	2
4	+2x, +2y, +2z	1
5	+2x, -2y, +2z	1

Vector 2 has components on a plane referred to as a Harker section. Vector 3 has components on a line and is referred to as a Harker line.[49] Vectors 4 and 5 are called satellite peaks.

Referring to Table 4.3.4.1. we note that peak 3 cor-

responds to vector 3 in Table 4.3.4.2. One solves for the y-value. Once obtained, one proceeds to the vector 2 which can be seen from the tables as corresponding to peak 2. (The fact that the vector and peak numbers mateh is purely coincidental.) One then solves for x and z. The values obtained are: x = 0.2302, y = -0.2376 and z = -0.2319. Verification by the satellites corresponds to peak 4 in the first table. That 2x = 0.4604is inconsequential since this is simply the symmetry-related value of 1 - 2x = 0.5496. It is observed by inspection that the coordinates of the satellite peaks correspond quite well with the xyz-values calculated from the vectors of the second table. The position of the heavy atom is then inserted into the unit cell and a structure factor calculation is performed. As previously stated (4.2.5.) the phases of the structure are essentially dominated by the heavy atom and the implication is that, once this step is completed, the phases of many $|F_{hkl}|$ become fixed. Completion and refinement of the structure ought to be more or less a straight forward process of least-squares refinements and difference Fourier syntheses.

5.EXPERIMENTAL CRYSTALLOGRAPHY

5.1.GENERAL

Geometric data collection by reciprocal lattice photography was performed using Weissenberg and precession cameras manufactured by the Charles Supper Co.[46] Both cameras were mounted upon a Picker Nuclear model 809B x-ray generator. X-rays were produced by a common 4-port beryllium-windowed Dunlee model DZ-1B fine-focus Molybdenum x-ray tube with cameras in a 180° configuration. Kodak "No Screen" x-ray film was used for Weissenberg photography while Polaroid "type 57" high-speed casette film was used for precession photography. Photographic chemicals were Kodak GBX Developer and Kodak Rapid Fixer. Unit cell measurements were calculated from precession photographs using a Charles Supper film measuring device.

Single crystal intensity data were collected using a Picker Nuclear Facs-1 fully automated four-circle diffractometer coupled with a Picker Nuclear 2861 radiation analyzer. Radiation was produced by a Marconi Avionics TX8 fine-focus Molybdenum x-ray tube powered by a Picker Nuclear model 6238E x-ray generator. Intensity data were detected using a Tl-doped NaI-crystal scintillation counter operated at 1kV with radiation analyzer set to receive 100% Mo K radiation. Ni-foil attenuators were automatically inserted for peaks of intensity greater than 10^4cps.

The instrument was interfaced to a dedicated Digital

PDP 8/a minicomputer. Programs controlling data collection and all subsequent data processing were the NRC of Canada Single Crystal Data Collection Package[47]. All data collections were performed using the aforementioned hardware. Data processing for the x-ray crystal structure of $RhCo_3(CO)_9[HC(PPh_2)_3]$ was accomodated at NRC Ottawa, Montreal Road Facility (Chemistry Division) using a Digital Vax minicomputer under supervision of Dr. E. J. Gabe.[47]

Structure factor calculations and least squares refinements were accomplished using the program LSTSQ[47] and all Fourier symtheses were performed using the program FOURR.[47]

Molecular structure graphics were produced by ORTEP[52] using the Concordia University Cyber 835 facility and Nicolet Zeta plotter except for $RhCo_3(CO)_9[HC(PPh_2)_3]$ which was plotted using PLTMOL[47] and a Tectronix plotter.

5.2.1. CRYSTAL AND MOLECULAR STRUCTURE OF $Mo(CO)_4[HC(PPh_2)_3]$

A pale yellow crystal of the complex was mounted in an arbitrary orientation a goniometer head. Weissenberg and precession photographs revealed the space group to be unequivocally P $2_1/c$. The crystal was then mounted upon the diffractometer after readjusting the goniometer arcs to Weissenberg settings. Thirteen non-axial reflections, well spaced through reciprocal space, were automatically aligned along with their Friedel equivalents and were used to calculate a refined orientation matrix. Unit cell dimensions thus determined are listed in Table 5.2.1.1.

Table 5.2.1.1. Unit Cell Dimensions (A, "O") with e.s.d.'s

a = 11.00983	b = 19.64966	c = 21.34026
σ (a) = 0.0095034	σ (b) = 0.0100173	σ (c) = 0.0185952
α = 90.0	β = 119.197	γ = 90.0
$\sigma(\alpha)$ = 0.058	$\sigma(\beta)$ = 0.067	$\sigma(\gamma)$ = 0.058

Data collection was driven by the program DIFFRAC[46,47] Three reference reflections { 0 12 0, 0 1 10, 6 0 6 } were checked every fifty reflections during the data collection. Out of 5254 reflections collected for $3.5^{\circ} \leq 2\theta \leq 45^{\circ}$ in segments hkl and $\bar{h}kl$, 4244 reflections were considered to be observed. Data reduction was performed by the program DATRD2.[47] Lorentz and polarization corrections were applied but no absorption corrections were performed. Data were scaled, grouped and normalized. Structure solution

was accomplished by a Patterson synthesis using the program FOURR[47]. The Mo atom was easily located and three cycles of isotropic least squares refinement using the program LSTSQ[47] were performed in which the thermal parameters were not refined. The residual index was 0.6299. Three more cycles in which B was permitted to refine yielded an R-factor of 0.6335. A difference Fourier synthesis was calculated. Three peaks of significantly greater magnitude than the rest were assigned as phosphorus atoms. A geometry calculation was performed to verify their proximity to the Molybdenum atom using the program DISPOW.[47] These seemed plausible and were edited into the cell as P1, P2 and P3 using the program CDEDIT[47]. Three more cycles of isotropic refinement brought the R-factor to 0.4860. Another difference Fourier synthesis was performed followed by a geometry calculation including Fourier peak data which permitted identification of the complete Molybdenum coordination sphere including all carbonyl oxygens and all phenyl carbons. These atoms were edited into the cell and six cycles of isotropic refinement were performed driving the R-factor down to 0.1820. Two more cycles of isotropic refinement afforded an R-factor of 0.1691 and R_w of 0.2524 with a G.O.F. equal to 1.4648. Another difference Fourier revealed still more atoms. These were attributed to a molecule of solvent. A geometry calculation showed no bonding contacts between this fragment and the Molybdenum complex and permit to be identified as an acetone molecule. It was edited

into the cell and refined as such. Nine anisotropic refinement cycles using the block-diagonal approximation gave the final indices R = 0.0662, Rw =0.1060 and a goodness-of-fit (G.O.F.) = 1.8604. Hydrogen atoms were not placed in idealized positions on the phenyl carbons or the central TRIPOD methane carbon. A final difference map was featureless. Molecular drawings were made using ORTEP.[52] (Figs. 5.2.1.1. - 5.2.1.3.). Positional and thermal parameters are listed in Tables 5.2.1.2. and 5.2.1.3., respectively. Selected interatomic distances and angles are listed in Tables 5.2.1.4. and 5.2.1.5.

Fig. 5.2.1.1. ORTEP [52] plot of $Mo(CO)_4[HC(PPh_2)_3]$ illustrating near-mirror symmetry.

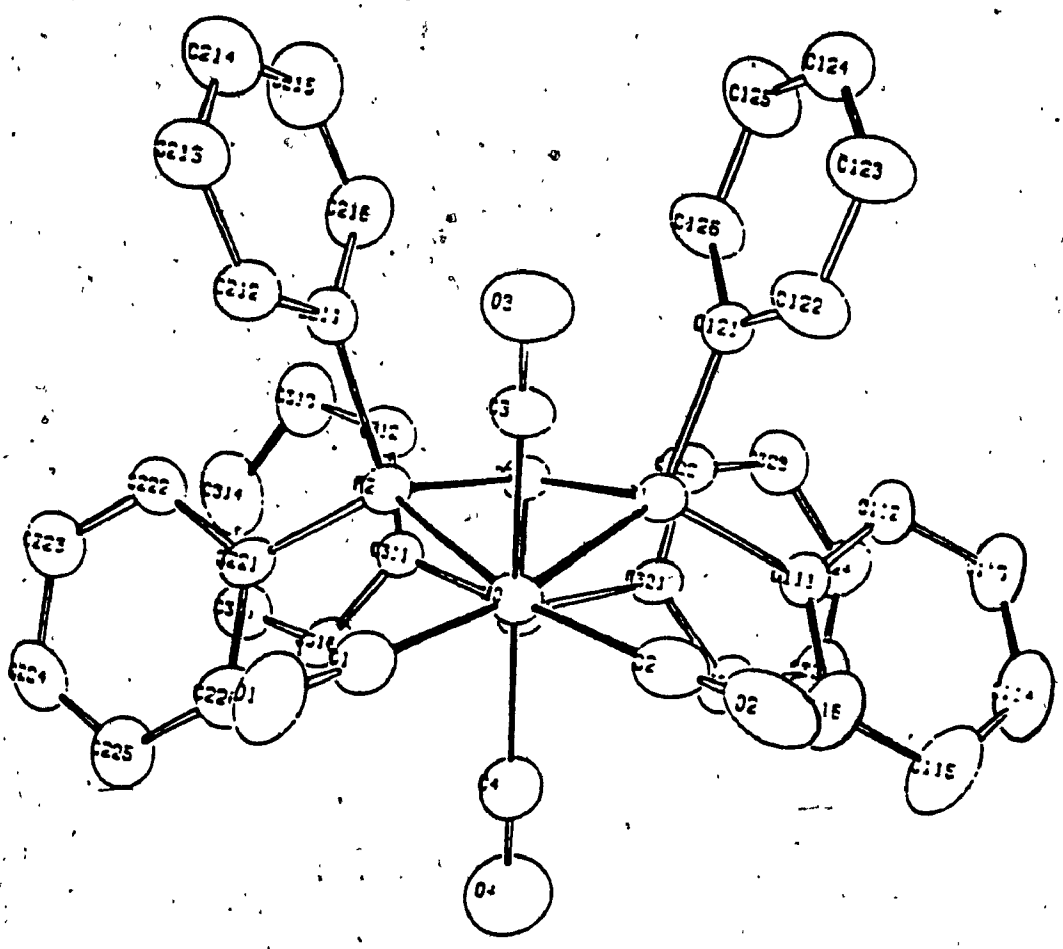

Fig. 5.2.1.2. Perspective view of the formula unit.

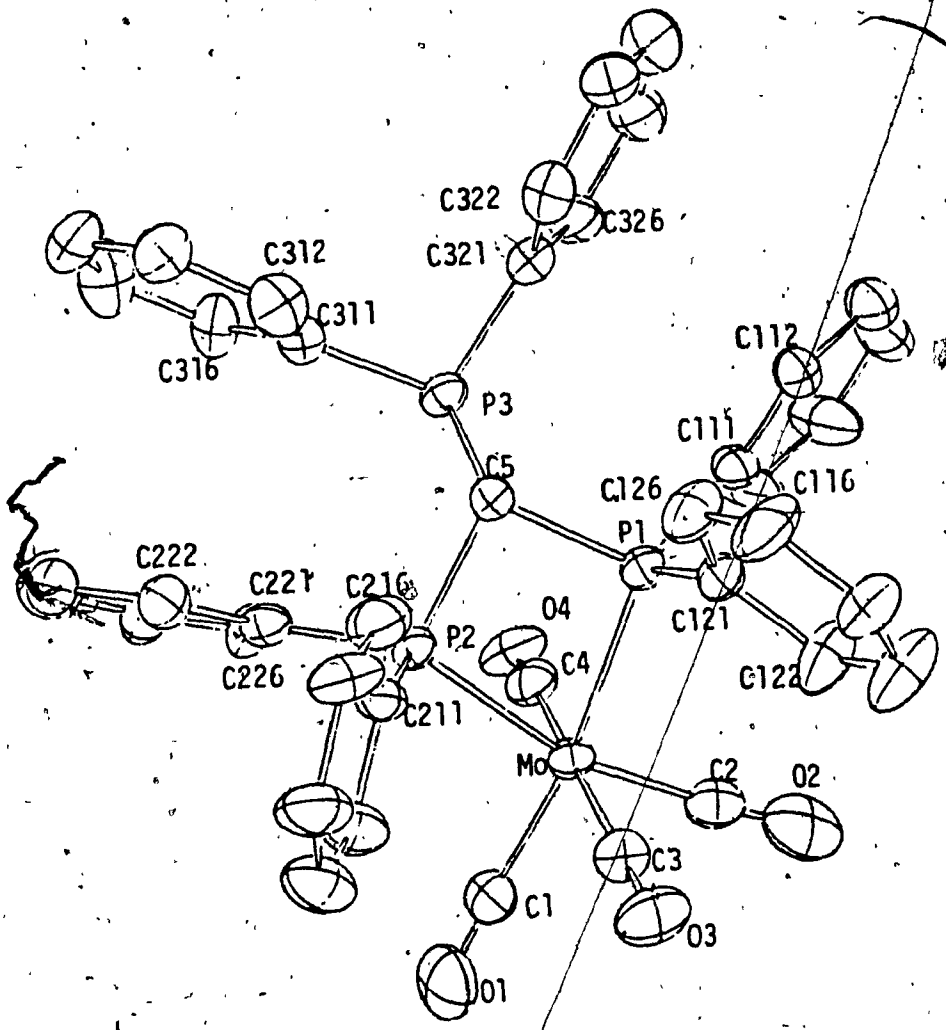

Fig. 5.2.1.3. Stereo packing diagram showing acetone solvate

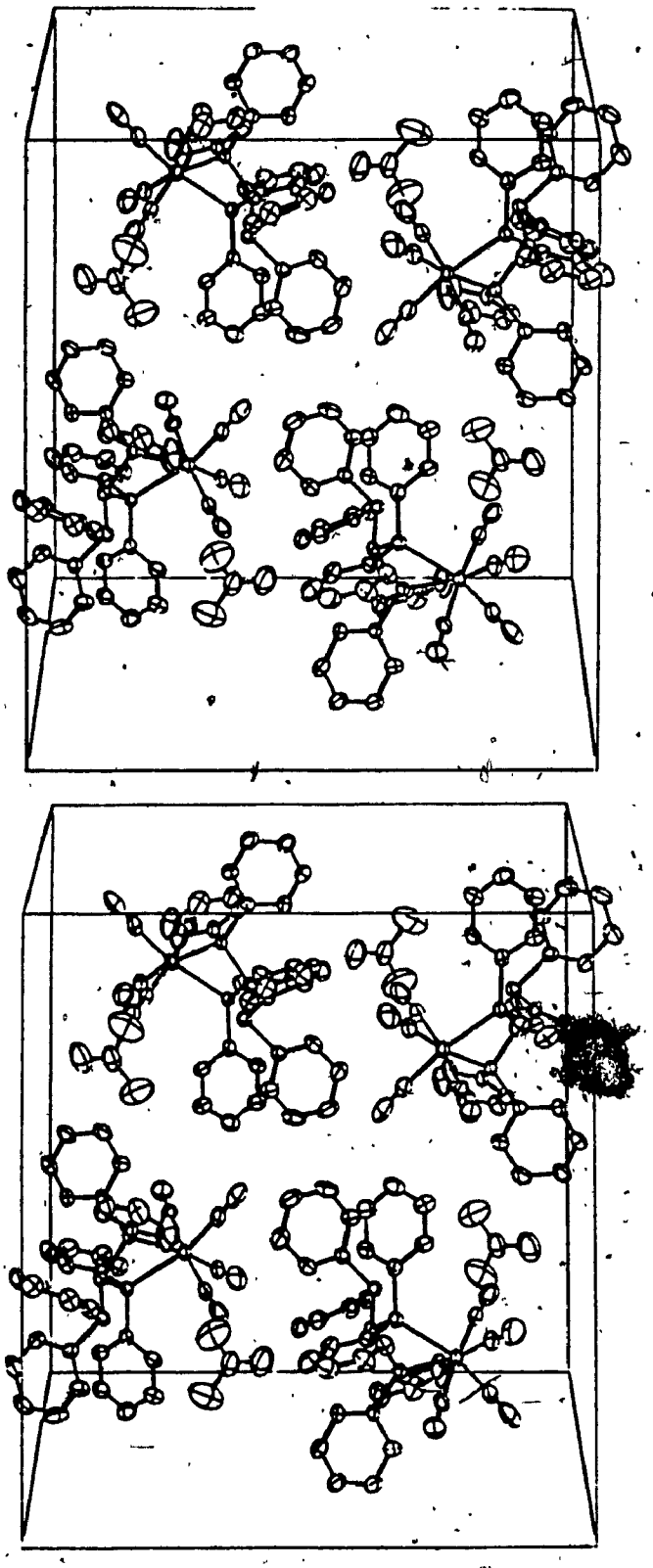

Table 5.2.1.2. Positional parameters for $Mo(CO)_4[HC(PPh_2)_3]$

ATOM	X	Y	Z	BISO
MO	0.23320(5)	0.23847(3)	-0.23172(3)	3.60(3)
P1	0.39460(16)	0.16669(8)	0.33472(8)	3.36(7)
P2	0.18569(16)	0.15584(8)	0.19408(8)	3.47(7)
P3	0.48104(16)	0.12029(9)	0.22185(9)	3.95(8)
O1	-0.0035(6)	0.3577(4)	0.1639(3)	8.0(4)
O2	0.3577(7)	0.3640(3)	0.3952(4)	8.3(4)
O3	0.0285(6)	0.2169(3)	0.3238(3)	6.1(4)
O4	0.4266(6)	0.3297(3)	0.2164(3)	6.4(4)
C1	0.0868(8)	0.3219(4)	0.2017(4)	4.8(4)
C2	0.3092(8)	0.3265(4)	0.3468(4)	5.4(4)
C3	0.1024(7)	0.2315(3)	0.3040(4)	4.5(3)
C4	0.3607(7)	0.3022(3)	0.2348(4)	4.8(4)
C5	0.3535(6)	0.1114(3)	0.2543(3)	3.3(3)
C111	0.5790(6)	0.1778(3)	0.3929(3)	3.5(3)
C112	0.6591(7)	0.1277(4)	0.4407(3)	4.3(3)
C113	0.7987(8)	0.1391(4)	0.4882(4)	5.5(4)
C114	0.8540(9)	0.1999(5)	0.4890(5)	6.6(6)
C115	0.7794(9)	0.2499(4)	0.4420(6)	7.0(7)
C116	0.6396(8)	0.2384(4)	0.3931(5)	5.5(5)
C121	0.3487(6)	0.1153(3)	0.3902(3)	3.7(3)
C122	0.3340(10)	0.1509(4)	0.4434(4)	7.5(6)
C123	0.3021(11)	0.1144(5)	0.4909(5)	9.2(7)
C124	0.2785(8)	0.0448(4)	0.4816(4)	6.6(4)
C125	0.2932(10)	0.0137(4)	0.4317(4)	7.6(7)
C126	0.3315(9)	0.0478(4)	0.3862(4)	6.3(5)
C211	0.0487(6)	0.1009(3)	0.1894(3)	3.8(3)
C212	0.9211(7)	0.1321(4)	0.1650(4)	5.6(4)
C213	0.8065(8)	0.0927(5)	0.1573(4)	6.8(5)
C214	0.8208(9)	0.0270(5)	0.1730(5)	7.6(6)
C215	0.9448(9)	-0.0031(5)	0.1973(5)	7.4(5)
C216	0.0622(8)	0.0326(4)	0.2063(4)	5.8(4)
C221	0.1530(6)	0.1536(3)	0.1019(3)	3.9(3)
C222	0.0803(7)	0.1000(4)	0.0556(4)	4.8(4)
C223	0.0549(8)	0.3956(4)	0.4852(4)	5.4(4)
C224	0.1035(8)	0.3475(5)	0.4606(4)	6.0(5)
C225	0.1729(9)	0.2058(5)	0.0060(4)	6.2(5)
C226	0.1977(7)	0.2055(4)	0.0753(4)	5.1(4)
C311	0.4138(6)	0.0576(3)	0.1488(3)	3.9(3)
C312	0.3625(8)	-0.0062(4)	0.1532(4)	5.4(4)
C313	0.6780(9)	0.4463(4)	0.4021(4)	6.3(4)
C314	0.6675(11)	0.4662(5)	0.4641(4)	7.8(6)
C315	0.3829(9)	0.0295(5)	0.0325(4)	7.2(6)
C316	0.4228(7)	0.0746(4)	0.0881(4)	5.2(4)
C321	0.6352(6)	0.0761(3)	0.2886(3)	3.9(3)
C322	0.6357(8)	0.0107(4)	0.3144(4)	5.2(4)
C323	0.2391(9)	0.4786(4)	0.1404(4)	5.7(4)
C324	0.8876(8)	0.0135(4)	0.3799(4)	6.1(5)
C325	0.8867(7)	0.0768(5)	0.3579(4)	5.9(5)
C326	0.7597(7)	0.1091(4)	0.3103(4)	5.0(4)
C1'	0.6935(10)	0.3547(5)	0.2020(6)	8.4(7)
O'	0.6607(10)	0.4125(4)	0.1968(6)	13.3(8)
C2'	0.7700(15)	0.3257(11)	0.2695(8)	14.5(17)
C3'	0.6453(19)	0.3094(11)	0.1364(9)	16.9(17)

Table 5.2.1.3. Thermal Parameters for $Mo(CO)_4[HC(PPh_2)_3]$

ATOM	U11	U22	U33	U12	U13	U23
MO	4.77(3)	3.48(3)	5.42(3)	-0.36(2)	2.75(3)	-0.28(2)
P1	4.53(9)	3.58(8)	4.65(8)	0.17(7)	2.43(7)	0.27(7)
P2	4.14(8)	4.09(9)	4.94(9)	0.19(7)	2.60(7)	0.35(7)
P3	4.54(9)	4.86(10)	5.60(10)	0.10(7)	3.12(8)	0.57(7)
O1	9.6(5)	11.0(5)	9.9(5)	2.4(4)	2.4(4)	2.6(4)
O2	12.0(5)	10.2(5)	13.2(6)	-3.1(4)	6.5(5)	-6.4(4)
O3	9.3(4)	9.4(4)	12.1(5)	-0.6(4)	8.1(4)	-0.6(4)
O4	10.0(4)	8.9(4)	12.9(5)	-1.1(3)	8.0(4)	1.9(4)
C1	6.6(4)	4.8(4)	6.9(4)	0.4(3)	2.8(4)	0.4(3)
C2	6.9(5)	5.1(4)	8.5(5)	-0.7(4)	4.2(4)	-1.2(4)
C3	5.9(4)	4.8(4)	6.4(4)	0.4(3)	3.5(4)	-0.7(3)
C4	6.5(4)	4.7(4)	7.1(5)	-0.1(3)	3.5(4)	0.9(3)
C5	4.1(3)	4.1(3)	4.5(3)	0.3(3)	2.3(3)	0.1(3)
C111	4.7(3)	3.8(3)	4.8(3)	-0.3(3)	1.7(3)	0.1(3)
C112	5.0(4)	6.2(4)	5.3(4)	-0.3(3)	1.5(3)	0.6(3)
C113	6.5(5)	7.3(5)	6.9(5)	-1.0(4)	1.4(4)	1.3(4)
C114	6.7(5)	9.9(7)	8.4(6)	-2.3(5)	0.1(4)	0.9(5)
C115	6.1(5)	6.3(5)	14.3(9)	-1.2(4)	1.0(6)	2.1(5)
C116	5.2(4)	5.2(4)	10.4(6)	-1.6(3)	1.2(4)	0.9(4)
C121	4.7(3)	4.3(3)	4.8(3)	0.2(3)	2.6(3)	0.3(3)
C122	13.8(8)	7.1(5)	7.6(5)	1.1(5)	7.5(6)	0.9(4)
C123	16.2(9)	7.9(6)	10.8(7)	2.6(6)	10.6(7)	2.7(5)
C124	8.8(6)	7.6(5)	8.5(5)	0.7(4)	6.0(5)	2.1(4)
C125	14.3(9)	5.8(5)	8.8(6)	-2.0(5)	7.3(6)	0.9(4)
C126	11.7(7)	4.5(4)	7.7(5)	-1.1(4)	6.1(5)	-0.4(4)
C211	4.1(3)	5.4(4)	5.0(4)	-1.0(3)	2.4(3)	-0.6(3)
C212	5.5(4)	7.2(5)	8.5(5)	-0.5(4)	3.9(4)	-1.4(4)
C213	5.8(5)	10.8(7)	9.4(6)	-1.7(5)	4.4(4)	-2.9(5)
C214	7.5(5)	11.6(7)	9.9(6)	-3.7(5)	5.9(5)	-2.3(5)
C215	8.7(6)	8.6(6)	10.9(7)	-3.1(5)	5.3(6)	1.2(5)
C216	6.9(5)	6.5(5)	8.7(5)	-0.6(4)	3.8(4)	1.6(4)
C221	3.9(3)	4.5(4)	6.3(4)	0.4(3)	2.9(3)	0.5(3)
C222	6.1(4)	6.7(5)	5.4(4)	-0.1(4)	3.2(3)	-0.3(3)
C223	7.0(5)	7.8(5)	5.8(4)	-0.6(4)	3.1(4)	0.1(4)
C224	7.3(5)	9.4(6)	6.2(5)	-2.3(5)	3.2(4)	-2.2(4)
C225	8.3(5)	8.7(6)	6.7(5)	0.1(5)	4.2(4)	1.5(4)
C226	7.0(5)	6.6(5)	5.8(4)	0.7(4)	3.7(4)	1.5(4)
C311	4.2(3)	5.5(4)	5.0(4)	0.6(3)	2.7(3)	0.0(3)
C312	7.5(5)	6.7(5)	6.5(5)	0.4(4)	3.7(4)	-1.3(4)
C313	8.8(6)	7.4(6)	7.9(5)	-1.2(5)	3.1(5)	1.5(4)
C314	12.3(8)	10.5(7)	6.8(5)	-3.0(6)	4.7(5)	1.9(5)
C315	8.6(6)	12.5(8)	6.3(5)	3.1(5)	4.5(5)	-0.0(5)
C316	5.4(4)	8.6(5)	5.9(4)	3.0(4)	3.4(3)	1.6(4)
C321	5.1(3)	4.2(3)	5.5(4)	0.7(3)	3.2(3)	0.4(3)
C322	6.9(5)	6.4(5)	6.4(4)	1.4(4)	3.6(4)	0.7(4)
C323	8.5(5)	5.7(5)	7.6(5)	-1.2(4)	3.6(4)	0.4(4)
C324	6.0(5)	8.5(6)	8.8(6)	1.6(4)	3.2(4)	1.0(5)
C325	5.4(4)	8.7(6)	8.3(6)	0.4(4)	2.3(4)	0.9(4)
C326	4.3(4)	7.1(5)	7.7(5)	0.1(3)	3.2(4)	0.6(4)
C1'	9.8(7)	7.4(6)	14.6(9)	0.3(5)	7.5(7)	1.6(6)
O'	17.2(8)	10.8(6)	22.6(10)	0.3(6)	13.4(8)	3.1(6)
C2'	12.6(11)	26.8(21)	15.7(13)	5.8(13)	4.2(10)	9.3(13)
C3'	20.6(17)	25.7(21)	17.7(14)	-4.6(16)	12.2(14)	-7.3(14)

TEMP=-2(PI)**2(U11*H*H*ASTAR*ASTAR+---+2*U12*H*K*ASTAR*BSTAR+---)

THE UIJ VALUES HAVE BEEN MULTIPLIED BY 100.

Table 5.2.1.4. Selected Interatomic Distances for $Mo(CO)_4[HC(PPh_2)_3]$

Mo - P1	2.486(2)	P2 - C5	1.874(6)
Mo - P2	2.507(2)	P2 - C211	1.817(6)
Mo - P3	4.332(2)	P2 - C221	1.819(6)
Mo - C1	1.946(7)	P3 - C5	1.852(6)
Mo - C2	1.942(7)	P3 - C311	1.836(6)
Mo - C3	2.018(7)	P3 - C321	1.818(6)
Mo - C4	2.025(7)	C1 - O1	1.163(9)
P1 - C5	1.891(6)	C2 - O2	1.165(9)
P1 - C111	1.804(6)	C3 - O3	1.121(8)
P1 - C121	1.805(6)	C4 - O4	1.117(8)

E.S.D.'s ( ) refer to the last digit printed.

Table 5.2.1.5. Selected Internal Angles for $Mo(CO)_4[HC(PPh_2)_3]$

Mo - P1 - C5	97.20(.19)	C1 - Mo - C2	94.82(.32)
Mo - P2 - C5	96.96(.19)	C1 - Mo - C3	87.95(.30)
Mo - C1 - O1	176.89(.68)	C1 - Mo - C4	88.37(.29)
Mo - C2 - O2	177.89(.72)	C2 - Mo - C3	87.30(.29)
Mo - C3 - O3	172.83(.61)	C2 - Mo - C4	87.90(.30)
Mo - C4 - O4	174.28(.63)	C3 - Mo - C4	173.70(.27)
P1 - Mo - P2	67.06(.08)	C5 - P1 - C111	112.68(.27)
P1 - C5 - P2	94.23(.26)	C5 - P1 - C121	104.72(.27)
P1 - C5 - P3	113.28(.30)	C5 - P2 - C211	105.95(.29)
P2 - C5 - P3	111.90(.30)	C5 - P2 - C221	109.83(.26)
P1 - Mo - C1	186.46(.22)	C5 - P3 - C311	100.85(.27)
P1 - Mo - C2	96.53(.24)	C5 - P3 - C321	104.49(.27)
P1 - Mo - C3	90.51(.20)	C111 -P1- C121	101.35(.28)
P1 - Mo - C4	94.10(.20)	C211 -P2- C221	101.81(.28)
P2 - Mo - C1	101.55(.22)	C311 -P3- C321	100.37(.28)
P2 - Mo - C2	163.55(.24)		
P2 - Mo - C3	91.68(.19)		
P2 - Mo - C4	94.07(.21)		

E.S.D.'s ( ) refer to the last digit printed.

5.2.2. CRYSTAL AND MOLECULAR STRUCTURE OF $Mo(CO)_2Cl(\eta^3\text{-allyl})[HC(PPh_2)_3]$ 5

A brilliant orange crystal was mounted on the goniometer in a preferred orientation to facilitate alignment of the reciprocal lattice zones. Preliminary Weissenberg and precession photography allowed unambiguous assignment of the space group as P $2_1/c$. Goniometer arcs were reset to Weissenberg positions and the assembly was mounted on the diffractometer. Automatic alignment of nineteen well-spaced reflections throughout reciprocal space permitted calculation of a least-squares refined orientation matrix from which unit cell dimensions were calculated. (Table 5.2.2.1.)

Table 5.2.2.1. Unit Cell Dimensions (A,"O") with e.s.d.'s.

a = 13.93862	b = 18.19383	c = 15.47242
σ(a) = 0.010558	σ(b) = 0.0112862	σ(c) = 0.0092620
α = 90.207	β = 106.689	γ = 90.022
$\sigma(\alpha)$ = 0.052	$\sigma(\beta)$ = 0.055	$\sigma(\gamma)$ = 0.058

Intensity data collection was driven by the program DIFFRAC.[47] Three reference reflections { 6 0 0, 0 7 1, 0 0 6 } were monitored every 50 reflections which varied less than $\pm$ 5% over the acquisition period. 4879 reflections were measured in the order hkl and $\bar{h}$kl of which 3612 were considered observed. The data were reduced using the

program DATRD2[47] and the Molybdenum atom was located by solving the Patterson. It was edited into the cell using the program CDEDIT.[47] A structure factor calculation and three isotropic refinement cycles in which the thermal parameters were not refined were performed using the program LSTSQ.[47] Three more isotropic refinement cycles were performed with refinement of the thermal parameter. This yielded an R-factor of 0.5954. This was followed by a difference Fourier synthesis from which four peaks were identified as C1, P1, P2, and P3. These were edited into the cell and three more isotropic refinements were performed. The R-factor decreased to 0.4327. Another difference Fourier followed by a geometry calculation permitted location of all remaining non-hydrogen atoms. These were edited into the cell and six isotropic cycles of least squares refinement reduced the R-factor to 0.1488. The phenyl carbon C123 seemed an erroneous peak assignment and hence a structure factor calculation without this atom was performed. A difference Fourier at this point revealed the true position of the incorrectly assigned C123 and it was edited into the cell. Six more isotropic refinements were then performed bringing the R-factor down to 0.1130. The coordination sphere was then permitted to refine anisotropically for three cycles bringing the R-factor down to 0.1057. The whole structure was then permitted to refine anisotropically for three block-diagonalized least-squares cycles dropping the R-factor down to 0.0933. A final diffe-

rence Fourier exhibited no significant residual electron density. Nine more cycles of refinement yielded the final residual indices: $R = 0.0578$ and $R_w = 0.0969$. The G.O.F. was 1.7025. Hydrogen atoms were not edited into idealized positions.

Molecular structure diagrams were performed using ORTEP[52] (Figs. 5.2.2.1. - 5.2.2.3) Positional and thermal parameters are listed in Tables 5.2.2.2. and 5.2.2.3 respectively. Selected interatomic distances and bond angles are listed in Tables 5.2.2.4. and 5.2.2.5.

Fig. 5.2.2.1. Perspective view of the chloro-allyl complex.

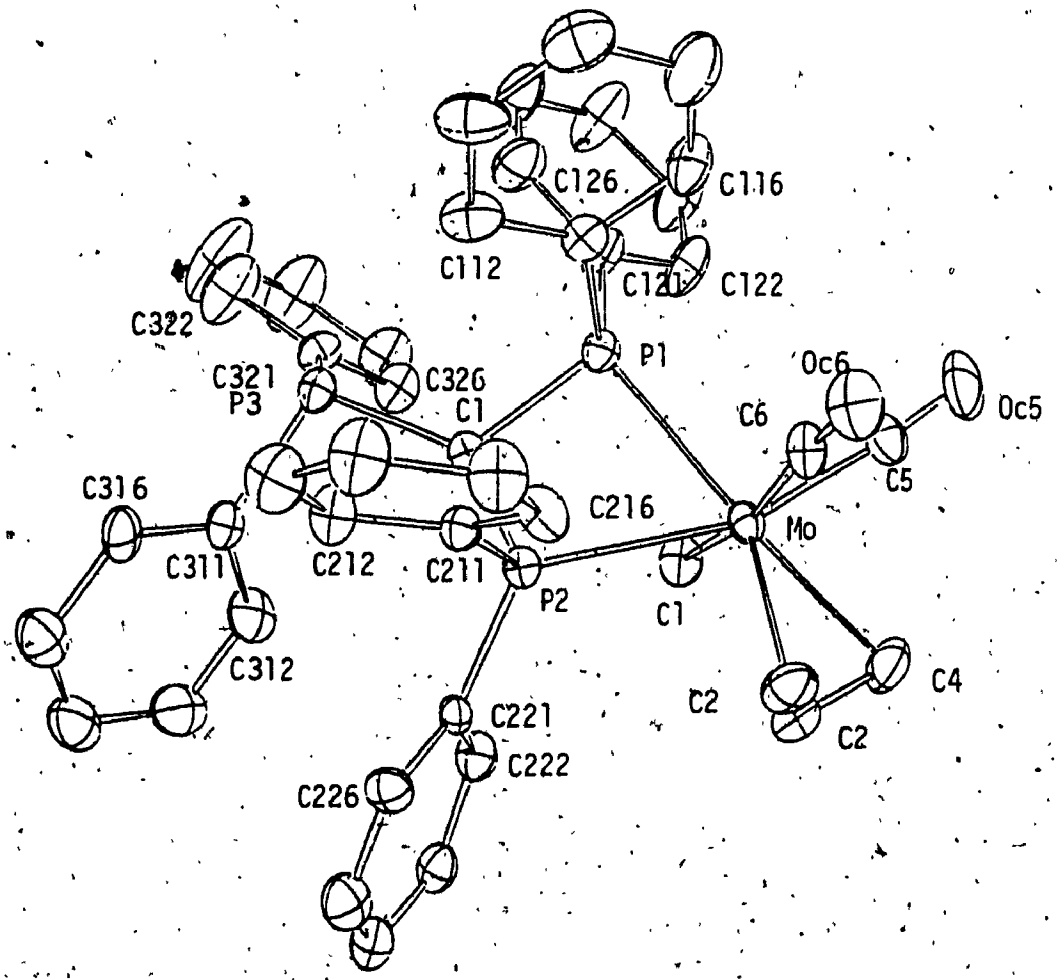

Fig. 5.2.2.2. Stereo view of formula unit.

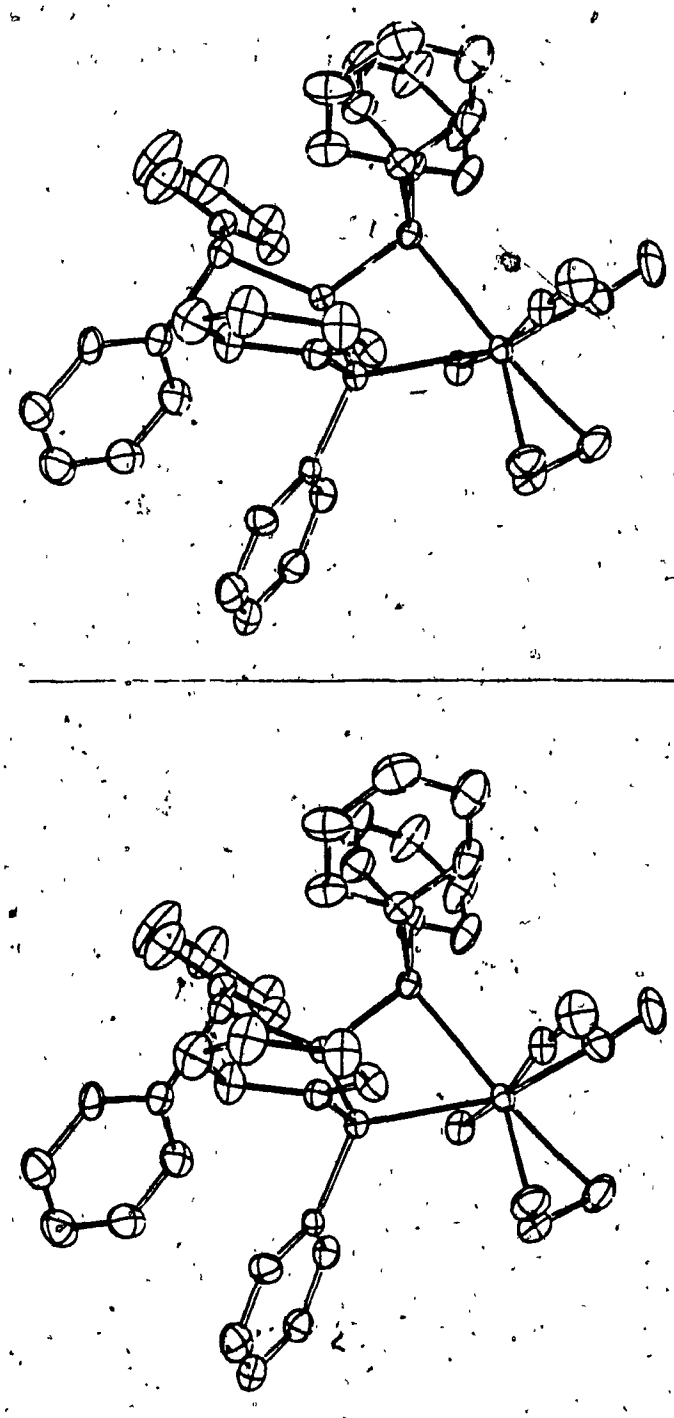

Fig. 5.2.2.3. Stereo packing diagram.

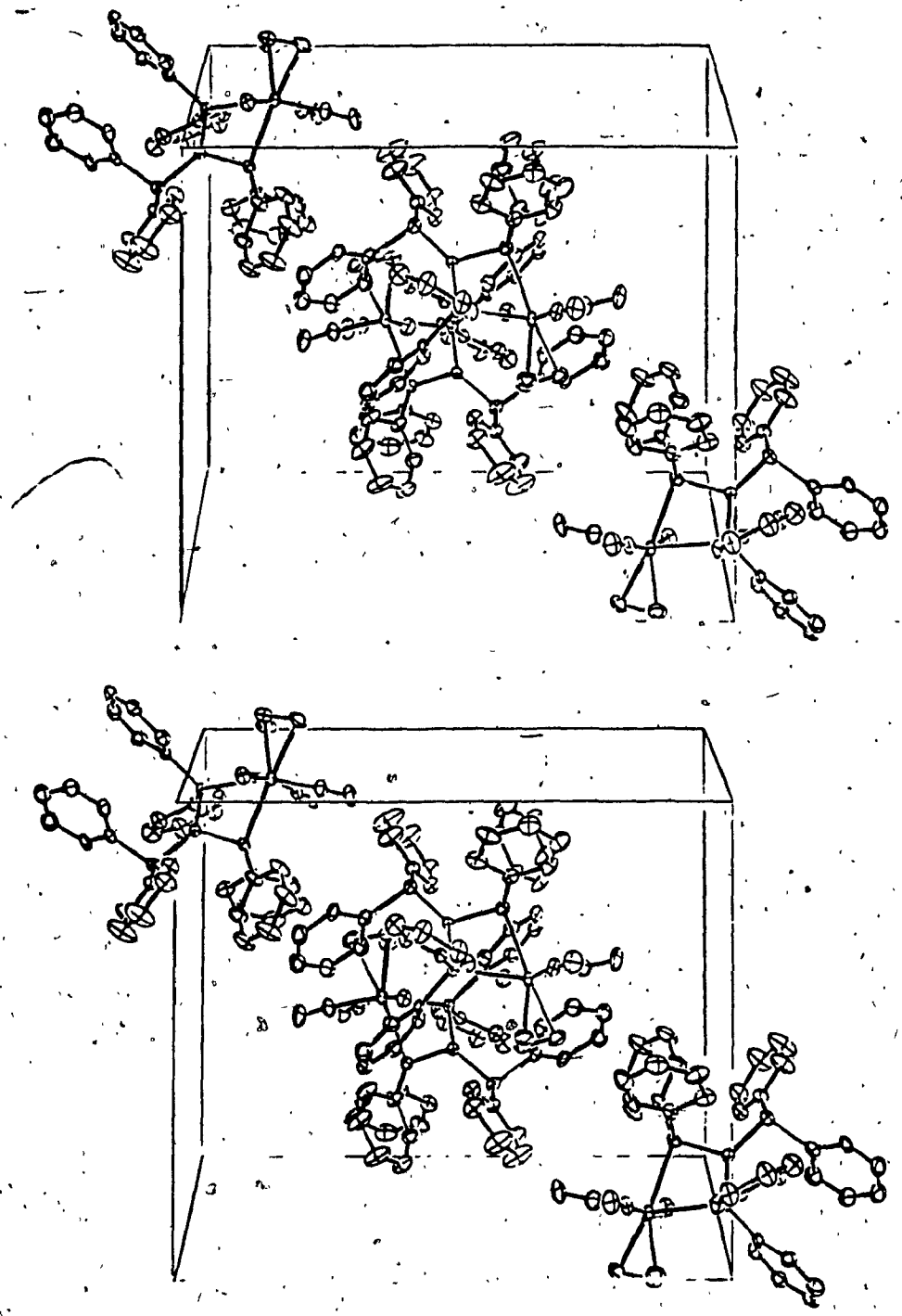

Table 5.2.2.2. Positional Parameters for $Mo(CO)_2Cl(\pi\text{-allyl})[HC(PPh_2)_3]$

ATOM	X	Y	Z	RISO
MO	0.22742(4)	0.14027(3)	-0.07727(3)	2.506(25)
CL	0.40983(12)	0.40291(10)	0.45894(12)	3.53(8)
P1	0.22632(12)	0.40723(9)	0.26946(11)	2.63(7)
P2	0.82521(11)	-0.00440(9)	0.10966(10)	2.39(7)
P3	0.75801(12)	0.08129(10)	0.27432(11)	2.80(8)
C1	0.7539(4)	0.0052(3)	0.1932(4)	2.2(3)
C2	0.2412(7)	0.1289(5)	0.0695(5)	4.7(4)
C3	0.1391(7)	0.1294(5)	0.0288(5)	5.2(5)
C4	0.2926(7)	0.1953(5)	0.0656(5)	5.3(5)
C5	0.2701(6)	0.2589(4)	0.4073(5)	4.1(4)
C6	0.0981(5)	0.3145(4)	0.3722(5)	3.6(3)
OC5	0.2883(5)	0.1990(3)	0.3931(5)	7.0(4)
OC6	0.0258(4)	0.2820(3)	0.3450(4)	5.1(3)
C111	0.1091(5)	0.3949(4)	0.1794(4)	3.2(3)
C112	0.0461(5)	0.4531(5)	0.1338(5)	4.2(5)
C113	0.9605(6)	0.4340(6)	0.0661(5)	5.5(6)
C114	0.9384(6)	0.3628(5)	0.0411(6)	5.6(6)
C115	0.0001(6)	0.3053(5)	0.0876(6)	5.9(5)
C116	0.0837(5)	0.3223(4)	0.1535(5)	4.2(4)
C121	0.3169(5)	0.3848(4)	0.2094(5)	3.7(4)
C123	0.4630(6)	0.3220(6)	0.1980(6)	6.3(6)
C122	0.3932(5)	0.3350(5)	0.2469(5)	4.6(4)
C124	0.4541(7)	0.3536(6)	0.1169(6)	6.9(7)
C125	0.3727(7)	0.4006(5)	0.0776(6)	6.5(6)
C126	0.3048(6)	0.4151(5)	0.1235(5)	5.1(5)
C211	0.9560(5)	0.0192(3)	0.1662(4)	2.8(3)
C212	0.9808(5)	0.0865(4)	0.2088(5)	3.8(3)
C213	0.0775(6)	0.1052(5)	0.2550(6)	5.2(5)
C214	0.1534(6)	0.0546(5)	0.2566(6)	5.1(5)
C215	0.1286(6)	-0.0138(5)	0.2109(6)	4.8(5)
C216	0.9697(5)	0.4709(4)	0.3345(5)	3.4(3)
C221	0.7822(4)	0.0640(3)	0.0212(4)	2.5(3)
C222	0.6844(5)	0.4363(4)	0.4713(4)	3.4(3)
C223	0.6499(5)	0.3873(4)	0.3989(5)	3.9(4)
C224	0.7160(6)	0.3371(4)	0.3779(5)	4.0(4)
C225	0.8150(6)	0.3377(4)	0.4305(5)	4.4(4)
C226	0.8474(5)	0.1149(4)	-0.0011(5)	3.4(3)
C311	0.7382(5)	0.1631(4)	0.2025(4)	3.1(3)
C312	0.6549(5)	0.1712(4)	0.1243(5)	4.0(4)
C313	0.6443(7)	0.2350(5)	0.0750(6)	5.3(5)
C314	0.7134(8)	0.2916(5)	0.1015(6)	6.3(6)
C316	0.8065(5)	0.2188(4)	0.2290(5)	4.0(3)
C315	0.7946(6)	0.2849(4)	0.1783(6)	5.2(4)
C321	0.6342(5)	0.0772(4)	0.2912(4)	3.4(3)
C322	0.6222(6)	0.1192(6)	0.3594(6)	6.6(6)
C323	0.5300(9)	0.1245(8)	0.3796(8)	10.0(10)
C324	0.4521(7)	0.0872(7)	0.3293(8)	8.2(8)
C325	0.4592(6)	0.0435(5)	0.2563(6)	5.3(5)
C326	0.5504(5)	0.0405(4)	0.2377(5)	3.8(4)

Table 5.2.2.3. Thermal Parameters for

$Mo(CO)_2Cl(\pi\text{-allyl})[HC(PPh_2)_3]$

ATOM	U11	U22	U33	U12	U13	U23
MO	3.04(3)	2.79(3)	3.69(3)	-0.19(2)	0.64(3)	-0.05(2)
CL	3.02(8)	5.07(10)	5.31(10)	0.24(7)	0.16(8)	-0.48(8)
P1	3.04(9)	3.46(9)	3.51(9)	-0.08(7)	0.58(7)	-0.56(7)
P2	2.64(8)	2.96(9)	3.46(8)	-0.05(7)	0.80(7)	-0.11(7)
P3	2.98(9)	3.87(10)	3.78(9)	0.14(7)	0.52(7)	-0.61(7)
C1	2.1(3)	3.4(3)	3.0(3)	0.1(3)	0.8(3)	-0.0(3)
C2	7.6(6)	6.4(5)	4.0(4)	-0.0(4)	1.8(4)	-0.6(4)
C3	6.9(5)	7.7(6)	5.2(5)	-2.0(5)	3.2(4)	-0.9(4)
C4	8.3(6)	6.7(6)	5.1(4)	-1.7(5)	1.9(4)	-2.5(4)
C5	5.0(5)	4.5(4)	6.1(5)	0.5(4)	0.9(4)	0.5(4)
C6	4.3(4)	3.6(4)	5.9(4)	0.0(3)	1.4(3)	-0.8(3)
OC5	11.8(5)	3.8(3)	11.2(5)	2.3(3)	4.3(4)	-0.5(3)
OC6	4.2(3)	6.4(4)	8.9(4)	-2.1(3)	0.9(3)	-1.1(3)
C111	3.4(4)	4.8(4)	4.0(4)	-0.4(3)	1.1(3)	-0.5(3)
C112	2.9(4)	8.3(6)	4.8(4)	-0.7(4)	0.0(3)	0.5(4)
C113	5.1(5)	10.7(7)	5.1(5)	-0.6(5)	0.3(4)	2.1(5)
C114	4.8(5)	10.7(8)	5.7(5)	-1.2(5)	0.0(4)	-0.7(5)
C115	6.4(6)	8.3(7)	7.9(6)	-2.3(5)	2.1(5)	-3.1(5)
C116	4.2(4)	5.7(5)	6.0(5)	-1.1(4)	-0.1(4)	-2.5(4)
C121	3.8(4)	5.6(4)	4.5(4)	-1.2(3)	1.4(3)	-2.4(3)
C123	4.0(5)	11.0(8)	9.0(6)	-0.1(5)	1.6(4)	-5.6(6)
C122	3.4(4)	8.0(6)	6.1(5)	0.8(4)	0.9(4)	-3.6(4)
C124	5.8(6)	12.6(9)	7.8(6)	-2.8(5)	3.0(5)	-5.9(6)
C125	8.3(7)	9.5(7)	7.0(6)	-2.4(5)	4.2(5)	-4.2(5)
C126	6.3(5)	7.6(6)	5.5(5)	-0.9(4)	3.0(4)	-1.2(4)
C211	3.1(3)	3.9(4)	3.5(3)	-0.4(3)	0.5(3)	-0.1(3)
C212	3.3(4)	4.8(4)	6.2(4)	-0.3(3)	1.6(3)	-1.2(3)
C213	4.5(5)	7.6(6)	7.7(6)	-1.5(4)	1.0(4)	-1.1(5)
C214	3.2(4)	7.3(6)	8.7(6)	-0.3(4)	0.2(4)	-1.9(5)
C215	3.5(4)	6.5(5)	8.4(6)	0.4(4)	0.6(4)	-0.9(4)
C216	2.6(3)	4.3(4)	6.1(4)	-0.8(3)	0.6(3)	0.5(3)
C221	3.7(3)	2.5(3)	3.2(3)	-0.4(3)	0.5(3)	-0.2(3)
C222	3.6(4)	4.4(4)	4.9(4)	-0.1(3)	0.7(3)	-0.8(3)
C223	4.8(4)	5.4(4)	4.9(4)	-0.1(4)	1.8(3)	-0.8(3)
C224	5.5(5)	4.4(4)	5.3(4)	-0.4(4)	1.5(4)	-1.2(4)
C225	5.2(5)	5.1(4)	6.6(5)	1.0(4)	2.3(4)	-0.3(4)
C226	4.0(4)	4.7(4)	4.4(4)	-0.7(3)	1.5(3)	0.2(3)
C311	3.3(3)	3.7(4)	4.6(4)	0.8(3)	1.7(3)	-0.8(3)
C312	4.4(4)	4.6(4)	6.4(5)	1.4(4)	1.0(4)	-0.1(4)
C313	7.3(6)	6.7(6)	6.3(5)	2.4(5)	2.3(4)	0.8(4)
C314	10.7(7)	5.1(5)	8.3(6)	1.6(5)	5.3(6)	0.6(4)
C316	5.2(4)	3.6(4)	6.2(4)	-0.1(3)	3.2(4)	-1.5(3)
C315	7.2(5)	4.7(5)	7.9(5)	0.5(4)	4.2(5)	-0.1(4)
C321	3.8(4)	5.3(4)	3.7(4)	0.2(3)	0.9(3)	-0.2(3)
C322	5.1(5)	11.7(8)	8.5(7)	-1.3(5)	3.4(5)	-4.6(6)
C323	8.2(7)	18.6(13)	11.0(9)	-4.1(8)	4.6(7)	-9.1(9)
C324	4.7(5)	14.9(10)	11.4(8)	-2.5(6)	4.4(6)	-5.9(8)
C325	3.9(4)	8.4(6)	7.8(6)	-0.2(4)	2.2(4)	-1.5(5)
C326	3.6(4)	5.7(5)	5.3(4)	0.2(3)	1.1(3)	-0.9(4)

TEMP=-2(PI)**2(U11*H*H*ASTAR*ASTAR+---+2*U12*H*K*ASTAR*BSTAR+---)

Table 5.2.2.4. Selected Interatomic Distances for $Mo(CO)_2Cl(\pi\text{-allyl})[HC(PPh_2)_3]$

Mo - Cl	2.574(8)	P1 - C121	1.801(9)
Mo - P1	2.503(11)	P2 - C1	1.832(9)
Mo - P2	2.593(19)	P2 - C211	1.845(9)
Mo - P3	5.083(27)	P2 - C221	1.822(10)
Mo - C2	2.218(13)	P3 - C1	1.855(11)
Mo - C3	2.301(11)	P3 - C311	1.831(13)
Mo - C4	2.358(13)	P3 - C321	1.815(8)
Mo - C5	1.965(16)	C2 - C3	1.391(14)
Mo - C6	1.942(9)	C2 - C4	1.416(15)
P1 - C1	1.872(15)	C5 - OC5	1.156(12)
P1 - C111	1.845(11)	C6 - OC6	1.145(9)

E.S.D.'s ( ) refer to the last digit printed

Table 5.2.2.5. Selected Internal Angles for $Mo(CO)_2Cl(\ -allyl)[HC(PPh_2)_3]$

Mo - P1 - C1	94.56(.37)	Cl - Mo - C3	120.52(.38)
Mo - P2 - C1	92.63(.23)	Cl - Mo - C4	79.66(.44)
Mo - C2 - C3	75.36(.59)	Cl - Mo - C5	89.89(.36)
Mo - C2 - C4	77.46(.49)	Cl - Mo - C6	166.26(.21)
Mo - C5 - OC5	174.65(.70)	C2 - Mo - C3	35.37(.39)
Mo - C6 - OC6	173.89(.62)	C2 - Mo - C4	35.89(.40)
P1 - C1 - P2	93.47(.31)	C2 - Mo - C5	105.31(.47)
P1 - C1 - P3	122.21(.52)	C2 - Mo - C6	105.10(.47)
P2 - C1 - P3	128.09(.39)	C5 - Mo - C6	80.45(.43)
P1 - Mo - P2	63.90(.16)	C3 - C2 - C4	116.37(.80)
P1 - Mo - Cl	81.42(.39)	C1 - P1 - C111	111.89(.31)
P2 - Mo - Cl	87.75(.29)	C1 - P1 - C121	107.92(.31)
P1 - Mo - C2	154.04(.31)	C111 -P1- C121	100.97(.43)
P2 - Mo - C2	97.74(.28)	C1 - P2 - C211	107.66(.42)
P1 - Mo - C5	97.75(.36)	C1 - P2 - C221	109.01(.39)
P2 - Mo - C5	161.64(.27)	C211 -P2- C221	105.93(.46)
P1 - Mo - C6	90.18(.45)	C1 - P3 - C311	103.50(.60)
P2 - Mo - C6	98.34(.40)	C1 - P3 - C321	101.97(.39)
Cl - Mo - P3	71.87(.30)	C311 -P3- C321	97.23(.38)
Cl - Mo - C2	86.74(.45)		

E.S.D.'s ( ) refer to the last digit printed.

5.3.1. CRYSTAL AND MOLECULAR STRUCTURE OF $RhCo_3(CO)_9[HC(PPh_2)_3]$

A dark purple crystal of the complex was mounted within a fine lithium borate capillary using "5 minute epoxy. The crystal was oriented such that the long edge of the crystal ran parallel to the capillary axis. Preliminary reciprocal lattice photography revealed no systematic absences for six reciprocal lattice zones. The space group was assigned tentatively as $P\bar{1}$. The goniometer was mounted on the diffractometer after resetting the head arcs to the Weissenberg positions. Initial orientation matrix and least-squares refinement from alignment of fifteen axial reflections and their Friedel equivalents gave unit cell parameters tabulated in Table 5.3.1.1.

Table 5.3.1.1. Unit Cell Dimensions (A, "O") with e.s.d.'s.

a = 14.58287	b = 21.50459	c = 17.25984
σ(a) = 0.008670	σ(b) = 0.016129	σ(c) = 0.011665
α = 90.348	β = 114.701	γ = 103.351
$\sigma(\alpha)$ = 0.064	$\sigma(\beta)$ = 0.049	$\sigma(\gamma)$ = 0.057

Data collection was driven by program DIFFRAC[47]. Three reference reflections, { 9,0,0; 0,0,10; 0,8,0 }, were measured every 47 reflections for the duration of data acquisition. Out of 8840 independent reflections measured over the range $3.5^\circ < 2\theta < 40^\circ$, 5529 were found to be greater

than 3 I. Four segments were collected in the order: hkl, $h\bar{k}l$, $hk\bar{l}$ and $\bar{h}kl$.

Although a relatively large data collection was performed the low 2θ-limit (3.5^{o}) may have not permitted some strong, structurally significant reflections to have been recorded. Also, a relative decrease in the intensities of the standard reflections of up to 50% over the period of data collection (attributed to sample decomposition) was observed.

Data reduction was accomplished using the program DATRD2[47]. Lorentz and polarization corrections were applied but no correction was applied for absorption. The data were scaled in linear segments, grouped, reduced and normalized.

The data were statistically phased using MULTAN.[40] Trial solution of the structure by a three dimensional Patterson synthesis yielded no simple assignments of the heavy atoms. The best solution set from MULTAN by the criteria outlined in Sec. 4.2.6. yielded an E-map which duplicated the Patterson, differing only in the choice of origin.

The next best MULTAN solution set produced an E-map with the first six peaks possessing significantly higher intensities than the rest, that the first two peaks were assigned to Rhodium atoms and the next four were assigned as Cobalt atoms. A structure factor calculation followed editing these atoms into the cell. Three cycles

of isotropic least squares followed by applying UNIMOL,[47] a program used to find unique molecular fragments in the asymmetric unit, indicated two molecules to be present in the asymmetric unit. PLTMOL[47] was used to plot the electron density in stereo projection. This revealed two formula units which seemed at this point to be quite similar.

Although the presence of false peaks obscured the plot each formula unit appeared to contain a tetrahedral metal skeleton with the outline of the TRIPOD ligand capping one triangular face containing a Rhodium atom. A difference Fourier followed by the plotting procedure above revealed a clearer view of the skeleton as well as the phosphino functions, partial phenyl rings and several carbonyl groups in bridging and terminal positions. Identified atoms were edited into the cell file and three more cycles of full-matrix least squares refinement dropped the residual index to about 0.30. Another difference Fourier allowed most non-hydrogen atoms to be identified. These too were edited into the cell file at which point the asymmetric unit could be identified as two tetranuclear mixed-metal carbonyl clusters with a Rhodium-containing triangular face triply coordinated by the TRIPOD ligand. Three more least squares cycles of full matrix refinement were performed while permitting the metal skeleton to refine anisotropically. This brought the residual index down to just above 0.20. Inspection of the metal thermal parameters indicated anomalous behavior. The occupancies of these atoms were

permitted to refine inthe three subsequent completely anisotropic full-matrix least squares cycles bringing the R-factor to ≅ 0.17. A check of the occupancies indicated there were indeed three Cobalt atoms and one Rhodium atom contained in the skeleton, however, their locations from one cell to the next were not unique. The Rhodium atom is always in one of the three basal positions of the Tripod capped tetrahedron and the apical metal is always Cobalt. A final difference synthesis permitted location of all atoms except for two terminal carbonyl carbons in Molecule 1. These are the carbons labelled Ct3 and Ct6 in Fig. 5.3.1.2.

The final residual index was calculated to be 0.1559. A stereo projection is provided in Fig. 5.3.1.1. and the labelled formula unit is shown in Fig. 5.3.1.2. Positional and thermal parameters are tabulated in tables 5.3.1.2. and 5.3.1.3. respectively. Table 5.3.1.4. contains selected interatomic distances and Table 5.3.1.5. contains selected bond angles obtained from the program DISPOW.[47]

Fig. 5.3.1.1. Stereo view of the asymmetric unit.

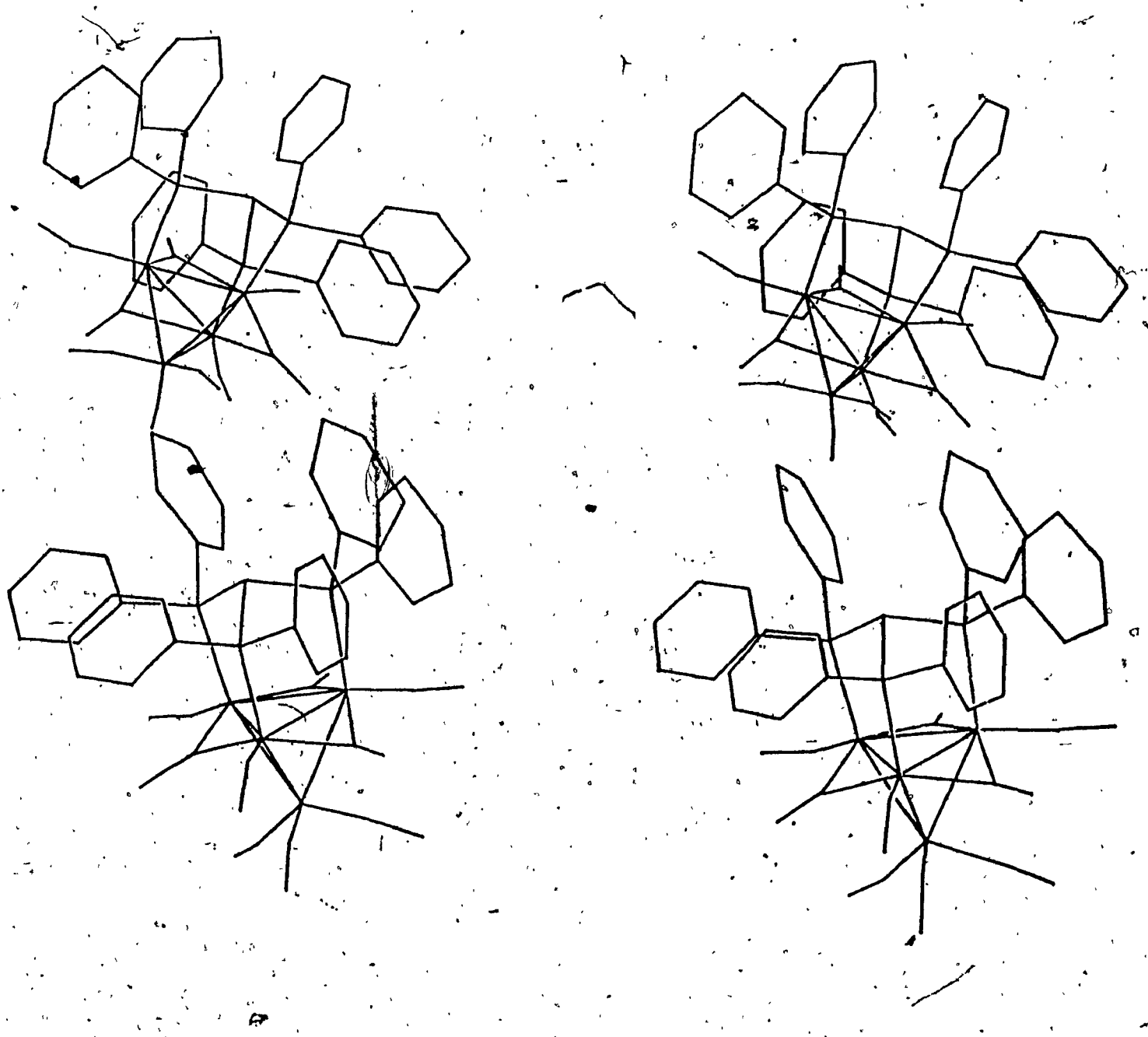

Fig. 5.3.1.2. Labelled asymmetric unit.

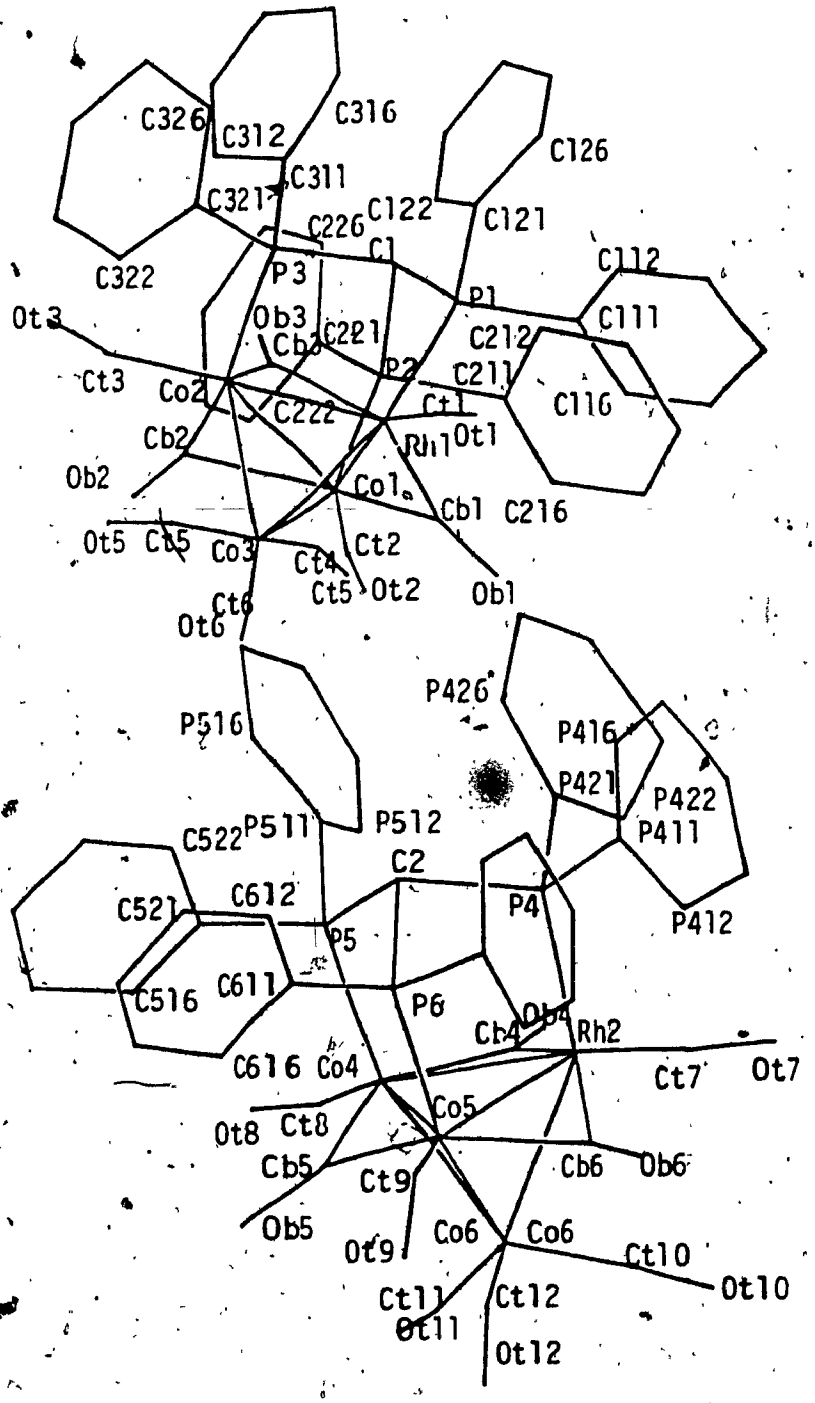

Table 5.3.1.2. Positional Parameters for

$RhCo_3(CO)_9[HC(PPh_2)_3]$

TABLE . ATOMIC PARAMETERS X, Y, Z AND BEQ.
E.S.DS. REFER TO THE LAST DIGIT PRINTED.

	X	Y	Z	BEQ
Rh1	0.1867 (4)	0.66255(24)	0.4339 (3)	3.0 (3)
Co1	0.2849 (4)	0.57174(23)	0.4920 (3)	4.3 (3)
Co2	0.3725 (3)	0.67129(22)	0.4352 (3)	4.3 (3)
Co3	0.2094 (6)	0.5863 (3)	0.3299 (4)	7.0 (5)
P1	0.2587 (10)	0.7239 (6)	0.5630 (8)	4.8 (8)
P2	0.3533 (10)	0.6152 (6)	0.6292 (8)	5.0 (8)
P3	0.4663 (9)	0.7241 (6)	0.5685 (7)	4.6 (8)
C1	0.388 (3)	0.7097 (20)	0.6319 (23)	3.7 (27)
C111	0.176 (4)	0.712 (3)	0.620 (3)	4.9 (36)
C112	0.094 (4)	0.664 (3)	0.598 (3)	7.0 (39)
C113	0.028 (4)	0.656 (3)	0.638 (3)	7.5 (44)
C114	0.066 (5)	0.703 (3)	0.718 (3)	7.6 (48)
C115	0.159 (5)	0.755 (3)	0.734 (4)	7.5 (43)
C116	0.216 (4)	0.763 (3)	0.691 (4)	7.3 (46)
C121	0.295 (4)	0.8125 (20)	0.565 (3)	3.8 (31)
C122	0.368 (4)	0.853 (3)	0.636 (3)	4.7 (35)
C123	0.386 (4)	0.916 (3)	0.638 (4)	7.1 (45)
C124	0.321 (5)	0.9437 (25)	0.559 (4)	6.4 (44)
C125	0.249 (4)	0.900 (3)	0.487 (3)	5.6 (38)
C126	0.230 (3)	0.8361 (25)	0.487 (3)	5.5 (35)
C211	0.269 (3)	0.600 (3)	0.682 (3)	6.5 (37)
C212	0.196 (4)	0.529 (3)	0.660 (4)	8.1 (45)
C213	0.135 (5)	0.510 (4)	0.702 (4)	12.4 (55)
C214	0.163 (4)	0.552 (3)	0.777 (4)	6.4 (38)
C215	0.233 (4)	0.616 (3)	0.807 (4)	7.0 (48)
C216	0.292 (4)	0.6382 (23)	0.762 (3)	5.6 (36)
C221	0.470 (3)	0.5911 (19)	0.702 (3)	4.8 (29)
C222	0.513 (4)	0.6064 (21)	0.792 (3)	5.9 (36)
C223	0.606 (4)	0.5891 (22)	0.857 (3)	7.4 (38)
C224	0.646 (3)	0.5519 (24)	0.814 (4)	7.5 (40)
C225	0.602 (4)	0.5331 (24)	0.724 (3)	6.4 (37)
C226	0.527 (4)	0.5578 (22)	0.670 (3)	5.9 (33)
C311	0.586 (3)	0.7055 (20)	0.635 (3)	3.9 (29)
C312	0.623 (3)	0.7146 (20)	0.724 (3)	5.8 (32)
C313	0.727 (4)	0.7043 (19)	0.7673 (25)	5.9 (35)
C314	0.779 (4)	0.680 (3)	0.719 (5)	10.5 (58)
C315	0.735 (5)	0.675 (3)	0.630 (4)	8.3 (44)
C316	0.640 (4)	0.6831 (23)	0.589 (4)	6.8 (39)
C321	0.519 (3)	0.8159 (20)	0.574 (4)	4.7 (32)
C322	0.588 (4)	0.8462 (22)	0.658 (3)	5.7 (36)
C323	0.630 (4)	0.911 (3)	0.662 (3)	5.6 (37)
C324	0.598 (4)	0.9406 (21)	0.586 (4)	5.5 (36)
C325	0.524 (4)	0.9100 (22)	0.506 (3)	5.2 (35)
C326	0.477 (4)	0.8402 (24)	0.497 (3)	4.8 (35)

Table 5.3.1.2. (cont'd)

Cb1	0.156 (4)	0.5709 (24)	0.462 (4)	8.5 (42)
Ob1	0.074 (3)	0.5442 (16)	0.4586 (17)	6.6 (26)
Cb2	0.399 (4)	0.5788 (19)	0.470 (3)	5.3 (35)
Ob2	0.4632 (24)	0.5623 (15)	0.4536 (21)	6.7 (25)
Cb3	0.256 (5)	0.721 (3)	0.373 (4)	14.7 (47)
Ob3	0.248 (3)	0.7622 (19)	0.3273 (22)	7.9 (30)
Ct1	0.082 (7)	0.672 (4)	0.404 (5)	17.1 (73)
Ot1	-0.018 (4)	0.6847 (24)	0.369 (3)	10.8 (40)
Ct2	0.278 (4)	0.482 (3)	0.511 (3)	6.3 (39)
Ot2	0.265 (4)	0.4340 (21)	0.530 (3)	5.3 (33)
Ct3				
Ot3	0.4929 (23)	0.7187 (13)	0.3648 (17)	8.5 (21)
Ct4	0.165 (4)	0.5092 (22)	0.322 (3)	8.0 (44)
Ot4	0.143 (3)	0.4541 (17)	0.3071 (22)	8.3 (26)
Ct5	0.091 (4)	0.5985 (25)	0.280 (4)	10.7 (39)
Ot5	0.011 (3)	0.6037 (20)	0.2285 (22)	11.7 (33)
Ct6				
Ot6	0.291 (3)	0.6118 (15)	0.2271 (22)	10.9 (26)
Rh2	0.71456	0.92406	0.14337	4.50
Co4	0.62173	0.82443	0.02437	3.89
Co5	0.80343	0.82827	0.15309	4.10
Co6	0.79144	0.90414	0.03658	4.45
P4	0.64322	0.88233	0.23364	4.65
P5	0.52313	0.77100	0.09096	4.22
P6	0.73197	0.77030	0.23093	4.58
C2	0.60108	0.78677	0.21196	2.96
C411	0.52544	0.90826	0.22793	5.17
C412	0.49483	0.94840	0.16182	6.51
C413	0.40394	0.97185	0.15313	9.92
C414	0.36437	0.94952	0.21492	8.11
C415	0.39186	0.90568	0.28457	5.48
C416	0.48774	0.89499	0.28455	6.94
C421	0.73168	0.90377	0.34623	4.16
C422	0.70258	0.86479	0.40302	3.83
C423	0.76351	0.88317	0.49701	3.79
C424	0.83939	0.94518	0.50816	5.84
C425	0.86617	0.99362	0.45094	6.42
C426	0.80634	0.96357	0.36745	5.62
C511	0.46746	0.68946	0.05864	4.41
C512	0.51663	0.65758	0.01702	4.68
C513	0.46560	0.58685	-0.00335	5.19
C514	0.38459	0.55052	0.00546	6.25
C515	0.34376	0.57973	0.05122	9.57
C516	0.39403	0.65522	0.07724	6.21
C521	0.39922	0.79727	0.06762	5.98
C522	0.35869	0.82218	-0.01101	3.94
C523	0.26235	0.83444	-0.02923	8.91
C524	0.21625	0.82135	0.02511	6.34
C525	0.25430	0.79513	0.10571	4.94
C526	0.35930	0.78662	0.12319	4.48

Table 5.3.1.2. (cont'd)

C611	0.69384	0.68202	0.20778	3.99
C612	0.76313	0.65835	0.18070	5.03
C613	0.73565	0.59005	0.16596	5.19
C614	0.66362	0.55386	0.18879	5.42
C615	0.59724	0.57643	0.21985	4.57
C616	0.61724	0.64351	0.22837	4.70
C621	0.81210	0.78199	0.34548	3.37
C622	0.77699	0.73003	0.39029	6.29
C623	0.84591	0.73704	0.48806	6.70
C624	0.94597	0.79531	0.51511	5.46
C625	0.97911	0.84120	0.46675	5.56
C626	0.90681	0.83133	0.38305	3.64
Cb4	0.61875	0.92167	0.02854	8.00
Ob4	0.53484	0.93883	-0.01949	7.70
Cb5	0.72664	0.77440	0.04062	8.73
Ob5	0.73729	0.73406	0.00232	6.82
Cb6	0.85248	0.91643	0.20933	8.83
Ob6	0.93687	0.94633	0.26484	8.63
Ct7	0.74077	1.01045	0.16905	8.27
Ot7	0.73783	1.06201	0.18194	9.79
Ct8	0.53083	0.79159	-0.05770	13.61
Ot8	0.47976	0.77717	-0.15124	10.19
Ct9	0.91339	0.81624	0.18633	12.23
Ot9	1.00046	0.79658	0.22059	11.30
Ct10	0.81735	0.98314	0.04006	7.49
Ot10	0.84192	1.03962	0.04365	10.36
Ot11	0.68374	0.87605	-0.13344	12.58
Ot12	0.95342	0.87822	0.04805	12.74
Ct12	0.88525	0.89049	0.03436	7.90
Ct11	0.71159	0.88169	-0.05767	3.16

BEQ IS THE MEAN OF THE PRINCIPAL AXES OF THE THERMAL ELLIPSOID

Table 5.3.1.3. Thermal Parameters for $RhCo_3(CO)_9[HC(PPh_2)_3]$

TABLE OF U(I,J) OR U VALUES *100.
E.S.D.S. REFER TO THE LAST DIGIT PRINTED

	U11(U)	U22	U33	U12	U13	U23
Rh1	3.1 (4)	3.1 (4)	3.7 (3)	2.3 (3)	1.3 (3)	0.9 (3)
Co1	5.8 (4)	5.6 (4)	4.7 (3)	2.6 (3)	1.3 (3)	0.0 (3)
Co2	5.7 (4)	5.9 (4)	5.1 (4)	2.9 (3)	1.8 (3)	0.0 (3)
Co3	9.4 (7)	9.0 (7)	6.6 (6)	3.4 (5)	1.4 (5)	-0.9 (4)
P1	7.0 (10)	6.0 (10)	6.1 (9)	2.9 (8)	3.0 (8)	0.8 (7)
P2	5.9 (9)	6.7 (10)	5.4 (9)	1.9 (8)	1.3 (8)	-0.4 (8)
P3	5.6 (9)	7.2 (10)	5.4 (9)	2.6 (8)	2.6 (8)	0.7 (7)
C1	2.5 (25)	9.4 (38)	5.1 (29)	1.8 (25)	4.4 (23)	2.6 (26)
C111	2.4 (31)	13.2 (53)	5.3 (35)	4.3 (33)	2.7 (29)	-0.8 (35)
C112	1.8 (32)	11.4 (55)	10.4 (49)	1.5 (36)	-0.1 (36)	-0.6 (39)
C113	5.6 (39)	20.5 (65)	7.3 (41)	7.5 (42)	5.1 (34)	3.4 (42)
C114	14.8 (56)	19.7 (69)	5.5 (40)	14.4 (53)	9.6 (42)	5.2 (41)
C115	5.9 (44)	10.7 (54)	9.7 (51)	2.3 (41)	1.2 (40)	2.7 (41)
C116	10.7 (50)	16.0 (60)	8.5 (48)	9.7 (47)	7.7 (41)	6.9 (44)
C121	5.5 (33)	5.2 (35)	7.2 (36)	0.2 (30)	6.5 (30)	1.0 (32)
C122	7.1 (38)	5.2 (38)	8.2 (41)	0.0 (33)	6.7 (34)	-1.2 (33)
C123	11.2 (51)	8.6 (51)	10.7 (51)	4.8 (45)	6.9 (42)	-1.5 (42)
C124	8.0 (44)	8.6 (47)	12.5 (53)	-0.5 (38)	10.3 (43)	-0.8 (44)
C125	10.0 (46)	5.9 (40)	7.8 (42)	3.1 (38)	5.5 (36)	4.8 (35)
C126	6.2 (37)	7.3 (44)	8.1 (40)	3.1 (35)	3.2 (31)	4.9 (33)
C211	4.4 (32)	17.7 (58)	5.0 (35)	0.2 (36)	5.7 (29)	-0.4 (38)
C212	6.5 (45)	10.8 (51)	14.3 (61)	5.9 (41)	3.3 (41)	8.3 (45)
C213	10.1 (53)	28.7 (93)	4.5 (40)	13.1 (60)	-4.6 (37)	-7.8 (51)
C214	4.5 (38)	11.5 (51)	10.5 (45)	5.5 (37)	3.4 (34)	9.1 (40)
C215	9.1 (50)	11.1 (54)	13.2 (58)	5.0 (43)	9.9 (45)	6.0 (46)
C216	8.9 (44)	8.3 (44)	4.3 (34)	7.8 (39)	0.1 (30)	-0.1 (31)
C221	6.7 (34)	5.1 (33)	3.1 (30)	2.4 (28)	-1.5 (26)	0.7 (24)
C222	11.6 (46)	7.3 (38)	4.7 (34)	3.7 (35)	4.0 (34)	0.8 (29)
C223	5.6 (37)	6.0 (38)	15.3 (55)	3.4 (31)	2.3 (38)	2.4 (35)
C224	5.5 (37)	9.5 (46)	12.9 (55)	4.3 (34)	2.0 (37)	0.2 (40)
C225	11.3 (47)	11.6 (47)	1.9 (29)	5.3 (40)	2.2 (31)	-0.2 (31)
C226	7.0 (38)	8.1 (40)	6.8 (37)	5.9 (33)	0.3 (31)	-1.3 (30)
C311	4.9 (32)	7.8 (37)	3.6 (30)	3.5 (28)	2.1 (27)	1.4 (26)
C312	6.0 (36)	6.6 (37)	5.2 (37)	0.8 (29)	-1.2 (30)	2.9 (29)
C313	11.4 (47)	2.3 (30)	3.3 (30)	0.0 (31)	-0.9 (34)	0.7 (23)
C314	6.9 (47)	11.3 (57)	26.3 (84)	6.6 (43)	9.2 (56)	3.7 (60)
C315	11.2 (56)	11.8 (51)	7.2 (41)	3.8 (44)	2.0 (43)	-0.6 (39)
C316	5.3 (37)	5.7 (38)	15.9 (56)	-0.8 (32)	6.7 (41)	-0.6 (36)
C321	2.1 (27)	4.4 (34)	12.3 (46)	0.3 (25)	4.4 (31)	-4.4 (35)
C322	8.0 (39)	1.4 (31)	11.1 (47)	0.6 (29)	3.3 (35)	-1.0 (31)
C323	9.1 (42)	9.3 (49)	5.0 (35)	4.2 (38)	4.1 (33)	3.0 (34)
C324	7.5 (40)	5.2 (38)	9.6 (43)	0.6 (32)	5.7 (38)	-2.7 (37)
C325	10.1 (43)	2.9 (34)	9.1 (42)	-1.2 (30)	7.8 (37)	-1.6 (30)
C326	6.7 (38)	8.8 (46)	6.4 (35)	5.5 (35)	4.3 (31)	6.2 (32)

Table 5.3.1.3. (cont'd)

Cb1	11.3 (48)	8.1 (39)	19.1 (57)	-3.4 (34)	15.5 (47)	8.0 (34)
Ob1	14.6 (34)	11.1 (32)	2.1 (18)	7.2 (28)	4.3 (23)	4.8 (19)
Cb2	12.0 (47)	4.3 (32)	8.2 (36)	8.3 (34)	5.2 (34)	8.7 (27)
Ob2	8.8 (28)	6.6 (26)	13.2 (31)	3.4 (22)	6.9 (24)	1.2 (21)
Cb3	20.2 (58)	6.5 (43)	15.9 (58)	15.3 (45)	-10.7 (47)	-6.0 (38)
Ob3	10.0 (32)	13.3 (40)	9.3 (30)	8.2 (31)	3.8 (25)	0.9 (26)
Ct1	24.9 (87)	19.2 (79)	14.9 (77)	-22.3 (72)	17.5 (79)	-10.4 (62)
Ot1	20.4 (50)	11.7 (40)	10.1 (35)	3.2 (44)	8.3 (40)	-0.9 (28)
Ct2	6.5 (35)	18.8 (72)	1.3 (27)	-4.4 (45)	8.0 (26)	2.2 (37)
Ot2	9.8 (42)	4.0 (35)	5.6 (35)	-2.8 (32)	4.9 (31)	3.0 (26)
Ct3						
Ot3	12.9 (32)	7.7 (28)	13.7 (32)	3.4 (25)	-1.5 (26)	-3.0 (23)
Ct4						
Ot4	11.8 (28)	6.6 (23)	6.4 (21)	3.7 (22)	-3.6 (20)	-4.7 (18)
Ct5	14.9 (53)	-0.5 (31)	14.2 (53)	0.4 (36)	5.1 (42)	0.4 (32)
Ot5	11.2 (31)	8.4 (30)	12.2 (30)	4.0 (28)	4.7 (25)	-0.2 (26)
Ct6	7.1 (42)	9.9 (47)	13.3 (51)	5.9 (37)	-7.1 (36)	-9.1 (39)
Ot6	15.1 (40)	18.4 (43)	8.0 (29)	10.6 (36)	-0.9 (27)	-3.2 (28)
Rh2	6.80	5.13	5.73	3.01	2.48	0.60
Co4	6.91	4.46	3.27	2.75	1.41	0.97
Co5	5.21	5.17	5.42	2.52	1.88	0.36
Co6	9.78	3.36	4.52	2.32	3.43	1.91
P4	5.89	5.89	5.89	1.51	2.54	0.68
P5	5.34	5.34	5.34	1.37	2.30	0.62
P6	5.80	5.80	5.80	1.49	2.50	0.67
C2	3.75	3.75	3.75	0.96	1.61	0.43
C411	6.55	6.55	6.55	1.68	2.82	0.76
C412	8.24	8.24	8.24	2.12	3.55	0.96
C413	12.56	12.56	12.56	3.23	5.41	1.46
C414	10.27	10.27	10.27	2.64	4.43	1.19
C415	6.94	6.94	6.94	1.78	2.99	0.81
C416	8.79	8.79	8.79	2.26	3.79	1.02
C421	5.27	5.27	5.27	1.35	2.27	0.61
C422	4.86	4.86	4.86	1.25	2.09	0.56
C423	4.79	4.79	4.79	1.23	2.07	0.56
C424	7.40	7.40	7.40	1.90	3.19	0.86
C425	8.13	8.13	8.13	2.09	3.50	0.94
C426	7.11	7.11	7.11	1.83	3.07	0.83
C511	5.59	5.59	5.59	1.44	2.41	0.65
C512	5.93	5.93	5.93	1.52	2.56	0.69
C513	6.58	6.58	6.58	1.69	2.83	0.76
C514	7.91	7.91	7.91	2.03	3.41	0.92
C515	12.12	12.12	12.12	3.11	5.22	1.41
C516	7.86	7.86	7.86	2.02	3.39	0.91
C521	7.57	7.57	7.57	1.94	3.26	0.88
C522	4.99	4.99	4.99	1.28	2.15	0.58
C523	11.29	11.29	11.29	2.90	4.86	1.31
C524	8.03	8.03	8.03	2.06	3.46	0.93
C525	6.26	6.26	6.26	1.61	2.70	0.73
C526	5.67	5.67	5.67	1.46	2.44	0.66

Table 5.3.1.3. (cont'd)

C611	5.05	5.05	5.05	1.30	2.18	0.59
C612	6.37	6.37	6.37	1.64	2.75	0.74
C613	6.58	6.58	6.58	1.69	2.83	0.76
C614	6.87	6.87	6.87	1.76	2.96	0.80
C615	5.79	5.79	5.79	1.49	2.49	0.67
C616	5.95	5.95	5.95	1.53	2.56	0.69
C621	4.27	4.27	4.27	1.10	1.84	0.50
C622	7.97	7.97	7.97	2.05	3.44	0.92
C623	8.48	8.48	8.48	2.18	3.66	0.98
C624	6.92	6.92	6.92	1.78	2.98	0.80
C625	7.04	7.04	7.04	1.81	3.03	0.82
C626	4.62	4.62	4.62	1.19	1.99	0.54
Cb4	10.13	10.13	10.13	2.60	4.37	1.18
Ob4	9.75	9.75	9.75	2.51	4.20	1.13
Cb5	11.06	11.06	11.06	2.84	4.77	1.28
Ob5	8.64	8.64	8.64	2.22	3.72	1.00
Cb6	11.18	11.18	11.18	2.87	4.82	1.30
Ob6	10.93	10.93	10.93	2.81	4.71	1.27
Ct7	10.47	10.47	10.47	2.69	4.51	1.22
Ot7	12.40	12.40	12.40	3.19	5.34	1.44
Ct8	17.23	17.23	17.23	4.43	7.43	2.00
Ot8	12.91	12.91	12.91	3.32	5.56	1.50
Ct9	15.49	15.49	15.49	3.98	6.68	1.80
Ot9	14.31	14.31	14.31	3.68	6.17	1.66
Ct10	9.49	9.49	9.49	2.44	4.09	1.10
Ot10	13.13	13.13	13.13	3.37	5.66	1.52
Ot11	15.94	15.94	15.94	4.10	6.87	1.85
Ot12	16.13	16.13	16.13	4.15	6.95	1.87
Ct12	10.00	10.00	10.00	2.57	4.31	1.16
Ct11	4.00					

Table 5.3.1.4. Bond Distances - $RhCo_3(CO)_9[HC(PPh_2)_3]$

MOLECULE 1	Bond	Distance(A)	Std(A)
	Rh1-Co1	2.64232	0.00651
	-Co2	2.66332	0,00690
	-Co3	2.50630	0.00773
	-P1	2.27477	0.01224
	-Cb1	2.02485	0.04825
	-Cb3	2.01034	0.08919
	-Ct1	1.45570	0.10429
	Co1-Co2	2.64254	0.00773
	-Co3	2.59490	0.00773
	-P2	2.24632	0.01217
	-Cb1	1.72946	0.05580
	-Cb2	1.83319	0.05236
	-Ct2	1.94728	0.06483
	Co2-Co3	2.57731	0.00832
	-P3	2.25375	0.01197
	-Cb2	2.15726	0.03391
	-Cb3	2.13276	0.03853
	-Ct3	-------	-------
	Co3-Ct4	1.61683	0.04618
	-Ct5	1.65814	0.04895
	-Ct6	-------	-------
	C1-P1	1.86565	0.03602
	-P2	1.97377	0.04317
	-P3	1.85968	0.03596

Table 5.3.1.4. (cont'd)

MOLECULE 1	Bond	Distance(A)	Std(A)
	P1-C111	1.82198	0.04409
	-C121	1.84994	0.04459
	P2-C211	1.79001	0.04271
	-C221	1.83616	0.03965
	P3-C311	1.77509	0.03976
	-C321	1.93165	0.04454
	Cb1-Ob1	1.17755	0.04454
	Cb2-Ob2	1.20274	0.05676
	Cb3-Ob3	1.17486	0.08036
	Ct1-Ot1	1.41705	0.11698
	Ct2-Ot2	1.08418	0.07321
	Ct3-Ot3	-------	-------
	Ct4-Ot4	1.15198	0.05654
	Ct5-Ot5	1.17049	0.05971
	Ct6-Ot6	-------	-------

Table 5.3.1.4. (cont'd)

MOLECULE 2	Bond	Distance(A)	Std(A)
	Rh2-Co4	2.63150	0.04303
	-Co5	2.64701	0.04448
	-Co6	2.60322	0.04410
	-P4	2.29263	0.05495
	-Cb4	1.87986	0.05693
	-Cb6	1.89982	0.05127
	-Ct7	1.82048	0.04502
	Co4-Co5	2.63453	0.05438
	-Co6	2.59003	0.05102
	-P5	2.31150	0.05425
	-Cb4	2.10292	0.04702
	-Cb5	1.99555	0.04424
	-Ct8	1.49954	0.03071
	Co5-Co6	2.57187	0.06099
	-P6	2.24395	0.05691
	-Cb5	1.98029	0.04662
	-Cb6	1.95425	0.04263
	-Ct9	1.54663	0.04776
	Co6-Ct10	1.64801	0.04954
	-Ct11	1.47937	0.04262
	-Ct12	1.54374	0.05286
	C2-P4	1.98893	0.04724
	-P5	1.89694	0.05456
	-P6	1.91516	0.04487

Table 5.3.1.4. (cont'd)

MOLECULE 2	Bond	Distance(A)	Std(A)
	P4-C411	1.88991	0.04290
	-C421	1.80890	0.05370
	P5-C511	1.73114	0.04648
	-C521	1.90057	0.04520
	P6-C611	1.84134	0.04659
	-C621	1.80709	0.05538
	Cb4-Ob4	1.29827	0.05302
	Cb5-Ob5	1.16390	0.03695
	Cb6-Ob6	1.21971	0.05009
	Ct7-Ot7	1.14372	0.04316
	Ct8-Ot8	1.46279	0.05344
	Ct9-Ot9	1.32822	0.04938
	Ct10-Ot10	1.17769	0.04939
	Ct11-Ot11	1.19218	0.05431
	Ct12-Ot12	1.01941	0.04554

Table 5.3.1.5. Bond Angles - $RhCo_3(CO)_9[HC(PPh_2)_3]$

Molecule 1	Atoms	Angle	Std
	C1 -P1 -Rh1	109.83	1.22
	C1 -P2 -Co1	108.18	1.20
	C1 -P3 -Co2	110.53	1.24
	C1 -P1 -C111	110.36	1.84
	C1 -P1 -C121	110.70	2.03
	C111-P1 -C121	102.30	2.22
	C1 -P2 -C211	103.36	2.31
	C1 -P2 -C221	108.94	1.70
	C211-P2 -C221	104.44	2.27
	C1 -P3 -C311	104.61	1.92
	C1 -P3 -C321	108.14	1.82
	C311-P3 -C321	98.65	2.01
	P1 -C1 -P2	101.87	1.76
	P1 -C1 -P3	106.66	1.91
	P2 -C1 -P3	102.86	1.75
	P1 -Rh1 -Co1	95.36	0.35
	P1 -Rh1 -Co2	92.50	0.38
	P1 -Rh1 -Co3	147.94	0.39
	P2 -Co1 -Rh1	92.95	0.37
	P2 -Co1 -Co2	96.76	0.41
	P2 -Co1 -Co3	149.10	0.43
	P3 -Co2 -Rh1	95.53	0.36
	P3 -Co2 -Co1	92.11	0.40
	P3 -Co2 -Co3	148.42	0.44

Table 5.3.1.5. (cont'd)

Molecule 1	Atoms	Angle	Std
	Rh1 -Co3 -Co1	61.22	0.20
	Rh1 -Co3 -Co2	61.97	0.21
	Co1 -Co3 -Co1	61.45	0.22
	Rh1 -Co1 -Co2	60.51	0.19
	Rh1 -Co2 -Co1	59.76	0.19
	Co1 -Rh1 -Co2	59.73	0.19
	Rh1 -Ct1 -Ot1	175.00	6.39
	Co1 -Ct2 -Ot2	167.10	4.93
	Co2 -Ct3 -Ot3	------	----
	Co3 -Ct4 -Ot4	166.64	5.29
	Co3 -Ct5 -Ot5	165.28	5.20
	Co3 -Ct6 -Ot6	------	----
	Rh1 -Cb1 -Co1	89.15	1.80
	Rh1 -Cb3 -Co2	79.95	2.25
	Co1 -Cb2 -Co2	82.51	1.56
	Cb1 -Co1 -Cb2	152.53	2.23
	Cb2 -Co2 -Cb3	144.62	2.32
	Cb3 -Rh1 -Cb1	143.74	1.93

Molecule 2	Atoms	Angle	Std
	C2 -P4 -Rh2	109.66	1.75
	C2 -P5 -Co4	110.17	2.14
	C2 -P6 -Co5	111.39	2.46

Table 5.3.1.5. (cont'd)

Molecule 2	Atoms	Angle	Std
	C2 -P4 -C411	106.75	2.53
	C2 -P5 -C421	107.20	2.65
	C411-P6 -C421	101.67	1.99
	C2 -P5 -C511	110.72	2.85
	C2 -P5 -C521	105.25	1.96
	C511-P5 -C521	98.48	2.24
	C2 -P6 -C611	100.94	2.20
	C2 -P6 -C621	107.49	2.09
	C611-P6 -C621	102.05	2.68
	P4 -C2 -P5	103.00	2.54
	P4 -C2 -P6	100.19	2.12
	P5 -C2 -P6	103.68	2.00
	P4 -Rh2 -Co4	96.35	1.71
	P4 -Rh2 -Co5	92.03	1.81
	P4 -Rh2 -Co6	148.01	1.86
	P5 -Co4 -Rh2	93.71	1.58
	P5 -Co4 -Co5	95.12	1.96
	P5 -Co4 -Co6	150.39	1.95
	P6 -Co5 -Rh2	96.61	1.53
	P6 -Co5 -Co4	93.87	1.76
	P6 -Co5 -Co6	150.39	1.95
	Rh2 -Co6 -Co4	60.89	1.26
	Rh2 -Co6 -Co5	61.52	1.38
	Co4 -Co6 -Co5	61.38	1.52

Table 5.3.1.5. (cont'd)

Molecule 2	Atoms	Angle	Std
	Rh2 -Co4 -Co5	60.35	1.27
	Rh2 -Co5 -Co4	59.77	1.26
	Co4 -Rh2 -Co5	59.88	1.26
	Rh2 -Ct7 -Ot7	167.13	3.39
	Co4 -Ct8 -Ot8	151.74	3.46
	Co5 -Ct9 -Ot9	169.35	3.96
	Co6 -Ct10-Ot10	176.01	3.36
	Co6 -Ct11-Ot11	154.67	3.65
	Co6 -Ct12-Ot12	165.54	4.82
	Rh2 -Cb4 -Co4	82.50	2.11
	Co4 -Cb5 -Co5	83.00	1.69
	Co5 -Cb6 -Rh2	86.74	1.99
	Cb4 -Co4 -Cb5	137.41	2.31
	Cb5 -Co5 -Cb6	144.14	2.93
	Cb6 -Rh2 -Cb4	140.56	2.23

5.4. ATTEMPTED CRYSTAL STRUCTURE DETERMINATION OF PRODUCT OF REACTION BETWEEN $Co_2(CO)_8$ AND $HC(PPh_2)_3$

An orange crystal of the resultant complex from the preparation described in Section 3.2.7. was mounted on a glass capillary using 5-minute epoxy with a well-developed crystal face perpendicular to the capillary axis. The crystal was then mounted on a goniometer and aligned by oscillation photography. The two orthogonal exposures each revealed a rectangular cell projection. Preliminary reciprocal lattice photography displayed orthorhombic symmetry. Weissenberg photography of the 0kl and 1kl zones displayed systematic absences corresponding to no conditions for hkl and k = 2n for 0kl. Mirror symmetry was retained in the upper level. Precession photography of the zones hk0 and h0l exhibited absence conditions h = 2n and l = 2n, respectively. The upper levels showed no conditions. Lines h00, 0k0 and 00l gave conditions h = 2n, k = 2n and l = 2n also respectively. This uniquely determined the space group as Pbca. Unit cell dimensions were determined from precession photographs using a Charles Supper film measuring device. (These photographs have been used as examples in Section 4.3.1. on geometric data collection.)

Twelve axial reflections were automatically aligned along with their Friedel equivalents to create an initial least-squares refined orientation matrix from which unit cell dimensions were calculated along with their respective

standard deviations. (Table 5.4.1.)

Table 5.4.1. Unit Cell Dimensions (Å, °) with e.s.d's

a = 13.41292	b = 23.18790	c = 11.41308
$\sigma(a)$ = 0.0234084	$\sigma(b)$ = 0.0195639	$\sigma(c)$ = 0.0190998
α = 89.998	β = 89.939	γ = 90.141
$\sigma(\alpha)$ = 0.109	$\sigma(\beta)$ = 0.140	$\sigma(\gamma)$ = 0.120

Intensity data were collected for the octant hkl. Reference reflections 2 0 2, 3 0 2 and 0 6 0 varied less than ±5% over the duration of the data collection. 2299 reflections were collected for $2.5^\circ \leq 2\theta \leq 45^\circ$ of which 1976 were considered observed ($>3\sigma I$). Data reduction was performed to scale, reduce and normalise the data.

Trial solution by Patterson synthesis resulted in a map in which the strongest peaks did not correspond to any positions from solving the Patterson vectors for x,y and z. An attempt to scale the peak heights relative to the origin resulted in the possible identification of a vector corresponding to a Co-Co distance, however, positions calculated from the Patterson vectors did not seem to phase the data very well as observed by the reluctance of the residual index to decrease past 0.60.

The next trial solution was performed using MULTAN in which two of the eight solutions determined all the phases of the starting set. The criteria for choosing a correct solution indicated all solutions to be reliable. E-maps of

the two best solutions sets indicated that the solutions were probably the same but corresponded to different origins. Editing the two largest peaks into the cell followed by three cycles of isotropic least squares did not bring about an encouraging drop in residual index. A subsequent difference synthesis failed to resolve recognizable light atoms in any logically expected geometry. All attempts to edit remotely feasible atoms into the cell produced no convincing changes in terms of agreement between observed and calculated structure factors.

It is the belief of this investigator that the solution is possible, however, the combination of a non-apparent solution and non-green-fingered crystallography prevented the solution of the structure.

6. DISCUSSION

6.1. DISCUSSION OF RESULTS FROM $Mo(CO)_4[HC(PPh_2)_3]$ AND $Mo(CO)_2Cl(\pi\text{-allyl})[HC(PPh_2)_3]$

The two crystal structure determinations were performed to explore the feasibility of using mononuclear molybdenum-TRIPOD carbonyls in the step-wise synthesis of mixed-metal TRIPOD supported clusters and to explore the differences in the M-P3 distances between substituted and non-substituted TRIPOD carbonyls.

In the non-substituted carbonyl, a pseudo mirror-plane is defined by Mo, C3, O3, C4, O4, C5 and P3. This feature is obvious from Fig. 5.2.1.1. The dangling phosphino function is observed to lie below the equatorial plane of the coordination sphere of molybdenum. The chelating bite-angle of P1 and P2 to molybdenum is roughly 60° and the ring defined by Mo, P1, C5 and P2 is observed form four planar surfaces with vertices defined by vectors P1-to-P2 and Mo-to-C5 (Fig. 5.2.1.2.). The dihedral angle between the planes intersecting at edge P1-to-P2 is 21.476° while the dihedral angle between planes intersecting at edge Mo-to-C5 is 24.161°. The four carbonyl groups bend away from the ligand probably due to crowding from the phenyl groups although the proximity of the phenyl groups is not apparent from Fig. 5.2.1.3. since the protons are omitted.

The chloro-allyl TRIPOD complex of Section 5.2.2. was prepared by Dr. Ali Bahsoun,[3,4,5,8,10] and although the

predicted formulation was correct it was deemed that the x-ray structure would complement the structure of that in Section 5.2.1. The structure conforms to the expected geometry for complexes with the general formula, $[MoX(CO)_2L_2(\eta^3\text{-allyl})]$[50] in which L is a bridging diphosphene ligand such as dppm or dppe (Fig. 6.1.1.). In solution, complexes with this generic formula have been observed to be fluxional wherein the allyl may shift to the position trans to the halide[62] (Fig. 6.1.2.).

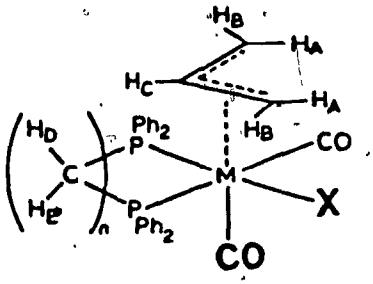

Fig. 6.1.1.

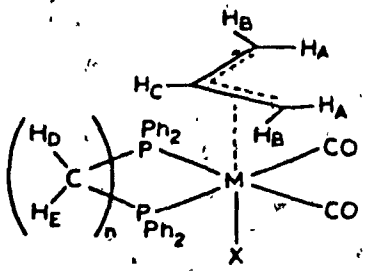

Fig. 6.1.2.

The coordination sphere of this substituted Tripod complex is quite unsymmetrical by comparison with the non-substituted one. Taking the Mo-Cl vector as the vertical reference, it is observed that the equatorial bonds are all less than 90° to Cl and that the carbonyl carbon, C6 is closest to being trans to Cl. Furthermore the bite angle of the chelating phosphino functions of the TRIPOD ligand is about 3° less than in the former structure. This is probably due to the allyl ligand in which two of the allyl carbons, C2 and C4, are observed to form similar angles with Cl and almost lie in the equatorial "plane." The

four-membered metallocycle comprised of Mo, P1, C1 and P2 forms four planes with vertices defined by vectors P1-P2 and Mo-C1. The dihedral angle between planes intersecting at vertex P1-P2 is 39.605° while the dihedral angle between planes intersecting at vertex Mo-C1 is 43.617°. The allyl C3 lies below this pseudo-plane, however, the distances from Mo to the allyl carbons would indicate it is indeed π-allyl. The net effect on the uncoordinated phosphino function is to impose a strain on the ligand forcing the P3 function to be 0.8 A further away from Mo than in the non-substituted TRIPOD carbonyl. The P3 function is observed to lie on the same side of the equatorial plane as C1. The dihedral angle between the plane defined by Mo, C5, C1 and the plane defined by allyl carbons C2, C3 and C4 is 17.112°. The allyl plane also forms a dihedral angle with the least-squares plane defined by atoms Mo, C5, C6, P2, and C1 which is calculated to be 17.518°.

In the case of the tetracarbonyl TRIPOD complex the Mo to carbonyl carbon distances are approximately 0.05A shorter for carbonyls trans to the chelating phosphino groups than for the two axial carbonyls. Alternatively in the chloro-allyl TRIPOD complex the difference in bond lengths between Mo and each carbonyl carbon is only 0.023A. The analogy between both complexes in terms of trans-influences is not easily made due to the degree of distortion from octahedral symmetry observed in the latter case. However, it is interesting to note that the longer of the two

bond distances for the latter case is that for which the carbonyl is transoid to the chloride.

The disparity between experimentally determined and calculated results for the elemental analysis for the complex $Mo(CO)_4[HC(PPh_2)_3]$ must be due to the presence of impurities in the form of starting reagents and/or solvent molecules. This may be stated with confidence since the crystal structure has been reliably determined. It should be noted that the solubility of both $Mo(CO)_6$ and the TRIPOD derivative are similar making purification by standard techniques difficult. The sample sent for analysis was not purified by crystallization.

6.2. $[RhCl\{HC(PPh_2)_3\}]_2$

Considering the difficulty in obtaining satisfactory spectra for this complex and the unsuccessful isolation of suitable single crystals for diffraction studies it is difficult at this point to unambiguously assign a definite composition to this compound. Both the rate of product formation and also the reaction yield (88%) are quite high providing the tentative formulation is correct. As pointed out in Section 3.2.4., the successful approach to immediate product recovery involved pouring wet, non-deoxygenated THF directly over a solid mixture of reactants in a 2:1 molar ratio of $HC(PPh_2)_3$ and $[RhCl(CO)_2]_2$ followed by rapid evacuation of the system. Rigourously deoxgenated sovlent

produced a color change when added to the solid reagent mixture, however, product recovery was not immediate. The actual product geometry depends upon whether or not the Cl-bridges were cleaved or not. The absence of CO absorption in the IR, indicated at least 4 CO molecules were displaced per molecule of the starting complex.

In excess PPh_3, the chlorocarbonyl trans bis-(triphenylphosphine) Rh(I) species is produced from the chlorodicarbonyl dimer.[54] Due to the constraint imposed by the TRIPOD ligand the trans product is ruled out. Providing the product is mononuclear the chloro - bridges would have to be cleaved by solvent (Fig. 6.2.1.).

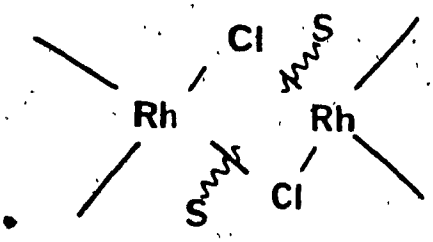

Fig. 6.2.1.

Alternatively the product may be polymeric since the third phosphino function could coordinate to a second Rhodium atom. The hypothesized polymeric structure is depicted in Fig. 6.2.2. on the following page.

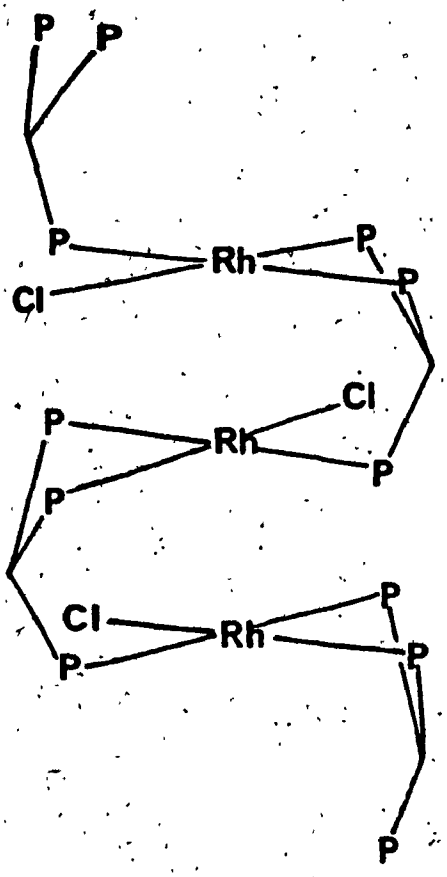

Fig. 6.2.2.

In a personal communication from the Osborn group, workers there report having isolated a complex they believe can be represented as that in Fig. 6.2.3. The room-temperature and low-temperature ^{31}P NMR spectra are observed to appear as in Fig. 6.2.4. This suggests that the possibility that two isomers are interconverting at room temperature. It may be possible that the complex prepared in this study is related to that of Osborn's group where the chloride would bridges two Rhodium centres and the counteranion would be simply chloride.

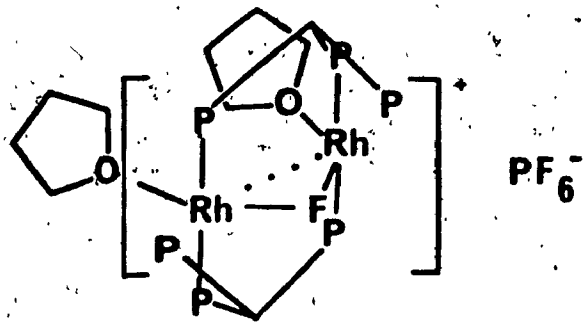

Fig. 6.2.3.

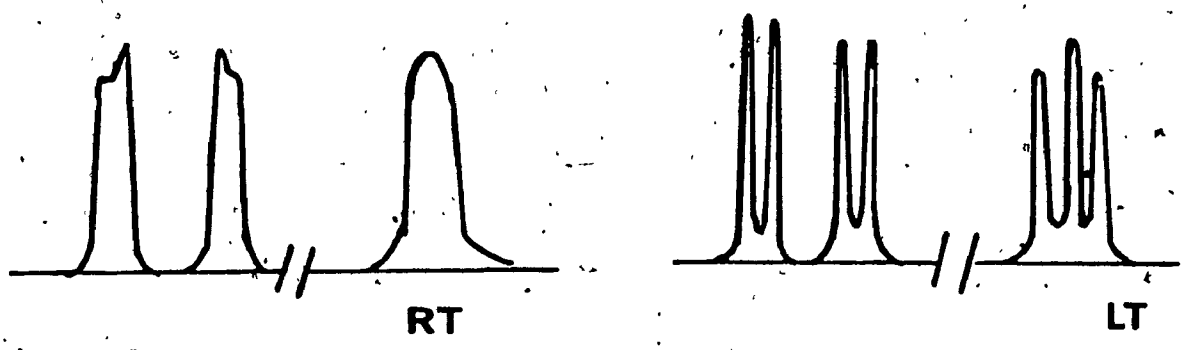

Fig. 6.2.4.

The proposed dimeric formulation would, however, suggest the best fit to the observed behavior of the molecule in terms of its reaction product with $Co_2(CO)_8$. The complex is insoluble in THF hence it is not likely that it contains THF. The proposed polymer would probably exhibit a similar $^{31}P\{^1H\}$ NMR spectrum to the one observed. In the chlorodicarbonyl dimer, the chloride bridges define the vertex of two intersecting planes. These planes are defined by the square planar coordination sphere of each Rhodium atom. The TRIPOD ligand can displace two CO molecules on each metal centre. However, the possibility of a number of isomers interconverting at room temperature exists. If the energy barrier to interconversion between these isomers is low, interpretation of the NMR spectrum

could be difficult. Two possible isomers are depicted in Fig. 6.2.5.

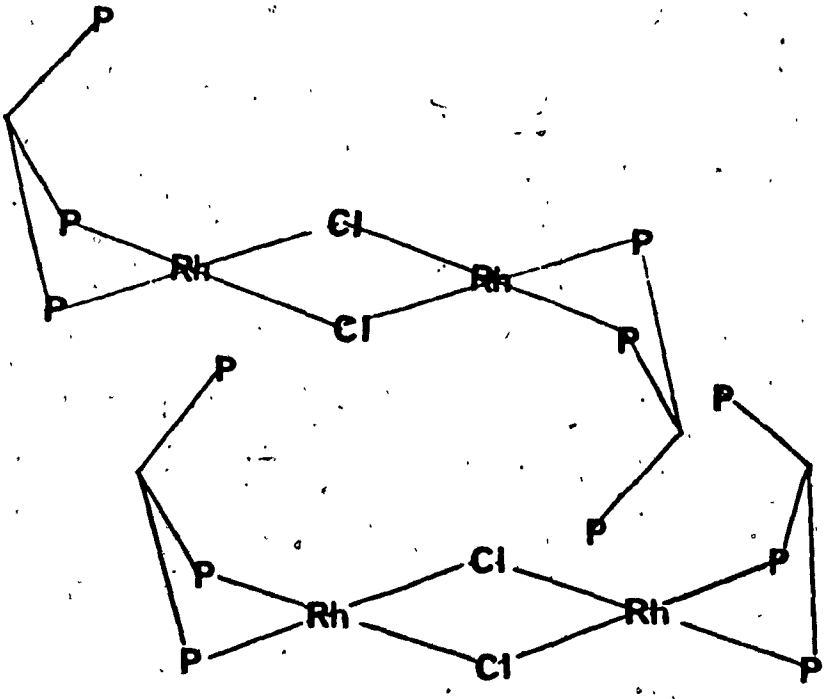

Fig. 6.2.5.

In addition, considering that the planes defined by the two Rhodium coordination spheres are not parallel in the parent carbonyl,[66,67] then a similar type of fluxionality may exist for the analogous postulated TRIPOD dimer.

The reaction is analogous to that used to prepare a compound for which a ^{31}P NMR study of phosphine exchange was performed. $[RhCl(PF_3)_2]_2$[54] was prepared by direct reaction of PF_3 and chlorodicarbonyl Rhodium(1) dimer. Hence, TRIPOD was substituted for PF_3 in making this complex. The trifluorophosphine complex has been found to undergo phosphorus exchange and facile interconversion to the PPh_3, CO and C_2H_4 derivatives. As well, in excess PPh_3 high yields of of tris-PPh_3 chloro Rhodium(I), also known as Wilkinson's catalyst[53] was obtained. This may well

support the mononuclear and polymeric formulations of the TRIPOD derivative prepared in this study. In any case, the possibility exists that the TRIPOD derivative could display interesting catalytic properties.

The results of the elemental analyses are well within the limits of experimental error. The similarity of this reaction by comparison with the reaction of PF_3 and chlorodicarbonylrhodium(1) dimer coupled with the absence of carbonyl absorption in the infrared spectrum infers that the chloro-bridged dimeric formulation is the correct one. The disparity between the calculated and observed values of the elemental analyses may be due to contamination from starting reagents and /or the presence of solvent. Difficulties with the solubility of this complex pre-empted purification by chromatography. Crystalline product isolation was not successful.

6.3. DISCUSSION OF RESULTS FOR $RhCo_3(CO)_9[HC(PPh_2)_3]$

6.3.1. X-RAY STRUCTURE

The structure exhibits two TRIPOD-capped tetranuclear carbonyl clusters. The $RhCo_3$ core demonstrates that the Rhodium atom is always contained in the basal plane and one unique, apical position is always held by a Cobalt atom. The formula unit adopts a somewhat helicopter-like appearance.

The asymmetric unit (Fig. 5.3.1.2.) should be referred to. The point group of the idealized molecular geometry of the formula unit is C_s. The observed symmetry of the crystalline material is C_1. The occupancies of the three metal atoms in the plane defined by coordination to the TRIPOD ligand should cause the idealized symmetry to correspond to C_{3v} providing the statistical distribution of the site symmetry for these atoms were completely random.

Molecule 2 is considered since all atoms were refined using correctly identified atomic scattering factors. Close inspection reveals the geometry of the plane defined by the phosphorus atoms is observed to be almost isosceles. The angles made by adjacent phosphorus atoms with the central methane carbon show the unique angle not to be opposite to Rh2 but opposite to Co5. This, however, may be the result of distortion induced by the packing of the molecules in the asymmetric unit. The metallic triangle defined by atoms coordinated by TRIPOD is almost isosceles as well but

approximates equilateral geometry more closely than the phosphorus triangle. The angle which deviates most from the equilateral configuration is that which has Co4 as vertex. The three angles from Co6 to the adjacent pairs of metal atoms in the plane coordinated by TRIPOD are close to being equal, however, the bond distance from Co6 to Co4 is observed to be significantly shorter than the other two. Bridging carbonyls Cb4, Cb5 and Cb6 form bond angles to adjacent metals in which the angle Rh2-Cb6-Co5 is notably larger than the other two. These carbonyls lie below the metal plane to which they are bound but a projection of the molecule along the line of sight from Co6 to the C2 carbon of the TRIPOD ligand reveals the edges from metal to carbonyl carbon to metal approximate 180°. Unfortunately plots exhibiting this feature are unavailable. It is reasonable to expect carbonyls to be more susceptible to distortion than the metallic skeleton but it should be pointed out that the large discrepancy between the observed and calculated structure factors make these observations somewhat less than reliable. The major sources of molecular asymmetry must be ascribed to distortions from idealized symmetry caused by molecular packing in the asymmetric unit as well as the fact that the structure is not optimal due to the questionable integrity of the intensity data.

6.3.2. RELATED CHEMISTRY

Although compounds with the same relative geometry have been previously prepared[3,8] this complex is unique in the sense that the three-Cobalt, one Rhodium tetrahedral metal skeleton was not prepared in the same fashion. The latter were prepared by direct action of the TRIPOD ligand on the corresponding tetranuclear carbonyl cluster.

The TRIPOD complex discussed in Section 6.2. was used as one of the precursors in preparing the TRIPOD-capped tetranuclear complex of this section. The reaction strategy was analogous to that using the trifluorophosphine complex, $Rh_2Co_2(CO)_8(PF_3)_4$[11] and Cobalt carbonyl to prepare the dicobalt-dirhodium $(PF_3)_4$ octacarbonyl complex.[11,55]

The parent carbonyl of the product in this study was found to be easily prepared from reaction of $RhCl_3$ and the anion $[Co(CO)4]^-$ by equation 1.[12]

$$3[Co(CO)_4]^- + RhCl_3 \text{ -- } RhCo_3(CO)_{12} + 3Cl^- \qquad (1)$$

Reaction of $[(PF_3)_2ClRh]_2$ and $Co_2(CO)_8$ affords a mixed metal tetranuclear complex containing four PF_3 ligands.

The reaction leading to Tripod-capped product with the $RhCo_3$ core was inspired by this reaction in an attempt to cap two triangular faces of the tetrahedral metal skeleton. Whether the bi-capped diRhodium diCobalt spe-

cies was first formed and subsequently disproportionated to the product or the chloro-TRIPOD Rhodium(I) species was fragmented to a monometallic species through attack of $Co_2(CO)_8$ remains undetermined. The reaction stoichiometry based on speculation regarding the 70% product yield can be formulated as

$$[RhCl\{HC(PPh_2)_3\}]_2 + 7/2Co_2(CO)_8 \text{ -- } 2RhCo_3(CO)_9[HC(PPh_2)_3] + CoCl_2 + 19CO \quad (2)$$

since the starting regent ratio of Co:Rh complexes was 4:1.

Filtering and washing may have removed unreacted starting material, however, $CoCl_2$ could have remained.

Regardless of the difficulties encountered characterizing the product the crystal structure presented a challenging problem in which the results are rather novel. Consideration of the unusual asymmetric unit, consisting of two disordered formula units as well as the space group symmetry P1 accounts for the exceptional unit cell size.

^{13}C and ^{31}P NMR studies indicate the parent carbonyl and the complex $Rh_2Co_2(CO)_8(PF_3)_4$ undergo exchange.[11,55] The carbonyl groups in the parent $RhCo_3$ carbonyl exchange terminal and bridging positions in what has been reported as two distinct processes[56] while carbonyl exchange in the homonuclear cluster analogues occurs by a single process.[57] While exchange has been investigated in some TRIPOD-capped tetranuclear clusters it is to be expected that the rigid nature of the ligand would tend to supress this mobility.

The carbonyl exchange in the TRIPOD-capped derivative of $Co_4(CO)_{12}$ exhibits only that the apical terminal carbonyls undergo exchange. While exchange studies indicate that ^{13}CO is incorporated statistically onto all CO sites of the molecule, intramolecular exchange (although slow) occurs more readily than intermolecular exchange.[3] Intramolecular exchange is impeded with increasing phosphine substitution of the cluster.[3] This has been ascribed to steric hindrance by phenyl groups in the case where the phosphine is the TRIPOD ligand, however, when the phosphines are less bulky the effect is still observed.[11] Perhaps the strong π-accepting quality of phosphines causes less electron density to be present in the tetrahedral metal skeleton. This may stabilize the system sufficiently to inhibit the exchange process from occuring.

When complexes $Rh_2Co_2(CO)_{12}$ and $Rh_2Co_2(CO)_8(PF_3)_4$ are mixed 1:1 in solution at room temperature,[13] the PF_3 units distribute themselves onto the Rhodium atoms forming two diphosphine derivatives in which each Rhodium is coordinated by one PF_3 unit. The dimer $[RhCl(PF_3)_2]_2$ also exhibits phosphine exchange when reacted with its parent carbonyl and ethylene precursors.[55] Due to the two individual processes found for carbonyl exchange by the parent carbonyl cluster[57] the TRIPOD product may display enhanced catalytic reactivity over its analogues while maintaining its structural integrity.

Differences between results of elemental analyses and

the calculated elemental composition can be partially rationalized by the possibility that a solvent molecule is present. This makes the fit for Rh, Co and P almost exact providing a molecule of 1,2-dichloroethane is present as a solvate. However, the results for carbon and hydrogen are still disparate. The resulting crystal structure, although not an excellent determination, refutes the elemental analyses in terms of carbon and hydrogen content. The ratios of the heavier elements present, however, are constant with respect to one another and hence disparity in the results for the lighter atoms may be explained by the presence of some decomposition product formed during the reaction. Solubility and crystallization difficulties were encountered with this product which did not facilitate purification.

6.4. Elemental Analysis for Product of Reaction Between $Co_2(CO)_8$ and $HC(PPh_2)_3$

The fit between the calculated and experimental values for the elemental analysis of this complex is improved if the complex is considered to be coordinated symmetrically by two of the three phosphino functions. This leaves one TRIPOD function dangling and the model now contains six CO ligands instead of five. Even though the agreement between observed and calculated results is improved the fit is not great. One confirming figure, however, is that the ratio of Co to P is a constant 2:3. The only way this can be formulated is by either of the two geometries which have been postulated in this study. Spectral evidence supports either structure and both are schematized in Fig. 6.4.1.

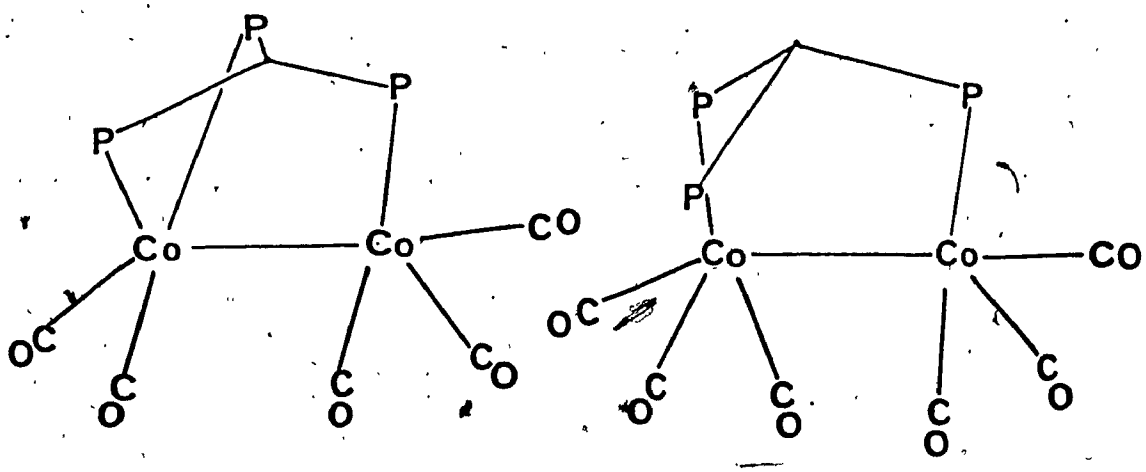

Fig. 6.4.1.

7. IMPLICATIONS FOR FURTHER STUDY

7.1 TRIPOD LIGANDS

Consideration of the complex $RhCl(PPh_3)_3$ (Wilkinsons' catalyst) is instructive in the design of homogeneous catalysts used for hydrogenation and polymerization. It has been observed that substitution of tertiary alkyl phosphines for triphenylphosphine deactivates the catalyst. Trialkylphosphines are stronger nucleophiles than aryl species and probably reduce the ability of the Rhodium centre to behave as a good π-acceptor for substrate attachment (i.e., oxidative addition).

Catalysts are required to release bound substrate once converted to product as well as having the ability to reform for the next catalytic cycle. If a ligand causes a substrate to bind too strongly, the catalyst becomes poisoned.

This imposes severe restrictions on the choice of ligand to be used in homogeneous catalyst design. A very delicate balance hinging on the ligand field strength and the central metal must be struck in order that a catalyst performs the desired function.

One idea is to modify the ligand so as to subtly adjust the ligand field strength. For the TRIPOD case this could include modification of the groups adjacent to the coordinating function and/or changing the coordinating

function itself. In doing this the functionality of the resulting catalyst may be optimized.

In TRIPOD-supporting carbonyl complexes, fluxionality of the carbonyl groups is inhibited by comparison to the parent carbonyl complex. The attractive feature of cluster complex supporting TRIPOD is their resistance to degradation under relatively vigorous conditions.[3]

It would present some challenging chemistry to observe the effects of varying the nucleophilicity of the archetypal TRIPOD, $HC(PPh_2)_3$. This could be achieved by introducing electron-withdrawing groups onto the aromatic rings. A second approach is to vary the steric effect of the ligand by preparing the analogous dicyclopentadiene compound. Furthermore, preparation of a chiral TRIPOD could lead to enantioselective catalysts. Finally changing the coordinating atom to As [3] or Sb should also alter the resulting complexes' behavior.

7.2. STEPWISE SYNTHESIS OF HETEROPOLYMETALLIC COMPLEXES

The nickel trimer described in the general introduction is an example of the stepwise synthesis of homopolymetallic cluster formation using the TRIPOD ligand. The Fe-Rh complex in the same section exemplifies stepwise heteropolymetallic cluster synthesis.

In the case of mononuclear molybdenum-TRIPOD chelates such as those for which crystal structures have been

performed in this study, coupling these to Rh(1) complexes as initially attempted, this investigation was not successful.

Results for the two structures indicate positively that room exists for the complexation of a second metal centre. The difference in the molecular geometry between the two complexes infers, however, that the chloro-allyl derivative may not form a metal-to-metal bond quite so easily as the plain carbonyl due to the configuration of the third phosphino function relative to the chloride. This geometry may undergo rearrangement to a more favorable configuration in the presence of a suitable metallic fragment. This may be possible through a trigonal twist mechanism.[61,62,63]

Molybdenum(0) tends not to form metal-metal bonds under mild conditions. The cyclopentadienyl carbonyl anion, however, may be dimerized in the presence of a suitable oxidizing agent (i.e., $Fe(NO)_3$).[64] This method may be employed in the preparation of heteropolynuclear Mo(0) complexes supported by the TRIPOD ligand. The tetracarbonyl TRIPOD derivative could be converted to a sodium salt using Na/Hg amalgam. This could be mixed with a Rh(1) complex in the presence of ferric nitrate possibly coupling the two species. This route might be employed to couple the molybdenum complexes to other fragments such as tungsten and iron cyclopentadienyl carbonyl anions.[58,59,65]

Another possibility for preparing TRIPOD clusters in a

stepwise fashion comes from the reaction leading to the $RhCo_3$ complex for which the crystal structure appears in Section 5.3.1. The Rhodium precursor of this complex may serve as a starting point for reactions with a number of mixed-metal clusters.

7.3. OTHER HETEROMETALLIC TRIPOD COMPLEXES

Isolation of the TRIPOD-capped derivative of the complex $(CO)CpFe(\mu\text{-}CO)_2Co(CO)_3$[14,15] was not satisfactory. Preparation of the TRIPOD-free complex is simple[15,65] however, reaction with TRIPOD results in the formation of a product which thwarted attemps at its characterization both by spectroscopic and crystallographic techniques. Other methods to attempt to isolate the desired product included reacting the anion $[CpFe(CO)_2]^-$ [58] with TRIPOD followed by reaction with $Co_2(CO)_8$. Failure by this route led to the preparation of the cation $[CpFe(CO)3]^+$.[59] This cation was then reacted with TRIPOD in a 1:1 molar ratio. The resulting product was reacted with $Co_2(CO)_8$ yielding a green solution which was more brilliant than the olive color obtained by direct reaction of the preformed hetero-complex with TRIPOD. Isolation of product ,however, was not successful. A third attempt was to try reacting the TRIPOD ligand with $CpFe(CO)_2I$. This complex in the presence of excess PPh_3 affords a mixture of 38% $CpFe(CO)PPh_3I$ and 50% $[CpFe(CO)_2PPh_3]^+I^-$.[60] The reaction did not give an

easily identifiable product. Due to time limitations and the successful isolation of the product which has been formulated as $Co_2(CO)_5[HC(PPh_2)_3]$ (Sec. 3.2.4.) work on the Cobalt–Iron target was terminated temporarily. The target molecule is given in Fig. 7.3.1.

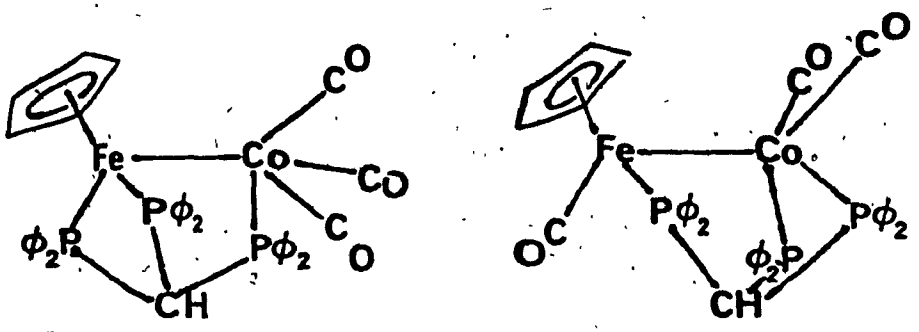

Fig. 7.3.1.

Considering the ease in which the TRIPOD ligand reacts with $Co_2(CO)_8$, further attempts to prepare this complex may be successful by reaction of the Cobalt-TRIPOD complex prepared in this study (as outlined in Section 3.2.4.) with one of the above-named cyclopentadienyl iron species.

REFERENCES

1. The Osborn Group: J. A. Osborn and A. A. Bahsoun.
2. K. Von Issleib, A P. Abicht, J. Prakt. Chem., 1970, 312, 456.
3. A. A. Bahsoun, J. A. Osborn, C. Volker, J. J. Bonnet, G. Lavigne, Organometallics, 1892, 1, 1114.
4. A. A. Bahsoun, J. A. Osborn, P. H. Bird, N. Nucciarone, A. V. Peters, J. Chem. Soc.; Chem. Commun. 1984, 2, 72.
5. A.A. Bahsoun, Personal Communication.
6. J. A. Osborn, G. G. Stanley, Angew. Chem., Int. Ed. Engl., 1980, 19, 1025.
7. M. M. Harding, B. S. Nicholls, A. K. Smith, J. Organometal. Chem.,1982, 226, C17.
8. A. A. Arduini, A. A. Bahsoun, C. Voelker, Angew. Chem. Int. Ed. Engl., 1980, 19, 1024.
9. J. A. Clucas, M. M. Harding, B. S. Nicholls, A. K. Smith, J. Chem. Soc; Chem. Commun., 1984, 5, 319.
10. A. A. Bahsoun, J. A. Osborn, J. P. Kitzinger, P. H. Bird, U. Siriwardane, Nouveau Journal de Chimie, 1984, Vol. 8, 2, 125.
11. Topics in Current Chemistry, 71 "CARBONYL CHEMISTRY" Springer Verlag Berlin Heidelberg, New-york, 1977
12. A. Martinengo, P. Chini, V. G. Albano, F. Cariati, T. Salvatore, J. Organometal. Chem., 1973, 59, 379.

13. H. E. Hosseini, J. F. Nixon, J. Organometal. Chem., 1975, 97, C 24.

14. T. Madach, H. Varenkamp, Chem. Ber., 1975, 113, 2675.

15. I. L. C. Campbell, F. S. Stephens, J. Chem. Soc., Dalton Trans., 1975, 22.

16. D. F. Shriver, "The Manipulation of Air Sensitive Compounds", McGraw Hill, N.Y., 1969.

17. R. F. Angelici, "Synthesis and Technique in Inorganic Chemistry", Saunders, 1977.

18. L. V. Azaroff, "Elements of X-Ray Crystallography", McGraw Hill, 1968.

19. M. M. Woolfson, "X-Ray Crystallography", Cambridge University Press, 1970.

20. E. W. Nuffield, "X-Ray Diffraction Methods", John Wiley & Sons, 1966.

21. C. H. Stout, L. H. Jensen, "X-Ray Structure Determination, A Practice Guide", Macmillan Publishing Co., New York, 1968.

22. M. J. Buerger, "Contemporary Crystallography", McGraw Hill Inc., New York, 1970.

23. M. J. Buerger, "X-Ray Crystallography", John Wiley & Sons, New York, 1942.

24. N. Friedrich, P. Knipping, M. Vonlauc, Sitzb. Math. Phys., Klasse Bayer Akad. Wiss., Munchen p.303, 1912.

25. N. L. Bragg, Proc. Camb. Phil. Soc., 1913, 17, 43.

26. P. P. Ewald, Proc. Phys. Soc., 1940, 52, 167.

27. D. T. Cromer, J. T. Waber, Acta Cryst., 1965, 18, 104.

28. "International Tables for X-Ray Crystallography", Vol. III, "Physical and Chemical Tables", Caroline H. MacGilvray, Gerard Rieck; Ed's., Kathleen Lonsdale; Gen. Ed., Kynoch Press, Birmingham, England, 1962.

29. A. L. Paterson, Z. Kryst., 1935, A90, 517.

30. M. J. Buerger, "Vector Space and its Application to Crystal Structure Investigation", John Wiley & Sons, New York, 1943.

31. "International Tables for X-Ray Crystallography, Vol.I, 1965, "Symmetry Groups", Norman F. M. Henry, Kathleen Lonsdale; Ed's., Kynoch Press, Birmingham, England, 1962.

32. H. Lipson, C. A. Taylor, "Fourier Transforms and X-Ray Diffraction", London: G.Bell, 1958.

33. "Theory and Practice of Direct Methods in Crystallography", M. F. C. Ladd, R. A. Palmer; Ed's., Plenum Press, New York, 1980.

34. C. Giacovazzo, "Direct Methods in Crystallography", Academic Press, London, New York, 1980.

35. J. Karle, H. Hauptman, Acta Cryst., 1980, 3, 181.

36. A. J. C. Wilson, Nature, London, 1942 50, 151.

37. "International Tables for X-Ray Crystallography", Vol. II., "Mathematical Tables", John S. Kasper, Kathleen Lonsdale; Ed's., Kynoch Press, Birmingham, England, 1959.

38. D. Sayre, Acta Cryst., 1952, 5, 60.

39. J. Karle, I. L. Karle, Acta Cryst., 1966, 21, 849.

40. "MULTAN"; A Multi-Solution Direct Methods Crystallographic Phase Determination Program written by P. Main, G. Germain, M. M. Woolfson, 1974.

41. A. D. Booth, Proc. Roy. Soc., (London), 1946, (A), 188, 77,; 1947, (A), 190, 482.

42. H. Lipson, W. Cochran, "The Determination of Crystal Structures", London: G. Bell, 1957.

43. User Manual for the Program, "DIFFRAC"; a Fortran Program Designed to Drive an Automated Data Collection, E. J. Gabe, T. Lepage, D. F. Grant, N.R.C. of Canada, (Ottawa).

44. K. Weisenberg, Z. Physik., 1942, 23, 229.

45. M. J. Buerger, "The Precession Method in X-Ray Crystallography", John Wiley & Sons, New York, 1964.

46. "The Charles Supper Co.", Natick, Mass.

47. "The Single Crystal Diffraction Software Package", N.R.C. of Canada, (Ottawa), E.J. Gabe, Y. Lepage.

48. A Feature of the "DIFFRAC" program (part of ref. 47) Which Increases Data Collection Efficiency by Estimating Background Radiation from the Peak Profile Rather than by Direct Measurement.

49. D. Harker, J. Chem. Phys., 1936, 4, 381.

50. "Comprehensive Organometallic Chemistry; The Synthesis, Reactions and Structures of Organometallic Compounds", Sir Geoffrey Wilkinson; Ed., F. Gordon Stone; Deputy Ed., Edward W. Abel; Exec. Ed., Pergammon Press,

Oxford, New York, Toronto, Sydney, Paris, Frankfurt, 1982., Vol. III, page 1156.

51. "Advanced Inorganic Chemistry", F. Albert Cotton, G. Wilkinson, 3rd Edition, Wiley Interscience; John Wiley & Sons, New York, Chichester, Brisbane, Toronto, 1980, pages 936-941.

52. "ORTEP"; Oak Ridge Thermal Ellipsoid Program, C. K. Johnson, Oak Ridge National Laboratory, Oak Ridge, Tennessee, 1966.

53. J. A. Osborne, F. H. Jardine, J. F. Young, G. Wilkinson, J. Chem. Soc., 1964, (A), 1711.

54. J. A. McCleverty, G. Wilkinson, Inorg. Synth., 1966, 8, 214.

55. D. A. Clement, J. F. Nixon, J. Chem. Soc., Dalton Trans., 1972, 2553.

56. B. F. G. Johnson, J. Lewis, T. W. Matheson J. Chem. Soc., Chem. Commun., 1974, 441.

56. F. A. Cotton, L. Kruczynski, B. L. Shapiro, L. F. Johnson, J.A.C.S., Aug. 23, 1972, 94:17, 6191.

58. L. Busetto, R. J. Angelici, Inorg. Chim. Acta., Dec. 1968, 2:4, 391.

59. ibid; J.A.C.S., 1968, 90, 3283.

60. P. M. Treichel, R. L. Shubkin, K. W. Barnett, D. Reichard, Inorg. Chem., 1966, 5,7, 1177.

61. H. tom Dieck, H. Friedel, J. Organomet. Chem., 1968, 14, 375.

62. R. G. Hayter, J. Organomet. Chem, 1968, 13, P1.

63. B. J. Bridson, J. Organomet. Chem., 1977, 125, 225.

64. R. Birdwhistell, P. Hackett, A.R. Manning, J. Organomet. Chem. 1978, 157, 239.

65. "Comprehensive Organometallic Chemistry; The Synthesis, Reactions and Structures of Organometallic Compounds", Sir Geoffrey Wilkinson; Ed., F. Gordon Stone; Deputy Ed., Edward W. Abel; Exec. Ed., Pergammon Press, New York, Oxford, Toronto, Sydney, Paris, Frankfurt, 1982, Vol. VI, page 763.

66. J. G. Norman,Jr., D. L. Gmur, J. Am. Chem. Soc., 1977, 99, 1446.